KIT SCIENTIFIC REPORTS 7643

Annual Report 2012

Institute for Pulsed Power and Microwave Technology
Institut für Hochleistungsimpuls- und Mikrowellentechnik

John Jelonnek (ed.)

KIT Scientific Publishing

John Jelonnek (ed.)

Annual Report 2012

Institute for Pulsed Power and Microwave Technology
Institut für Hochleistungsimpuls- und Mikrowellentechnik

Karlsruhe Institute of Technology
KIT SCIENTIFIC REPORTS 7643

Annual Report 2012

Institute for Pulsed Power and Microwave Technology
Institut für Hochleistungsimpuls- und Mikrowellentechnik

edited by
John Jelonnek

KIT Scientific Publishing

Report-Nr. KIT-SR 7643

Impressum

Karlsruher Institut für Technologie (KIT)
KIT Scientific Publishing
Straße am Forum 2
D-76131 Karlsruhe
www.ksp.kit.edu

KIT – Universität des Landes Baden-Württemberg und
nationales Forschungszentrum in der Helmholtz-Gemeinschaft

KIT Scientific Publishing 2013
Print on Demand

ISSN 1869-9669

Institute for Pulsed Power and Microwave Technology

(Institut für Hochleistungsimpuls- und Mikrowellentechnik (IHM))

Director: Prof. Dr.-Ing. John Jelonnek

The Institute for Pulsed Power and Microwave Technology (Institut für Hochleistungsimpuls- und Mikrowellentechnik (IHM)) is doing research in the areas of pulsed power and high power microwave technologies. Both, research and development of high power sources as well as related applications are in the focus. Applications for pulsed power technologies are ranging from material processing to bioelectrics. Microwave technologies are focusing on RF sources for electron cyclotron resonance heating and on applications for material processing at microwave frequencies.

IHM is doing research, development, academic education and, in collaboration with the KIT Division IMA and industrial partners, the technology transfer. Projects have been conducted within six HGF Programs: Renewable Energies (EE), FUSION, NUKLEAR, NANOMIKRO, Efficient Energy Conversion and Use (REUN) and Technology-Innovation and Society (TIG).

R&D work has been done in the following topics: fundamental theoretical and experimental research on the generation of intense electron beams, strong electromagnetic fields and their interaction with plants, materials and plasmas; application of these methods in the areas of generation of energy through controlled thermonuclear fusion in magnetically confined plasmas, in materials processing and in energy technology.

Research areas require additionally the deep knowledge on modern electron beam optics, vacuum technologies, material technologies, high voltage technologies and high voltage measurement techniques.

The R&D program of the IHM is summarized as follows:

Department for Pulsed Power Technologies:
(Head: Dr. Georg Müller)

In environmental- and bio-technology the research and development is devoted to pulsed power technology with repetition rates up to 20 Hz, power in the Giga-Watt range and electric field strengths of 10^5-10^7 V/m. The research is concerned with short pulse (µs) - and with ultra-short pulse (ns) treatment of biological cells (electroporation). The focus is related to large-scale applications, treatment of large volumes, to the realization of a high component life time and to the overall process integration. Main directions of work in this field are the electroporation of biological cells for extraction of cell contents (KEA process), the dewatering and drying of green biomass, the treatment of micro algae for further energetic use and sustainable reduction of bacteria in contaminated effluents. Another key research topic is related to the surface modification and corrosion protection of metals and alloys using high-energy, large-area pulsed electron beams (GESA process). The research is focused on electron beam physics, the interaction of electron beams with material surfaces and the corresponding material specific characterization investigations. The goal is to develop a corrosion barrier for improved compatibility of structural nuclear reactor materials in contact with heavy liquid metal coolants (Pb or PbBi) (Programs: EE, NUKLEAR, TIG).

- For expanding experimental capabilities, microalgae culti¬vation capacity was increased by a second 26 ltr annular photobioreactor (PBR). Also, in collaboration with IBLT/BVT, a 1000 ltr flat panel PBR to be installed at the greenhouse area of IHM has been designed. (Program: EE, HGF-Portfolio BioEconomy)
- For optimizing downstream processing a detailed study on the lipid yield by ethanolic extraction after PEF treatment was performed after refinement of the biochemical and gravimetric diagnostic methods. A 4-fold increase in lipid extraction yield after PEF treatment could be revealed in average. Solvent extraction efficiency at appropriate treatment energy values was close to 100 %. Special emphasis was laid on the extraction from wet biomass, since energy consumption for PEF treatment is low compared to the energy needed in conventional lipid extraction for drying and cell disruption. Furthermore, PEF-processing of microalgae allows for selective extraction of water-soluble components and lipids. In addition to saving processing energy, this may open new processing possibilities for microalgae fractioning. (Program: EE)
- Nanosecond pulse exposition has been shown to stimulate growth of microalgae cultures. At current state of work an average increase of 10-20% in biomass yield could be achieved by nsPEF-treatment. (Program: EE).
- A modular trigger generator for over-voltage triggering based on the mentioned transformer concept has been build. This device is a 20-stage device. Each stage comprises a part of the transformer's secondary winding, two separate primary windings, each connected to one IGBT-switch for pulse generation, a capacitor bank providing the pulse energy, and the related driving- and control circuitry. All stages are triggered synchronously by a main control unit via fibre-optic links. The device is a two-terminal device, which will replace one charging coil of a Marx generator and is designed to be powered by the generator's charging current. (Program: EE).
- Fe-Cr-Al alloys are of large interest for practical applications at high-temperatures in reactive environments, thanks to their corrosion resistance, which is due to the formation of an alumina protective scale at the surface and are therefore good candidates as protection barriers in for the use in heavy liquid metals-HLM. To define the minimum Al content for the formation of an alumina scale in oxygen containing Pb, 10 compositions belonging to this alloy system were exposed in liquid Pb between 400 -600°C. An oxide map illustrating the stability domain of alumina grown on Fe-Cr-Al-alloys when exposed to molten, oxygen containing lead was drawn. The alumina stability domain border shifts with lower temperatures to higher chromium and aluminum concentrations. (Program: NUKLEAR).
- An extensive experimental campaign of fretting tests was continued in the frame of the GETMAT project. In particular, fretting corrosion tests in accelerated but still reactor relevant conditions (concerning temperature and oxygen content of Pb) were performed to investigate the role of the main affecting parameters, such as temperature, amplitude of the slip and applied load. Three different materials were selected among the candidate alloys for lead cooled nuclear systems, namely: f/m steel T91, austenitic steel 15-15Ti and GESA treated T91 (after LPPS (Low Pressure Plasma Spray) of FeCrAlY powder). The interaction of the fretting process with the corrosion mechanisms occurring in liquid lead and with the protecting oxide scale/corrosion barrier required for reactor components was also matter of study. Based on the concept of fretting maps all obtained data was analyzed with respect to the specific fretting coefficient. This data was then

applied to prognost parameters like load and amplitude at which tolerable fretting corrosion is expected. (Program NUKLEAR).

- Numerical assessments of MGI in the tokamaks JET and ITER has been done. The modelling is performed with the 2D tokamak code TOKES. The code calculates the motion of the plasma across and along the magnetic field lines, the motion of injected gas and atoms after recombination, and the gas motion in the injector. Validation of TOKES against JET are continued aiming at the heat transport during TQ and magnetic energy evolution at CQ onset. The modelling for ITER concerns maximal possible temperature T_{wmax} for the Be and W wall and a gas amount (argon) sufficient for plasma cooling with t_c < 5 ms. (Program: FUSION).

Department for High Power Microwave Technologies:

(Head: Dr. Gerd Gantenbein)

The High Power Microwave Department is focusing on RF sources (gyrotrons) for electron cyclotron resonance heating and current drive (ECRH&CD) of magnetically confined nuclear fusion plasmas and on the application of microwaves to materials and composites.

- Collaboration within the project PMW for planning, construction and testing of the 10 MW CW, 140 GHz electron cyclotron resonance heating (ECRH) system for the stellarator W7-X at IPP Greifswald. In particular, 1 MW CW, 140 GHz gyrotrons have been developed in cooperation with EPFL-CRPP Lausanne and Thales Electron Devices (TED), Vélizy, France. The first series tube delivered world record parameters in long-pulse operation with 0.92 MW at 30 min pulse length, an efficiency of approximately 45% and a mode purity of 97.5%. In 2010, series tube SN4R reached 1.02 MW. SAT for SN6 has been finalized at IPP Greifswald. SN7 has been delivered to KIT for first FAT tests, but resent to Thales for refurbishment. Final FAT acceptance of SN7 is expected for early 2013. Finalization date for the 10 MW ECRH system is targeted for 2014. The quasi-optical transmission system and the high-voltage modulators for the gyrotrons have been developed in cooperation with IPF, University of Stuttgart. With the development of major components for the ECRH system KIT makes a significant contribution to W7-X (HGF program FUSION).

- Within the European GYrotron Consortium (EGYC) and in collaboration with its industrial partner Thales Electron Devices (TED), Vélizy, France, EGYC is developing RF sources which will provide a total of 8 MW CW RF power at 170 GHz for the 24 MW CW ECRH system of ITER, Cadarache. Fusion for Energy (F4E) is coordinating the project for ITER which is done within the frame of the HGF program FUSION. Institutional partners are CNR, Italy, EPFL-CRPP, Switzerland and HELLAS, Greece. In 2012, F4E and EGYC have decided to switch to a conventional-cavity 1 MW CW 170 GHz $TE_{32,9}$-mode backup gyrotron replacing the EU 2 MW CW 170 GHz coaxial-cavity gyrotron. Its physical design did start in 2008 already. In 2012, the physical design of the $TE_{32,9}$-mode gyrotron has been finalized. Major improvements have been done in the physical design of the magnetron injection gun (MIG) and the quasi-optical system at the output of the gyrotron.

- Future fusion experiments will require frequency step-tunable gyrotrons. A step-tunable 1 MW gyrotron (105-163 GHz), including edge-cooled microwave vacuum window made of synthetic CVD-diamond for future ECRH systems of large-scale tokamak experiments is under test. In 2012, a new CVD diamond Brewster window has been tested in “cold” and “hot” experiments. “Hot” tests using the gyrotron did verify the proper Gaussian beam profiles for different frequencies and operating modes as measured in “cold” tests before. Previously observed parasitic oscillations at lower frequencies with BWO-like dependence on the cathode voltage and magnetic field did not appear for any measured mode. An experimental and theoretical study on the influence of the lateral misalignment between the axis of the annular electron beam and the cavity has been performed additionally.

- In 2012, studies on electron beam diagnostic systems have been continued during two experimental campaigns which took place at the IHM gyrotron facility in April and October 2012. The campaigns have been followed by periods of data processing. A diagnostic tool for determination of the energy distribution has been tested which is measuring the X-ray spectrum at the collector (collaboration with St. Petersburg State Polytechnical University, St. Petersburg, Russia).

- The physical and industrial design of a 10 kW / 28 GHz gyrotron has been finalized to evaluate the use of CPR emitters for gyrotron applications. CPR cathodes allow operation with higher current density (up to 50 A/cm^2) and provide much longer life time (~100000 h) compared to conventional emitters.

- Sintering of advanced functional and structural ceramics, in particular of nanostructured ceramics and metal powders and process technology in nano-mineralogy by means of high power millimeter waves at a frequency of 30 GHz delivered by a gyrotron. In further experiments, fundamental new non-thermal microwave effects are validated (HGF program NANOMIKRO).

- System studies on microwave applicators for various applications at the ISM (Industrial, Scientific, Medical) frequencies 0.915 GHz, 2.45 GHz and 5.8 GHz, such as for energy-efficient production of aircraft components made of carbon fibre composites by microwave process technology at 2.45 GHz. The new HEPHAISTOS CA3 system with a payload capacity of 7000 l and a microwave power of 25 kW is already in routine operation. This will, in development with industry, offer various applications and processes on a service basis. With the new facilities of the 2.45 GHz HEPHAISTOS-line significantly shorter processing times at slightly improved material properties compared with the conventional production in autoclaves have been achieved (Programm REUN, TIG and IMA).

IHM is equipped with a workstation cluster and a large number of experimental installations: KEA, KEA-ZAR, three GESA machines, eight COSTA devices, one abrasion and one erosion teststand, two gyrotron test facilities with one common power supply and microwave-tight measurement chamber, one compact technology gyrotron (30 GHz, 15 kW, continuous wave (CW)), several 2.45 GHz applicators of the HEPHAISTOS series, one 0,915 GHz, 60 kW magnetron system, one 5.8 GHz, 3 kW klystron installation and a low power microwave laboratory with several vectorial network analysers.

In 2012, Prof. John Jelonnek has started the new lecture course entitled “High Power Microwave Technologies (Hochleistungs-mikrowellentechnik)” for master students at KIT. Dr. Gerd Gantenbein has been teaching the part “heating and current drive” of the lecture “Fusionstechnologie B” by Prof. R. Stieglitz, IFRT. Dr.-Ing. Martin Sack hold the lecture course “Elektronische Systeme und EMV” at KIT.

At the turn of the year 2012/2013 the total staff with regular positions amounted to 40 (19 academic staff members, 5 engineers and 16 technical staff member and others).

In addition 11 academic staff members and 10 technical staff members (and others) were financed by acquired third party budget.

In course of 2012, 3 guest scientists, 11 PhD students (2 of KIT-Campus South, 6 of KIT-Campus North, 3 Scholarship), 1 DHBW student and 4 trainees in the mechanical and electronics workshops worked in the IHM.

Strategical Events, Scientific Honors and Awards

By Sept. 2012, Prof. Dr.-Ing. John Jelonnek has completed his first year as successor of Prof. Dr. Dr. h. c. Manfred Thumm as Director of IHM.

The organizational structure of IHM has been adapted. The department for high power microwave technologies is formed by three teams now, the team "gyrotron simulation and components", headed by Dr. Stefan Illy, the team "gyrotron verification and measurements techniques", headed by Dr. Tomasz Rzesnicki and the team "materials processing with microwaves" headed by Dr. Guido Link. The team "plasma-wall interactions", headed by Dr. Igor Landman has been moved to the department of pulsed power technologies.

IHM has organized the 4th Euro-Asian Pulsed Power Conference (EAPPC) in combination with the 19th International Conference on High-Power Particle Beams (BEAMS) which took place at Karlsruhe in September. Chair has been Dr. Georg Müller. The conference has been counted as very successful event.

Prof. Manfred Thumm received the "Heinrich-Hertz Preis" of KIT and EnBW Stiftung for his research work in the area of generation, transmission and conversion of high power microwaves for future magnetic confinement nuclear plasma devices.

Prof. Manfred Thumm received the "Excellent Teaching Award" for the Embedded Systems Engineering Executive Master Program of the HECTOR School of Engineering and Management at the KIT.

DI Andreas Schlaich received the "Student Paper Award – Honourable Mention" at the 39th IEEE Int. Conference on Plasma Science (ICOPS 2012) in Edinburgh, Scotland.

Longlasting Co-operations with Industries, Universities and Research Institutes

- Basics of the interaction between electrical fields and cells (Bioelectrics) in the frame of the International Bioelectrics Consortium with Old Dominion University Norfolk, USA; Kumamoto University, Japan; University of Missouri Columbia, USA; Institute Gustave-Roussy and University of Paris XI, Villejuif, France; University of Toulouse, Toulouse, France, Leibniz Institute for Plasma Science and Technology, Greifswald, Germany
- Desinfection of hospital wastewater by pulsed electric field treatment in cooperation with University of Mainz and Eisenmann AG
- Integration of the electroporation process for sugar production with SÜDZUCKER AG
- Development of protection against corrosion in liquid metal cooled reactor systems in the following EU-Projectes: LEADER, GETMAT, MATTER, HELIMNET, ESFR (Partner: CEA, ENEA, SCK-CEN, CIEMAT)
- Development of core- and structure materials for liquid lead reactor cooling systems in collaboration with the Japanese Atomic Energy Agency (JAEA)
- Development of large area pulsed electron beam devices in collaboration with the Efremov Institute, St. Petersburg, Russia
- Experiments on liquid Pb and PbBi-cooling of reactor systems with the Institute for Physics and Power Engineering (IPPE), Obninsk, Russia
- Development, installation and test of the complete 10 MW, 140 GHz ECRH Systems for continuous wave operation at the stellarator Wendelstein W7-X in collaboration with the Max-Planck-Institute for Plasmaphysics (IPP) Greifswald and the Institute for Plasmaresearch (IPF) of the University of Stuttgart
- Development of the European ITER Gyrotrons in collaboration in the frame of the European Gyrotron Consortiums EGYC and coordinated by Fusion for Energy (F4E). The other members of the Consortium are CRPP, EPFL Lausanne, Switzerland, CNR Milano, Italy, ENEA, Frascati, Italy, HELLAS-Assoc. EURATOM (NTUA/NKUA Athens), Greece. The industrial partner is the microwave tube company Thales Electron Devices (TED) in Paris, France
- Development of new diagnostic systems for improvement of electron guns for gyrotrons and cavity interaction calculations in collaboration with the St. Petersburg Polytechical University, Russia and the University of Latvia, Latvia
- Basic investigations of plasma-wall interaction in fusion reactors in collaboration with the State Research Center of Russian Federation Troitsk Institute for Innovation and Fusion Research (TRINITI), Troitsk, Russia and the Institute of Plasma Physics, Kharkov, Ukraine
- Fundamentals of application of gyrotrons for microwave materials processing in collaboration with the National Institute for Fusion Science (NIFS) in Toki, Japan and the University of Fukui, Japan
- Development of Microwave Systems of the HEPHAISTOS Series for materials processing with microwaves with the Company Vötsch Industrietechnik GmbH, Reiskirchen.

HGF program: FUSION

– Plasma Wall Interaction (PWI) –

(**EFDA Task WP12-IPH-A07-1-1-02/PS-01/KIT**: Analysis and computer simulation of disruption mitigation schemes of massive gas injection)

In ITER the disruptions can locally damage the wall surface. For protection of plasma facing components (PFC) a massive gas injection (MGI) of a noble gas into the confined plasma at the disruption onset is under investigation. During MGI the plasma thermal energy transforms into photonic load scattered over the surface. The MGI thermal quench phase (TQ) must outpace the disruption, which limits the acceptable MGI cooling time τ_c to a few ms. From MGI experiments it can be concluded that an effective ionization of injected atoms in the plasma and a radiating cooling wave into plasma bulk occur. Some moderate anomalous heat cross-transport develops in the bulk until the cooling wave reaches the magnetic surface of safety factor $q = 2$ ('resonance surface'); then the transport significantly rises.

Our purpose is the numerical assessments of MGI in the tokamaks JET and ITER. The modelling is performed with the 2D tokamak code TOKES. The code calculates the motion of the plasma across and along the magnetic field lines, the motion of injected gas and atoms after recombination, and the gas motion in the injector. Validation of TOKES against JET are continued aiming at the heat transport during TQ and magnetic energy evolution at CQ onset. The modelling for ITER concerns maximal possible temperature T_{wmax} of the Be and W wall and a gas amount (argon) sufficient for plasma cooling with $\tau_c < 5$ ms.

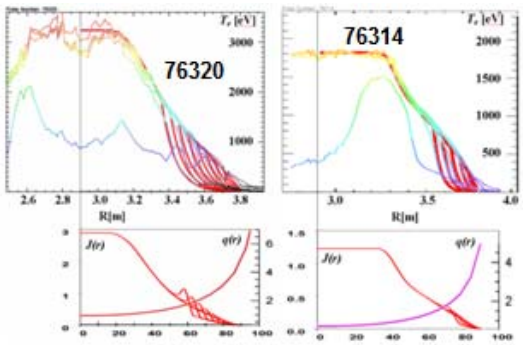

T_e profiles during the pre-TQ phase measured in JET and simulated with time step 0.2 ms. Shown are 2 pulses: JPN 76320 and JPN76314 with CFC wall. The simulated T_e, current density and q-profiles (lower panels) are plotted.

The simulated MGI process is divided into the pre-TQ, TQ itself and the current quench (CQ) phases. **Pre-TQ:** After the injected gas (G-gas, below argon) arrived at the separatrix, initially only the confined periphery plasma is cooled where G-gas is ionized and G-ions irradiate plasma energy (Fig. above). In the core T_e remains unchanged. The plasma current I_{tot} is almost constant which can indicate that the poloidal magnetic field B_θ does not evolve. The pre-TQ phase ends when T_e abruptly falls everywhere in the core as it is seen in Fig. 1. **TQ itself:** Fast drop of measured T_e indicates upon some fast anomalous cross transport. We suppose that it happens due to some ergodic behaviour of magnetic field (magnetic braiding). This anomalous transport mechanism is implied in TOKES simulations for fitting the calculations to the experiments. The anomalous thermal cross conductivity is proportional to the classical longitudinal one. It is also to note that the magnetic configuration cannot be reformed quickly (large inductance and small resistance of hot plasma) and thus a convective transport is not expected.

CQ onset: According to JET experiments, at the CQ onset the total plasma current I_{tot} reaches its minimum (next Fig.). We explained that effect. The current spike can indicate that the shrinking of current channel in the narrowed hot plasma column stops. Indeed, the poloidal magnetic flux $\Phi = I_{tot}L$ in the vessel holds until considerable cooling of plasma. In the contructing discharge the inductance L increases thus I_{tot} decreases until TQ end. Then the plasma gets cold and its resistivity increased, which effectively flattens current profile. This change decreases L, which results in the spike. We developed a simplified numerical model to prove that such behaviour of the discharge is possible. In the model we used energy conservation, the boundary conditions B_θ(wall) = 0 and the flux conservation at the wall. The resulting Φ gradually decreases, but nevertheless the plasma current shows a current spike like that of the experiment.

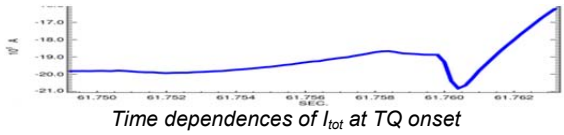

Time dependences of I_{tot} at TQ onset

In the ITER argon MGI simulation (next Fig.), T_{wmax} of Be or W wall after Ar massive gas injection was calculated with TOKES using short (flight length 35 cm) horizontal mid-plane injectors. The initial thermal energy and wall temperature are high (420 MJ and 500 K, respectively), which gives an upper estimation of the wall temperature after TQ.

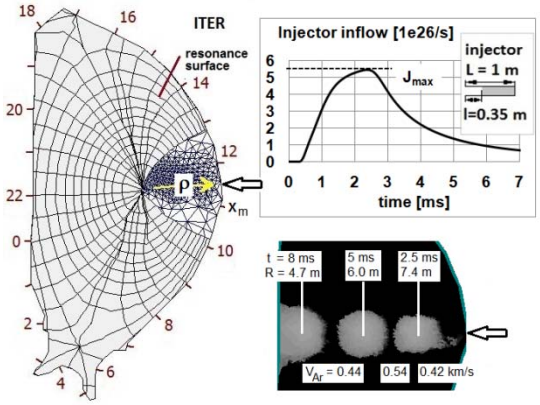

Magnetic flux coordinates, underground triangle meshes, wall surface coordinate X, minor radius coordinate ρ and injector location are shown. The maximum inflow J_{max} determines the MGI process. A gas propagation test is seen.

We assume that the position of the cooling front $x = x_c(t)$ drives the magnetic braiding in the whole confining region. Here x is a magnetic flux coordinate. The ratio $\eta = (x_c - x_s)/(x_r - x_s)$ is chosen as the driving parameter ($0 \le \eta \le 1$); x_s is the separatrix and x_r the resonance surface positions. For thermal conductivity $k_{\perp e}$ the fitting formula deduced from TOKES validations is applied:

$$k_{\perp e} = f \times 10^{20} \left(\frac{T_e(t,x,y)}{2.5\ \mathrm{keV}} \right)^{\frac{5}{2}} \begin{cases} 13\eta, & \eta < 1 \\ 260, & \eta > 1 \end{cases}$$

For ITER the factor $f \approx 8$ is obtained. At $\eta = 1$ the cooling front crosses the q=2 surface and $k_{\perp e}$ increases by a factor of 20.

In the ITER simulations the injected mass M_{Ar} was varied by one order of value ($17 < M_{Ar} < 160$ g). TQ starts after reaching the resonance surface at $t \sim 1$ ms. Then a powerful photon flash arises and T_e significantly decreases. The cooling front $x = x_c(t)$ increases its speed V_c with t. A slow decrease of radiation power after the flash occurs, which corresponds to the travel of front through the plasma until complete cooling.

With increasing M_{Ar} the cooling time τ_c decreases from 5 ms down to 2.8 ms. Decreasing $k_{i,e}$ (i.e. f down to 1) results in some redistribution of wall load in time but hardly changes τ_c and T_{wmax}.

For the W wall, MGI with the mid-plane injectors is always melt-free. For the Be wall this cannot be expected because T_{wmax} is obtained near the Be melting point. Therefore W is preferable at the most loaded position (wall coordinate $X \approx 11$ m). Due to the assumption of toroidal symmetry, the simulations give the lowest possible maximum of wall temperature and thus the minimal possible cooling time. In this way we addressed the question whether a melt-free MGI in ITER can be done at all in a few ms, even if using a large number of injectors in one poloidal plane.

(**EFDA Task WP12-IPH-A11-1-02/PS-01/KIT and WP12-IPH-A11-1-02/BS-01/KIT**: Modelling of W PFCs damage for TEXTOR and JET experiments under ITER relevant conditions.)

The disruptions can also decrease the ITER PFC durability not only by photonic heating or plasma impacts. It is expected that during several milliseconds of the disruption relativistic runaway electrons (RE) can be generated in the decaying plasma and produce additional damage to the first wall (FW). In earlier JET experiments with the carbon fibre composite (CFC) FW the RE beams were observed during the disruptions mitigated by Ar MGI. Since 2011 JET operates with the new ITER-like wall (ILW) covered with beryllium. In one ILW experiment with low density plasma a local melting of poloidal limiter due to RE impact was observed.

To numerically assess the melting of typical Be tiles caused by RE in next JET experiments aiming ITER, the KIT codes ENDEP and MEMOS are applied. An upgraded 3D version of MEMOS is now available for melt motion dynamics. In tokamaks the melt fluid can accelerate due to surface tension, applied plasma pressure and the **J×B** force of halo-, eddy-, and thermo-currents. 3D version was validated by TEXTOR experiments for long timescale (of several seconds) melt motion displacements and for RE impact on TEXTOR graphite limiter. Simulations of after effects of RE impact on the JET Be FW are performed including also the surface vaporization and determination of melting threshold W_{melt} for RE energy density W_{RE}.

In JET, detailed temperature evolution and spatial distributions as well as melting and evaporation erosion are simulated for single Be tile installed at the upper dump plate (next Fig.) accounting for geometrical peculiarities of it. The impact duration τ ranged from 1 to 4 ms. It is assumed that RE have exponential distribution function f(E)~exp(-E/E_0) on electron energy E, with the parameter E_0 below 10 MeV. The transversal electron energy E_{tr} is small: $E_{tr} << E_0$.

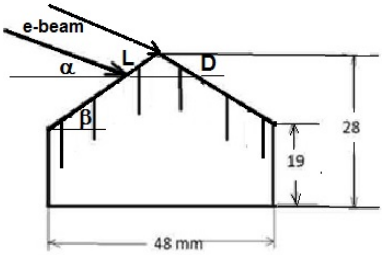

Sketch of Be tile of JET ILW

The simulations are divided into two steps. At first the volumetric energy deposition function is calculated with the Monte-Carlo code ENDEP. At the second the code MEMOS is applied for the calculations of temperature distribution in the material bulk. For the ILW wall we assumed that the RE beam parameters used in the simulations are equal to those from the JET experiments with CFC FW: typical RE current up to 0.5 MA and RE beam radius of 0.5 m, so that the current density up to 0.6 MA/m^2. The total wetted area of the impact is expected to be of 0.6 m^2.

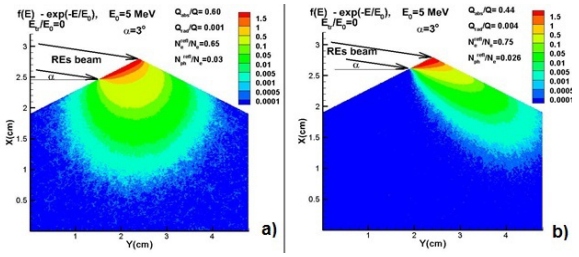

A normalized distribution function of energy absorbed in Be tile: a) L=1 cm, E_{tr}/E=0, b) L=0.5 cm, E_{tr}/E=0

The incident electrons gyrate about the magnetic force lines thus the incidence angle at the crossing of target surface depends on E_{tr}/E_e and the angle $\alpha \sim 20°$ of field line to the target surface. The simulations are done for E_{tr}/E_0 = 0 and 0.02; E_0 = 3, 5 and 8 MeV. Two scenarios with different width of wetted area along the tile surface: L=1 cm (i.e. D=3.4 mm) and L=0.5 cm (D=1.7 mm) are calculated (Fig. above) for rectangular time profile, pulse durations τ=1 to 4 ms and W_{RE} = 5 to 60 GW/m^2. In case of E_{tr}/E_e=0 and L=1 cm the impact energy is deposited rather uniformly inside the tile. Approximately 40% of energy is passing through the tile and escapes as primary and secondary electrons. RE current density J_{RE} drops by 35%. Increasing E_{tr}/E_e results in smaller absorption so that in case of E_{tr}/E_e=0.02 the J_{RE} drops less than for 26%.

The obtained RE energy distributions are used in the MEMOS simulations. Typical temperature distributions inside the tile at the end of the RE impact demonstrate the melting for both scenarios (next Fig.): $T_{wmax} > T_{melt}$ = 1560 K.

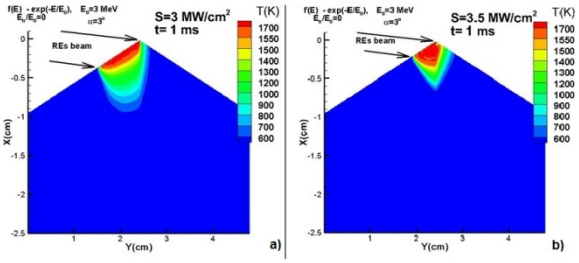

Temperatures inside the Be tile for RE loads with E_{tr}/E=0. Time moment 1 ms means the pulse end. a) L=1 cm; b) L=0.5 cm.

Dependences of T_{wmax} on W_{RE} and the current density J_{RE} are also obtained (next Fig.). The Be melting threshold J_{melt} was estimated to depend on pulse duration as 1/τ. The calculated J_{melt} ranged from 2 to 12 kA/m^2), which is much less than the J_{RE} expected in JET (up to 500 kA/m^2). Already small increase of J_{RE} above J_{melt} by 10-20% results in the melting pool deepness up to several hundred microns. The calculated solidification time is rather long: ~20 ms. With the expected wetted area of 0.6 m^2, J_{RE} ~10 kA would produce the melt layer of 0.5 mm thickness.

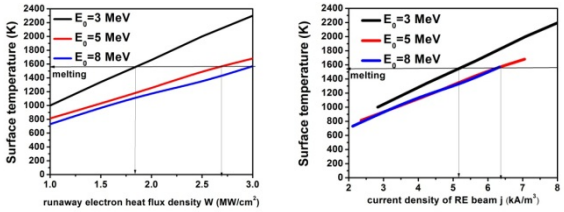

Maximum Be surface temperature against W_{RE} and J_{RE}.

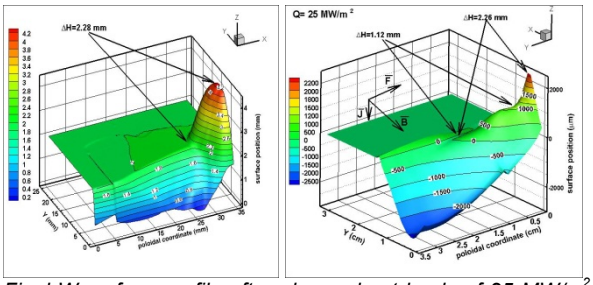

Final W surface profile after plasma heat loads of 25 MW/m^2 in TEXTOR experiments. Left: experiment, right: MEMOS results.

TEXTOR: The simulations were carried out for not castellated targets with the sizes 3.5×3.2×0.3 cm. For the thermo-emission current the Child-Langmuir model is used. Several scenarios of the duration 6 s with different maximum of W ranged from 21 to 27 MW/m^2 are calculated. The ENDEP and MEMOS codes validated against these TEXTOR experiments have reached at reasonable quantitative agreement of simulations with the experiment. For example (Fig. above), in case of W_{max} = 25 MW/m^2 the simulated final erosion profile on the target surface after the melt motion driven by the **J×B** force of thermo-currents is in a good agreement with the measurements. Furthermore, interactions of the RE electrons with TEXTOR graphite limiter have been investigated and then simulated with MEMOS. In the experiment mean RE energy about 4 MeV, the RE energy absorbed in the graphite limiter 3 kJ and RE pulse duration 10 ms was measured. The MEMOS contributed for calculations of target surface temperature in these experiments. In the simulations T_{wmax} up to ≈ 3500 K is demonstrated, which means a fast sublimation and brittle destruction of limiter.

(**F4E Grant GRT-315**: Simulation of ITER First Wall Energy loading during mitigated disruptions and runaway electrons)

This task implements the running collaboration between KIT and the ITER organization (IO) for numerical prediction of possible wall damage after the MGI mitigated disruptions of ITER baseline Q = 10 burning plasma discharge. So far only the first part of the project can be considered as finished: Be wall loading by photon radiation of injected and ionized neon during MGI TQ. TOKES MGI simulations were supported by MEMOS for elaborated calculation of wall surface temperature $T_w(X)$ and possible FW melting (without assessing melt motion).

TOKES calculated the impacting radiation flux on FW surface for different Ne amounts. At present ITER foresees three toroidally separated upper port MGI locations. Being 2D, the code cannot simulate such toroidally discrete gas injection. Instead, a single injection orifice is modelled as a gap in the FW poloidal plane contour, uniformly distributed toroidally such that the gas injection is toroidally symmetric in the code. IO suggested the simple geometric form for the injectors, incorporating a small bend to account for the need to direct the gas towards the plasma centre (see inset in next Fig.). (There is as yet no detailed design for the ITER injectors.)

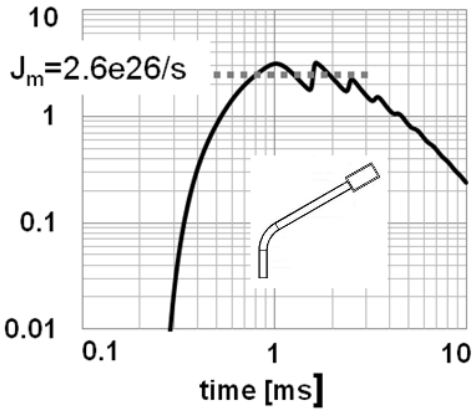

The inflow of Ne into the vessel as a function of t is shown. The median inflow The IO injector sketch is also shown.

Different MGI scenarios are examined by varying the initial pressure in the injector gas plenum from 500 bar down to 8 bar. The calculations considered several scenarios which cover the range of TQ time from 3 ms up to 12 ms. Physical parameter chosen for the injection intensity is the median gas inflow J_m (Fig. above) that characterizes the magnitude of oscillating injection; J_m was varied in the range (0.33 – 21)×10^{26} atom/s.

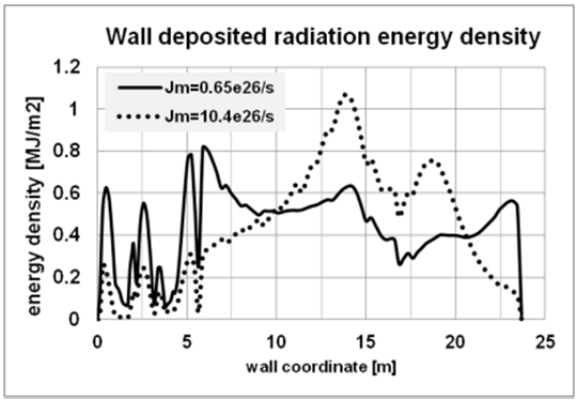

Comparison of Q_r for intense and moderate injection scenarios. The last moment of TQ phase is shown.

In the simulations a principal difference between the scenarios with $J_m < J_{m0} = 2.6\times10^{26}$/s and $J_m \geq J_{m0}$ was revealed (Fig. above). At the intence inflow ($J_m = 10.4\times10^{26}$/s) the cooling time τ_c is small (3.4 ms) and the maximum radiation load Q_{rmax} appears throughout in front of the injector - the ionized Ne has insufficient time to leave the injector location. At $J_m = 0.65\times10^{26}$/s, τ_c = 7.8 ms is obtained. This gives the ionized Ne more time to expand along the magnetic field lines, which decreases the load in front of injector. At $J_m = 10.4\times10^{26}$/s the maximum radiation flux reaches about 1.5 GW/m^2 in front of injector and about 1.2 GW/m^2 in the inner mid-plane. As to the case of $J_m = 0.65\times10^{26}$/s, typical radiation flux is ~0.5 MJ/m^2.

The radiation coming at the wall surface is transferred into the heat and the heat transported into the wall bulk by the thermal conduction mechanism. The heat penetration depth δ into the wall bulk on the timescale of the mitigated disruption heat pulse is small: $\delta \sim (\tau_c k/C)^{1/2} \sim 300$ μm, with k and C thermal conductivity and heat capacity of wall material, respectively. TOKES has a simplified algorithm for preliminary assessments of T_w. Improved temperature distributions are obtained with MEMOS (next Fig.), which takes into account the surface evaporation, melt and evaporation enthalpies, and the thermo-physical parameters of the material in their dependence on T_w.

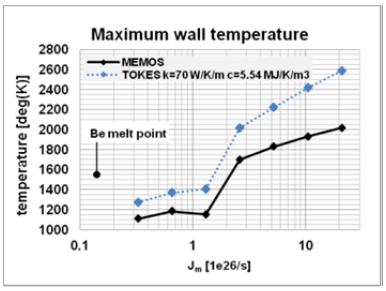

The T_{wmax} obtained with TOKES and MEMOS are shown. (T_{wmax} was achieved at different positions on the surface)

At $J_m < J_{m0} = 2.6\times10^{26}$/s, T_{wmax} is below the Be melting point and otherwise (intense injection) $T_{wmax} > T_{melt}$. The simulations demonstrated complete plasma cooling during 5.7 ms as a minimum TQ phase duration without the melting of Be wall surface. These results are obtained for the surface initial temperature $T_0 \sim 500$ K. The elaborated simulations with MEMOS allowed assessment of possible evaporation wear layer (~0.02 μm) and melt pool depth (~30 μm) over the beryllium surface (next Fig.). The melted area occupies on the first wall a rather wide stripe of the width 1-2 m in the vicinity of injector.

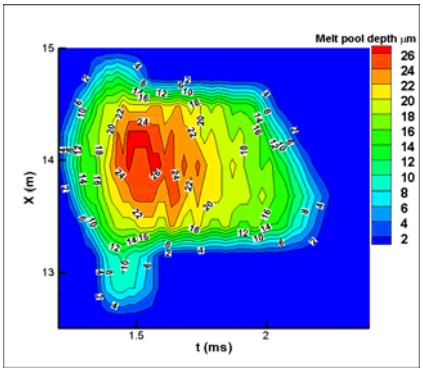

Distributions of Be melt pool depth vs X and t. $J_m = 21\times10^{26}$/s.

The distributions of $T_w(X,t)$ over the wall surface coordinate X and in time t is rather singular (next Fig.). Due to the radiation flash after switching on the anomalous transport mechanism a fast increase (about 100 K) of surface temperature occurs.

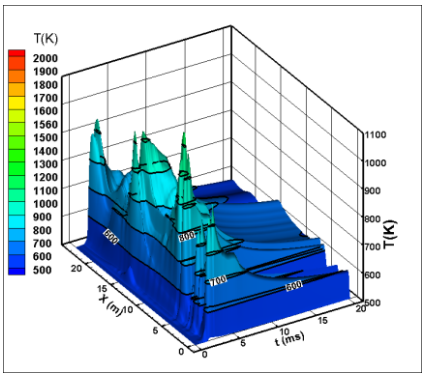

Be wall surface temperature vs X and t; $J_m = 1.3\times10^{26}$/s.

(**EFDA Task WP11-DAS-PLS-P02-01:** Design assessments for the FW blanket in DEMO Reactor)

The performance of PFC in DEMO is a fundamental issue affecting the technological feasibility of fusion power. Our aim is to determine the structure and coating thicknesses which maximize component lifetime against life limitations. At present, the most promising is a sandwich type W/EUROFER first wall module. We evaluated the expected power loading in steady-state and off-normal DEMO operation. We also consider ELMs and their effect on the tungsten armor melting and roughness formation due to the W vapor pressure. Then, the impact of VDE and RE on the FW is evaluated by taking into account the conversion of the magnetic energy stored in the RE current into heat through the ohmic dissipation of the eddy current. We also estimated the efficiency of helium gas as a coolant.

Simulation of power load during DEMO operation was performed by MEMOS and ENDEP codes. The net incoming transient heat flux Q onto the W armour is assumed in the range of 0.5-15 MW/m^2 which can be expected in DEMO. The parameters of off-normal events and ELMs in DEMO estimated based on ITER data and simple scaling arguments are summarized in the Tables:

events	Energy loads, GJ	Deposited area, m^2	Deposition time, sec	Energy density, MJ/m^2
Steady-state operation	radiation & c.-exch. atoms	FW, baffles etc	hours	0.5-20
VDE	$W_{th}(0.7)+40\%W_{mag}(1.2)$	~25-50	~0.5-1	~50
VDE"cold" w/o RE	$\sim40\%W_{mag}(1.2)$	~25	~0.5-1	~20-50*
VDE with RE	$\sim40\%W_{mag}(1.2)$	~16	~0.5	~30*
RE slow loss	$W_{RE,kin}(0.04)+40\%W_{RE,mag}$	~16	~0.5	≥70*
RE fast loss	$W_{RE,kin}(0.04)$	~16-50	0.01msec	~2.5

Description	ITER	DEMO
Thermal energy release during ELMs in outboard divertor, ΔW_{ELM}, MJ	10	~50
ELM frequency, Hz	50	~20
Energy deposition time on the FW, $\Delta\tau_{ELM}$, msec	0.3 (rising phase)-0.6(decay phase)	~0.17-0.34
FWHM,m (vertical plate)	0.05	~0.09
Max. energy density on outboard divertot, MJ/m^2	1-6	~12

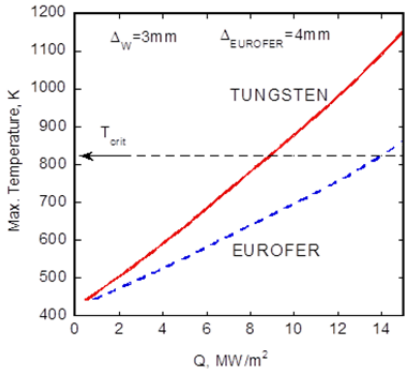

Maximum W and EUROFER temperature vs net incoming heat flux Q under steady-state DEMO operation.

In the case of steady-state operation the W surface temperature remains well below the vaporization and melting and the heat flux into coolant below critical heat flux thus avoiding severe degradation of the heat removal capability. Calculations for various values of armour thickness Δ_w and the EUROFER thickness $\Delta_{EUROFER}$ show that the optimal are the values of Δ_w =3 mm and of $\Delta_{EUROFER}$ = 4mm. (Fig. above) shows the FW armour surface temperature and the maximum EUROFER temperature (interlayer temperature) for different incoming heat flux values Q. When Q reaches~14 MW/m^2 the interlayer temperature exceeds the critical value Tcrit. ~ 550 ºC and EUROFER can experience irremediable thermal distraction.

In the case of off-normal events e.g. 'hot' VDE (accidental control loss) the energy deposition into the FW W armor causes surface melting up to 0.07 mm and evaporation up to a few mm. For 'cold' VDE, when vertical instability arises after thermal quench, current channel moves towards the wall during current decay and deposits remaining energy to the FW, the W/EUROFER structure can marginally tolerate the

energy loads. The RE fast losses does not cause the W armor melting because of a very short exposure time ~ 0.01 ms. In the case of RE slow losses electrons deposit their energy (magnetic and kinetic) deeper in armor layer which explains the W temperature decrease with increasing the armor thickness. In all cases (except for the RE slow loss) the armor temperature is quite independent on armor thickness, because heat deposition takes place in a thin surface layer. In the case of the RE slow loss heat deposition occurs deeper in armor and heating time becomes comparable with heat diffusion time for W thicknesses ≤ 1cm.

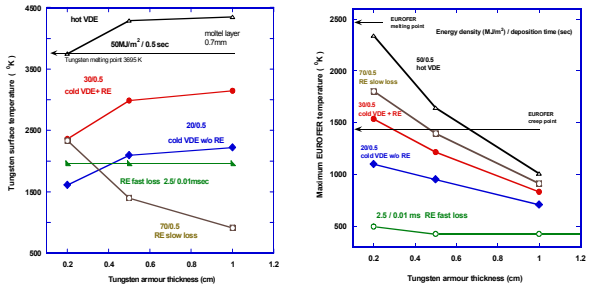

Fig. 8: The maximum W and EUROFER temperature as a function of W armor thickness for different off-normal events.

Calculations show that for ELMs with energy W_{ELM} ~12 MJ/m^2 the pressure gradient of the plasma shield is mainly responsible for an intensive melt motion of tungsten. The corresponding melt velocitiy is ~ 0.5 m/s and the surface roughness is about 0.1 µm. Due to the small melt velocity and the small re-solidification time of a few ms the melt splashing does not develop therefore all mass losses are due to target evaporation. For many ELMs, at fixed separatrix strike position (SSP) the maximum crater depth exceeds the evaporation thickness by a factor less than 5. Assumption on stochastic motion of SSP along the target surface essentially decreases the total erosion of W surface.

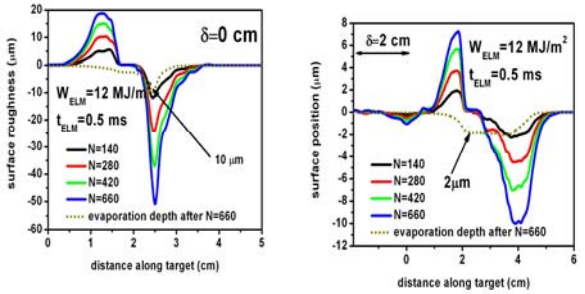

Fig. 9: The W surface roughness after N ELMs inpact for the Gaussian distribution of the separatris srike point with the dispersion δ= 0 and δ = 2 cm. N is the number of ELMs.

We found that under steady-state normal operation and He cooling the FW W/EUROFER blanket module can tolerate expected in DEMO heat loads without W armour melting and EUROFER thermal destruction. For Δ_W~3mm, $\Delta_{EUROFER}$~4mm the maximum tolerable heat flux is about 14MW/m^2. To achieve efficient heat transfer required for helium cooling of the FW blanket module in DEMO, a high flow velocity (≥ 100m/s) should be achieved. Direct conversion of the RE magnetic energy into heat within a metallic armor occurs due to ohmic dissipation of the return current of free electrons and depends on W surface temperature and RE pulse duration. In the case of hot VDE the W armor the heat load is not tolerate: it melts down to 0.07 mm and intensively evaporates up to a few mm during 0.5sec.The RE fast loss case does not cause the W armor melting because of a very short exposure time ~ 0.01 ms. For slow losses the RE deposit their energy (magnetic and kinetic) deeper in armor layer, which explains the W temperature decrease with increasing the armor thickness.

– Microwave Heating for W7-X (PMW) –

Introduction

Electron cyclotron resonance heating (ECRH) and current drive (ECCD) are the standard methods for localized heating and current drive in future fusion experiments. Thus, ECRH will be the basic day-one heating system for the stellarator W7-X which is currently under final construction at IPP Greifswald. It is expected that the ECRH system for W7-X will be finalized in 2014. In its first stage W7-X will be equipped with an 10 MW ECRH system operating at 140 GHz in continuous wave (CW).

The complete ECRH system is coordinated by the project “Projekt Mikrowellenheizung für W7-X (PMW)”. PMW has been established by KIT together with IPP and several EU partners in 1998. The responsibility of PMW covers the design, development, construction, installation and system tests of all components required for stationary plasma heating on site at IPP Greifswald. PMW coordinates the contribution from Institut für Plasmaforschung (IPF) of the University of Stuttgart too. IPF is responsible for the microwave transmission system and part of the power supply (HV-system). IPP Greifswald is responsible for the in-vessel components and for the in-house auxiliary systems. PMW benefits from the collaboration with Centre de Recherche de Physique des Plasmas (CRPP) Lausanne, Commissariat à l´Energie Atomique (CEA), Cadarache and Thales Electron Devices (TED), Vélizy.

A contract between CRPP Lausanne, FZK Karlsruhe and TED, Vélizy, had been settled to develop and build the series gyrotrons. First step in this collaboration was the development of a prototype gyrotron for W7-X with an output power of 1 MW CW at 140 GHz.

Seven series gyrotrons have been ordered from industrial partner Thales Electron Devices (TED), Vélizy. First operation and long pulse conditioning of these gyrotrons is being performed at the teststand at KIT. Pulses up to 180 s duration at full power are possible (factory acceptance test, FAT) whereas 30 minutes shots at full power are possible at IPP (necessary for site acceptance test, SAT). Including the pre-prototype tube, the prototype tube and the 140 GHz CPI-tube, in total 10 gyrotrons will be available for W7-X in final state. To operate these gyrotrons, in addition to the Oxford Instruments and Accel magnets, eight superconducting magnet systems have been manufactured at Cryomagnetics Inc., Oak Ridge, USA.

Most of the components of the transmission system, HV-systems and in-vessel-components have been ordered, manufactured, delivered and are ready for operation at IPP Greifswald. A part of the existing ECRH system has been already used to test new concepts and components for ECRH. A significant delay arose in the project due to unexpected difficulties in the production of the series gyrotrons.

Series Gyrotrons

In 2005, the first TED series gyrotron SN1 had been tested successfully at FZK and IPP (920 kW/1800 s). It met all specifications during the acceptance test, no specific limitations were observed. In order to keep the warranty SN1 has been sealed, one prototype gyrotron is routinely used for experiments.

Series gyrotrons following SN1 did show a more or less different behavior with respect to parasitic oscillations excited in the beam tunnel region. These oscillations resulted in an excessive heating of the beam tunnel components, in particular of the absorbing ceramic rings. The gyrotrons re-opened after operation showed significant damages due to overheating at the ceramic rings and the brazing of the rings. A possible solution was proposed and successfully tested by KIT. As the main difference to the usual beam tunnel this design features corrugations in the copper rings which handicap the excitation of parasitic modes.

The thermal loading of the collector depends very much on the efficiency of the interaction and on the pulse length. For CW high power operation this loading is close to what is feasible in terms cooling and lifetime of the collector. For the series tubes a sweeping procedure has been introduced which combines a vertical and radial displacement of the electron beam at the collector. This results in an almost constant power deposition at the inner wall along the axis and removes the particularly dangerous temperature peaks at the lower and upper reversal points of the electron beam. In 2012 complete sweeping systems for the series gyrotrons have been procured.

Modifications have been realized and already tested in order to reduce the internal absorption of stray RF power by covering stainless steel components with copper.

A possible corrosion in the water cooling circuit of the diamond window at the brazing structure is prevented by replacing the water by inert Silicon oil.

In 2012 long pulse conditioning and testing of the gyrotron SN6 was continued. SN6 is the first series gyrotron equipped with all improvements developed. The final acceptance tests of SN6 were finished successfully at IPP Greifswald showing above 900 kW RF output power and reliable operation at 30 min pulse length.

The next series gyrotron, SN7, was delivered to KIT in August 2012. During installation at KIT teststand a vacuum leak was detected in the copper of an internal cooling pipe. The tube has been repaired at Thales already, acceptance tests at KIT are starting at January 2013.

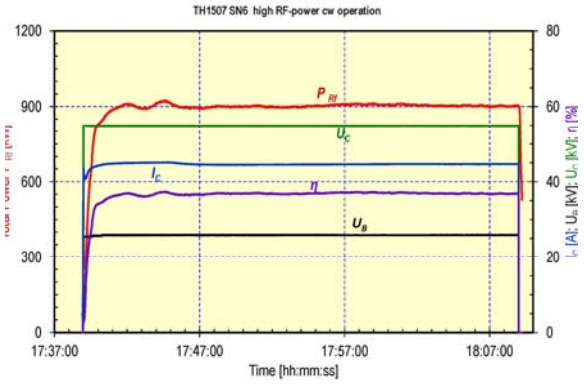

Output power P_{rf}, beam current I_c, efficiency and operating voltages U_c, U_B of series gyrotron SN6, measured at IPP Greifswald during long pulse operation (30 min.).

Transmission Line System

The transmission of the RF output power to the plasma happens via a quasi-optical system. It consists of different single-beam and multi-beam waveguide (MBWG) elements, which adds up in total more than 150 reflectors. For each gyrotron, a beam correcting assembly of four mirrors is used. It matches the RF power at the gyrotron output to a fundamental gaussian beam with the correct beam parameters, andit sets the appropriate polarization needed for optimum absorption in the plasma. A fifth mirror directs the beam to the beam combining optics, which is situated at the input plane of a multi-beam waveguide. This MBWG is designed to transmit up to seven beams (5x 140 GHz beams, 1x 70 GHz beam, and 1x channel connected to the N-port launchers via a switch) from the gyrotrons (entrance plane) to the stellarator hall (exit plane). To transmit the power of all gyrotrons, two symmetrically arranged MBWGs are used. At the output planes of the MBWGs, two mirror arrays separate the beams again and distribute them via two other mirrors and CVD-diamond vacuum barrier windows to individually movable antennas (launchers) in the torus.

The manufacturing and installation of the components of the basic transmission system has been completed. Cooling tube manifolds to supply the mirrors and stray radiation absorbers mounted in the towers in front of the stellarator were installed.

For beam diagnostics and power measurement of the gyrotron beams, linearization amplifiers for the detectors have been developed. The receivers attributed to the directional couplers on the mirrors M14 have been mostly built; present work concentrates on the design of the conical scan mechanics and electronics for the alignment control.

For gyrotron SN6 installed at IPP Greifswald, beam characterization and the subsequent design and manufacturing of the surfaces of the matching mirrors have been performed.

Within the site acceptance tests of gyrotron SN6, the "long load" (a 23 m long absorbing stainless steel tube with a water jacket) could be tested in more detail. Successful shots of 910 kW output power at the gyrotron window for 30 min pulses were performed using this load. As the long load operates as a pre-attenuator (attenuation typ. 77%), the residual power at the output was dumped in one of the calorimetric loads, which originally had been designed for short pulses (400 ms) at 1 MW. Nevertheless, cw operation was possible for an RF power of 210 kW, qualifying the design principle of the short-pulse load also for high-power CW loads.

In the past years, the ECRH system at IPP-Greifswald was used as a test bed for novel components, e. g. for the test of high-power diplexers. These devices are developed for use as a combiner for the RF output power of two gyrotrons as well as a fast directional switch (FADIS) between two RF output signals, and therefore are of potential interest for ITER. In 2012, the diplexer MC IIa was operated in the corrugated waveguide system at ASDEX Upgrade, and switching and in-line ECE experiments were performed successfully. An evacuated version (MQ IV) compatible with the ITER system has been designed, and mirrors are being manufactured. Provided that funding for the fabrication for the evacuated casing is available, high-power tests on the ITER test system at JAEA, Naka are foreseen.

For two of the N-ports of W7-X, "remote-steering" (RS) launchers are foreseen (RSL1 and RSL5). This is due to the fact, that front steering launchers as used in the A and E ports will not fit into these narrow ports. The remote-steering properties are based on multi-mode interference in a square waveguide leading to imaging effects: For a proper length of the waveguide, a microwave beam at the input of the waveguide (with a defined direction set by a mirror system outside of the plasma vacuum) will exit the waveguide (near the plasma) in the same direction.

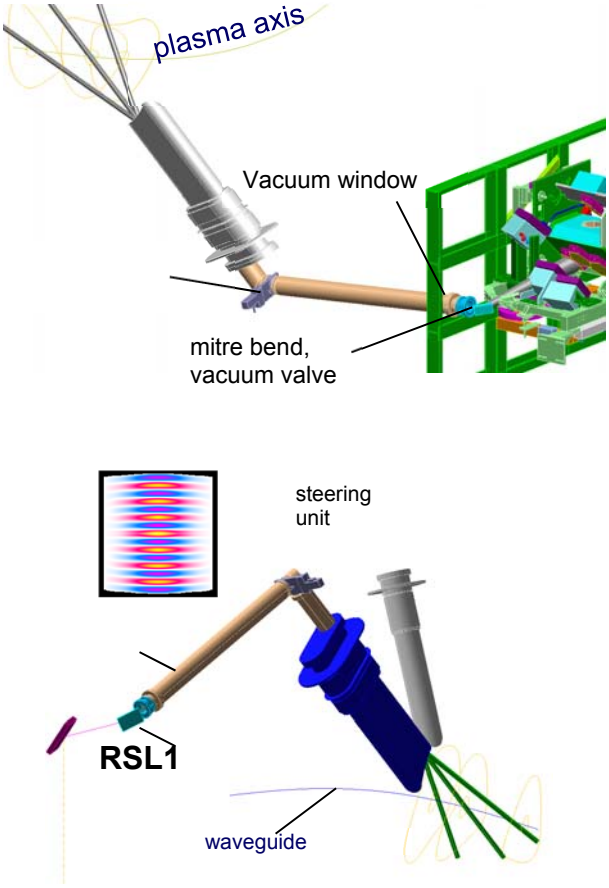

Conceptual design of the remote steering launchers RSL1 (top) and RSL5 (bottom), designed for the narrow N-ports of W7-X. The insert bottom,left shows the transverse field structure of an m= 15 mode in the slightly bulged waveguide cross-section of RSL5.

In autumn of 2012, the engineering design and manufacturing of the RS launchers was started within the frame of a "BMBF Verbundprojekt" with special funding by the German Bundesministerium für Bildung und Forschung (BMBF). The leading institution of the project is IPP with its branches at Greifswald and Garching. Partners of the project are the IPF Stuttgarttogether with two industrial partners, Neue Technologien GmbH, Gelnhausen (NTG), and Galvano-T electroforming-electroplating GmbH, Windeck (GT).

Within this Project FORMIK[3] ("Fortgeschrittene Mikrowellen-Heizsysteme für die kontrollierte Kernfusion"), the detailed design of the launchers as well as the preparation for manufacturing was started at IPP. Both launcher waveguides will consist of two straight corrugated square waveguides (total length typically 5 m), which will be connected via mitre bends to fit the antenna into the available space at W7-X, as seen in the figure below. The waveguide parts will be manufactured by electroforming techniques from copper. This method had been identified before as best suited for long, vacuum compatible corrugated waveguides, which need relatively strong water cooling. Within the FORMIK[3] project, NTG will care for the manufacture of the mandrels and the final machining of the waveguides, while GT will provide the electroforming works. A drawing of the RSL1 waveguide part to be situated in the vacuum vessel is shown below.

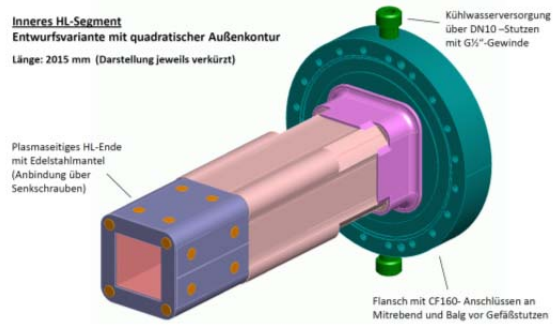

Design of the inner waveguide segment of RSL1 showing the port vacuum flange with connections for the water cooling of the waveguide, the outer machining and the plasma facing side with protection from stainless steel. Note the shortened view in the drawing, the real waveguide length is 2015 mm.

The RS launchers will be fed from the main transmission via one (RSL1) and two reflectors (RSL5), respectively. The optical beam path and the mirror parameters have been defined. The design of the reflectors, which will be similar to the reflectors of the main transmission system, has been started. In the construction phase, which is planned for the next year (2013), NTG will fabricate the mirror stainless steel blanks, the reflector mounts and the final mirror surfaces, and GT will provide the copper mirror surfaces with the cooling system embedded.

Prior to the start of the Verbundprojekt, basic research on the optimization of remote-steering antennas was continued at IPF Stuttgart. As the imaging characteristics of square waveguides diminish at steering angles > 12°, a prototype antenna waveguide with an optimized cross-section (square with outward bulges) with respect to the steering range was manufactured and tested. Antenna patterns recorded at a variety of steering angles show that an increase of the useful steering range up to 16° was reached, however, at the expense of a reduction of the quality of the antenna beam. A detailed analysis of the radiation patterns showed, that the dispersion relation for the deformed waveguide was optimal for the HE1,n modes, however, HE3,n modes, which also contribute to the antenna beam, did not obey the prescribed ideal dispersion. The results were confirmed by a resonator technique, for which the spectrum of the transverse resonances of the waveguide was measured and analysed.

A new simulation code was set up, which allows the simultaneous calculation of all propagation constants in the deformed waveguide; and calculations have started to find the best performing RS waveguide cross-section. Its application is foreseen for the RSL5 launcher; in contrast, RLS1 will be designed as square waveguide.

In-vessel components

The four ECRH-plug-in launchers have been equipped with water manifolds and flow sensors. One of the launcher was used to test the assembly within similar cramped geometrical conditions as they are expected for W7-X operation. Together with the assembly department at IPP-Greifswald a successful assembly procedure was elaborated which insures a reliable vacuum closure with a HelicoFlex- sealing.

The electron cyclotron absorption (ECA) diagnostics was developed and fabricated at IPP-Greifswald. It measures the transmitted ECRH power, the beam position and polarization. The waveguide vacuum interfaces had been slightly modified. A detailed leakage measurement showed that the entire helium penetration rate through the o-ring sealing of all 33 vacuum interfaces of one B-port plug-in would violate the

W7-X vacuum restriction. Alternative sealing methods had been investigated consequently. Finally, CF-type copper sealing with a glued mica window was chosen. It showed a sufficiently small helium penetration rate and a high mechanical reliability. The modified B-port insert passed the official W7-X vacuum leak test procedure successfully. Outside the vacuum vessel the microwave interfaces will be equipped by filigree components and detectors, which must be protected from mechanical damage. Therefore a protection bonnet had been designed, which also provides electrical connections and mechanical access. Finally the ECA-diagnostic had been officially committed to the assembly department for installation at the W7-X vacuum vessel.

–ITER ECRH Advanced Source Development–

F4E-2009-GRT-034-01: Analysis of Design Issues, Interfaces and Preparation of the Procurement Arrangement for the ITER Gyrotron

F4E-2009-GRT-049-01: Design and Development of the European Gyrotron

F4E-GRT-432: Design and Development of the European Gyrotron

Introduction

The development of an 2 MW, CW, 170 GHz coaxial cavity gyrotron for ITER is pursued within the European Gyrotron Consortium (EGYC, consisting of CRPP, Switzerland; KIT, Germany; HELLAS, Greece; CNR; Italy). EGYC acts as the scientific partner for Fusion for Energy (F4E). Within this consortium, KIT acts as the cooperation partner of ISSP, Latvia. The EU part to ITER is the delivery of RF sources (gyrotrons) to provide in total 8 MW of RF input power. In contrast to the other parties (Russia, Japan) delivering 1 MW, CW conventional cavity gyrotrons to ITER, the EGYC consortium planned to provide 2 MW, CW RF power units to reduce total costs and to limit the space requirements. Additionally, it would have offered to double the system power for ECH&CD.

While the industrial gyrotron prototype, built by Thales Electron Devices (TED, France), is tested at CRPP, KIT does the main part in the research and the development of the physical designs of thegyrotron components. It does low power tests of the different components and does high power tests at short-pulses. The latter are done using KIT's 2 MW modular pre-prototype gyrotron. KIT is responsible for the cavity, the uptaper and the mode converter system. It is simulating the beam generation, the interaction between the electrons and the RF field and the the electron-optical system up to the collector.

In 2011, the 2 MW industrial prototype gyrotron was successfully upstarting in short pulse operation with RF output powers up to 2 MW (@1 ms). However, after a fatal event in December 2012, at which a water leak destroyed the tube, F4E and EGYC decided together to move to the 1 MW fallback solution for the initial gyrotron installation of ITER. The corresponding physical design did start in 2007 already. Nevertheless, the 2 MW coaxial cavity design is continued towards a suitable design for an update of ITER and for future fusion devices.

In this chapter results of the coaxial cavity gyrotron development as well as the activities towards a conventional cavity gyrotron at 170 GHz for ITER will be described.

Recent modifications on the KIT Test Facility

The following modifications and improvements on the gyrotron test setup have been done in 2012:

(1) A normal conducting (NC) coil with improved cooling has been installed inside the bore hole of the KIT Oxford Instruments super-conducting (SC)-magnet. After that installation, the magnetic field of the SC magnet can be increased to the required value of 6.87 T in continuous-wave (CW) operation.

(2) The diode-type magnetron injection electron gun (MIG) has been redesigned to be identical to the corresponding components of the industrial CW gyrotron. Furthermore, the new construction of the electron gun allows a simple replacement of the emitter nose. In addition, an anode aperture (halo-shield) has been introduced in order to avoid electrons trapped between the cathode region and the magnetic mirror.

(3) The improved isolation between the gyrotron body and the top plate of the cryostat enables an operation of the gyrotron with single-stage depressed collector (SDC).

(4) A new design of the waveguide antenna (launcher) of the quasi-optical system has been installed. The launcher got a signficant smoother inner surface. Simulations predicts a significant reduction of the stray radiation.

Experimental results

In experiments the current flow to the newly introduced halo-shield (see Figure below) has been found. Further investigations have shown that at the position of the halo-shield the clearance between the electron beam and the wall is only about $\delta R_{beam\text{-}halo}$ =~0.2 mm in contrast to about 2.3 mm obtained from numerical calculations.

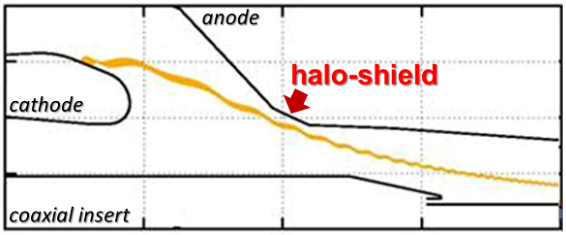

The profile of the gyrotron anode used in the experiment (halo-shield has been indicated).

It is assumed that the observed significant increase of the beam width is caused by electrons trapped between the cathode and the magnetic mirror. Mentioned effects have been accompanied by a rise of I_{body} and of the pressure inside the tube as well as the occurrence of parasitic low frequency oscillations. These parasitic oscillations could be responsible for the observed instabilities in the electron beam and further chaotic behavior of the gyrotron. The root cause of the instabilites is still under study.

Due to above mentioned instabilities the experiments could be continued with reduced pulse lengths only. Finally an RF output power of 1.9 MW and an electronics efficiency of 28% (without depressed collector, pulse length ~0.5 ms) has been obtained in single $TE_{34,19}$-mode operation at 170 GHz. Achieved results are shown in the Fig. 2 below (left). In addition, at high power the profile of the RF beam has been measured outside the gyrotron window with an IR camera. The analysis of the data confirmed the results of the low power measurements. The tube provides an excellent quality of the generated RF beam.

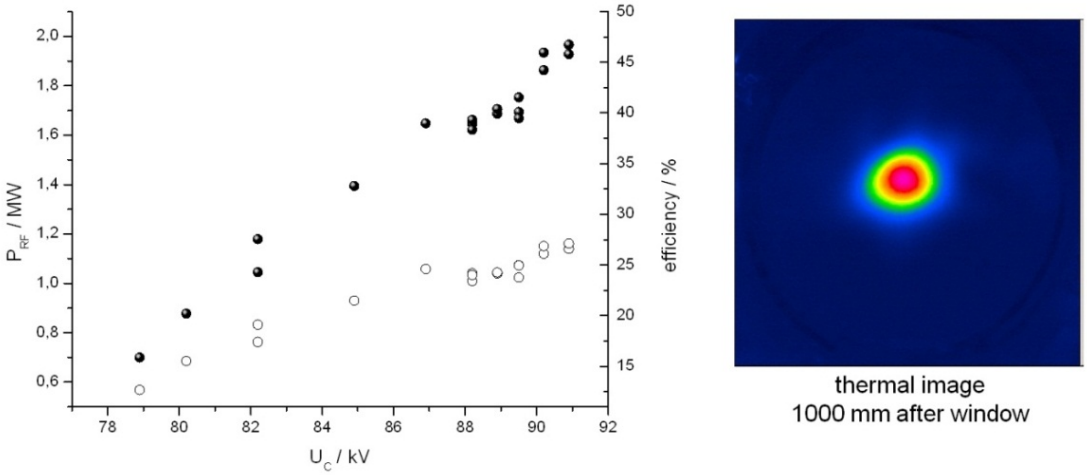

RF output power and gyrotron efficiency vs. cathode voltage measured at nominal magnetic field (left) and profile of the RF output beam measured 1000 mm after the gyrotron window (right).

For the first time, the KIT 2 MW pre-prototype has been operated with a single stage depressed collector. Reduced operation parameters has been used with respect to to the technical limitations of the body power supply and due to the above mentioned instabilities observed in a certain voltage range and accompanied by a sudden rise of the body current, I_{body}, . Final operating parameters have been an accelerating voltage ≤ 80 kV and a beam current <~70 A. Within the parameter limits a very stable operation of the tube has been demonstrated up to a depression voltage of 35 kV. With depression gyrotron efficiency increased from ~19% up to 37%. The RF output power at those conditions was measured to be about 1.2 MW.

First studies on an alternative method for the verification of the alignment of the electron beam with respect to the axis of the gyrotron cavity have been performed. The idea is based on the radial displacement of the electron beam inside the cavity by applying dipole coils and on the influence of the displacement on the excitation of a cavity mode. The figure shows the oscillation region of the $TE_{34,19}$ mode as obtained for two different beam currents in dependence of the dipole currents I_X and I_Y. The center of the measured values (I_X/I_Y=6.5A/3.2A) corresponds to a displacement of the beam inside the cavity.

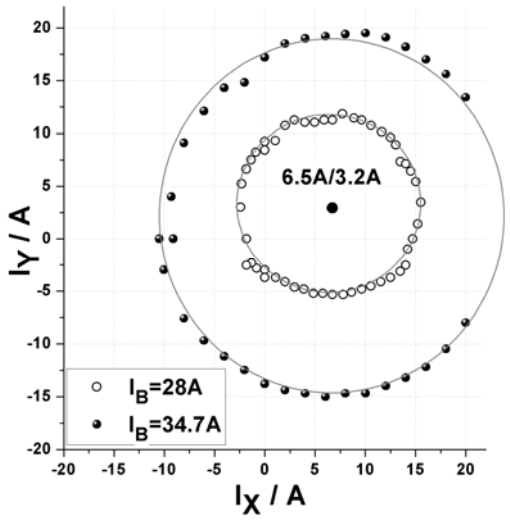

The oscillating area of the $TE_{34,19}$ mode in dependence of the transverse displacement due to the dipole field.

Out of this values a displacement of the electron beam with respect to the cavity axis by ~0.25 mm is obtained (I_{XY} = 1 A corresponds to a shift of 0.035 mm). This number is in agreement with measurements of the beam position relative to a capacitive probe in front of the cavity.

Studies on the electron gun

The attempt to employ the gun design of the industrial prototype in the KIT pre-prototype as far as possible did not lead to the desired performance. While the industrial prototype gun demonstrated all the desired improvements, with no trace of LF oscillations or voltage standoff problems, the refurbished KIT gun suffered from strong LF oscillations. The difference is obviously caused by the remaining design deviations. This observation may have some relation to halo electrons and to body currents.

The industrial prototype showed an unexpectedly high, but still acceptable body current. For the pre-prototype gyrotron with refurbished gun and halo shield, the body current was too high at nominal parameters. In the first experiment in this configuration, the magnetic field shape had to be changed to be able to operate. For this reason, the halo shield was removed in a second phase.

In frame of the 1 MW gyrotron development for ITER, important results on details of the emitter design where achieved. The thermal gaps around the emitter cause a high sensitivity to tolerances, which may be the reason for halo currents and low efficiencies which had not be understood before.

Experimental and theoretical investigations on RF parasitic oscillations

The suppression of parasitic oscillations is crucial for the performance of any gyrotron. Parasitic oscillations may occur in either the beam tunnel or in the after cavity region (ACI). A realistic simulation to understand these effects is still open.

Other parasitic oscillations may be generated in the uptaper as dynamic ACI as well as in the electron gun as LF parasitic oscillation. This later subject is strongly related to the studies on the electron gun and numerical simulations. In 2012 the aim has been to gain a better understanding on ACI.

In detail, the activities have been:

- Experimental studies of beam tunnel oscillations: in total, three experimental phases at KIT were performed, the first using the old 165 GHz electron gun at KIT combined with a beam tunnel with stacked corrugated copper and ceramic rings, the second one with the same beam tunnel, but the refurbished 170 GHz electron gun of KIT and the third employed a SiC beam tunnel instead. In all of these tests, no indication of any parasitic beam tunnel oscillation was found. In particular for the tests at KIT, it can be said that the RF spectrum was checked carefully and with high dynamic without any indication of spurious RF. This is a very robust validation of both beam tunnel concepts at the chosen operating parameters.

- Low frequency (LF) oscillations (around 80 MHz and 452 MHz) have been observed in recent experiments. The origin of the generation is still under study.

- Extensive measurements on dynamic ACI: the experiments with coaxial gyrotrons found no spurious RF signal at all. This is a particularly strong statement for the KIT experiments, where the measurement system described next was applied. This is a very good result for coaxial cavity devices, and is in agreement with simulations.

- For all these experimental studies, it was necessary to apply a suitable spectral diagnostic system (developed independently within a doctoral thesis) in parallel. This system permits unambiguous spectral measurements over a wide bandwidth and with high dynamic range, and was extended to also capture measurements of LF oscillations.

The main conclusions from the work in 2012 are:

- The chosen stacked beam tunnel concept appears successful and suitable, as well as the SiC beam tunnel which was checked in parallel. This is well proven by a wide band spectral measurement system with high dynamic range. On the other hand, it is still not possible to reliably simulate such beam ducts, so the determination of the limits of the chosen concepts still need essentially more background work.

- Other parasitic RF signals like ACI were not observed at all in the coaxial gyrotron, in strong contrast to any conventional gyrotron under investigation. While this is a very positive finding for coaxial cavity devices, the permanent appearance of spurious signals in conventional gyrotron operation has to be kept under observation and justifies extended work towards a full understanding of such spurious.

- Finally, LF oscillations are still not under control and need more investigation as well.

Improving the simulation codes for wave-beam interactions

This work was executed in coordinated efforts at KIT, CRPP, HELLAS and ISSP. This diversity is desired for cross-validation of results for which no experimental data are available.

In 2012 the following topics were investigated:

- Dynamic ACI: The generation of spectral lines indicating spuriouses caused by undesired gyrotron interaction in the cavity uptaper was assumed as a hypothesis. Same has been valid for their possible influence on the final gyrotron operation. Evidence has been gained that such spuriouses exist in reality and are not caused by artefacts in numerical simulations. Additionally, to measurements, such spectral lines appeared in the simulations using different numerical tools. However, work is still ongoing to verify the different simulations, and how far the results are depending on shortcomings of the employed simulation models. For this reason, it remains still unclear how far dynamic ACI influences gyrotron operation, and how far this can be predicted reliably. Additional efforts are necessary to improve the understanding of dynamic ACI.

- Non-uniform magnetic fields: In the uptaper the axial magnetic field starts to get non-uniform. Therefore, in the simulation this non-uniform magnetic field must be considered. That is particularly true for dynamic ACI, which is assumed to be to a high extend related to gyrotron interaction in regions of lower magnetic fields. The simulation code SELFT at KIT has been improved to consider non-uniform magnetic fields. The validation of and the final code and numeric simulations are still ongoing.

- Particle-in-Cell simulation (PIC approach): Self-consistent simulation is typically using a slow-variables approach for the electron trajectories. Additionally, the field amplitudes are taken as constant during the transit time of an electron through the cavity. This approach is becoming critical if changes in the slow variable fields take place during electron transit time. This is for example the case when a spurious frequency, generated by dynamic ACI, turns up in addition to the dominating cavity oscillation. To overcome the simplifications and to investigate their actual influence, it is necessary to drop the trajectory approach and to replace it by a PIC or PIC-like code. This was done for the EURIDICE code, while other PIC-code versions for SELFT and TWANG are still in work. It may be mentioned here that a simulation done using the full wave PIC code “HALO” of University of Stuttgart has already shown some dynamic ACI.

- Misalignment of the electron beam versus magnetic field axis: Effort has been spent on studies on the influence of electron beam misalignment. This effort was directly triggered by the observations made during the industrial prototype experiment at Lausanne, but it has a general importance beyond that. First results are that the influence of the electron beam misalignment on the beam parameters can be simulated with sufficient accuracy. It showed that misalignment is increasing mode competition and causes operation of counter-rotating modes.

Summary:

Dynamic ACI has been essentially substantiated by simulation and measurements. Still, most important influence factors e. g. boundary conditions and even correct modeling of the non-uniform magnetic fields need further investigation. It is quite natural that those discussions are arising at a point at which the existing cavity interaction codes are extended for usage in wider ranges of the gyrotron.First attempts on answering above questions were done by improving the simulation models regarding implementation of non-uniform magnetic fields, using particle-in-cell codes and by investigation of the implementation of boundary conditions for the cavity ports.

The investigation on electron beam misalignment serve purpose to ensure reliable series production and operation of gyrotrons at proper levels of output power and plug-in

efficiency. First results already indicate the strong influence of beam misalignment on gyrotron performance.

Design of highly efficient quasi-optical mode converters

The synthesis method for the waveguide antennas (launchers) of the quasi-optical system has been significantly improved. Namely, in the optimization, the wall surface is smoothed in terms of the spectrum reconstruction method.

On the base of the improved method, a new so-called smoothed launcher has been designed for the coaxial-cavity, $TE_{34,19}$-mode gyrotron.

The smoothed launcher as well as a new mirror system for the original launcher, featuring phase-correcting mirrors, were tested in a low power setup (see figure below). The new launcher was also installed into the pre-prototype gyrotron and tested in high power experiments as well. In preceding cold tests and another high power experiment, using the KIT 165 GHz electron gun, the launcher provided by IAP was measured for comparison as well. The complete quasi-optical system of the industrial prototype was also measured in low power, yielding a slightly reduced Gaussian mode content of 94.2% and the following results:

- The Gaussian mode contents for all tested systems remained high (~96%) as before.
- The stray radiation of the system featuring the smoothed launcher (4%) was reduced by nearly to its half, compared to the unsmoothed design (7%). This is a major step for reliability due to reduced heat loads in the mirror box. For comparison, the IAP launcher featured a stray radiation value of 5.5%.

In parallel, a new method for fast simulation of tapered launchers was developed and applied to the launchers of the coaxial gyrotron. This method permits fast simulations of tapered launchers, which could until now only be simulated with slow methods (SURF3D).

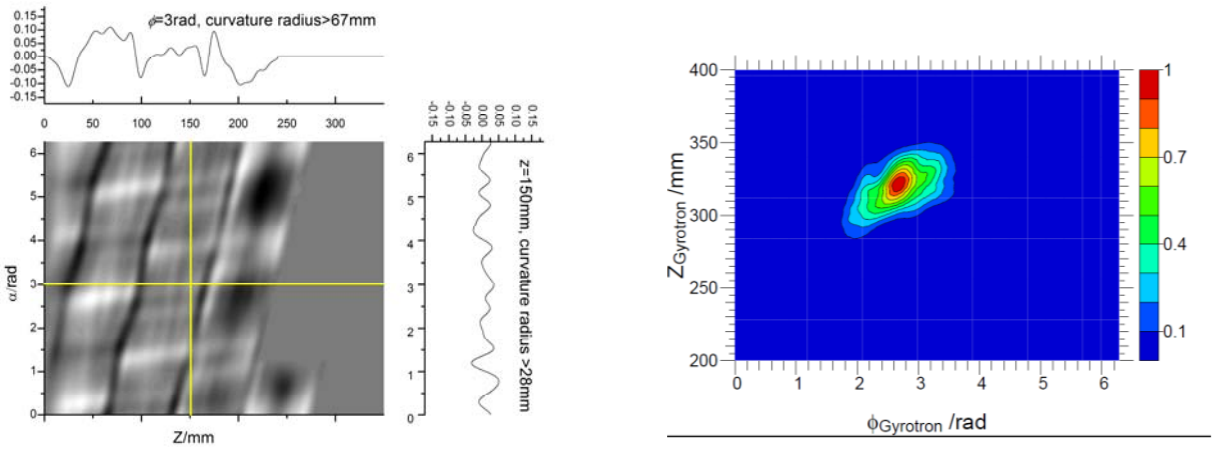

New smoothed launcher: Perturbation profile (left) with -0.166mm<δr<0.183mm, R_z>678mm and Rϕ>28mm; Radiated field (SURF 3D calculation) (right).

There are major discrepancies between the measured stray radiation and the simulated values. The reasons for these discrepancies are under investigation. Furthermore, there is no method to determine stray radiation in low power tests. In consequence, the stray radiation of a system is only known after high power tests, which is the last step of the development.

The development of the improved launcher synthesis method and its application in a new launcher design represents a major step towards reliable gyrotron operation. The alternative method of applying phase correcting mirrors is another approach of interest which may in future be combined with smoothed launchers as well.

For future work, it is highly recommendable to finalize the stray radiation measurements of the phase correcting mirror system and to refine the methods for Gaussian mode content calculation. It is furthermore highly desirable to determine the reasons for discrepancies between calculations and measurements of the stray radiation, with the goal of predicting realistic values for the stray radiation in the simulations.

– Advanced Gyrotron Development –

Studies on electron beam diagnostic systems

One of the big unknowns in experimental gyrotron diagnostics is still the electron energy distribution at the collector. Even though the distribution can be simulated with many tools today, a measurement in full operation is impossible yet. On the other hand, the energy distribution at the collector determines the possible energy recovery. Additionally, measurements of the energy distribution at the collector would provide valuable insight into the interaction mechanisms, as well as it would be a good tool for further code validation.

One possibility to create a diagnostic tool for determination of the energy distribution is to measure the X-ray spectrum at the collector. The X-ray sprectrumresults from the bremsstrahlung of the electrons which are reaching at the collector. One of the related problems is to reconstruct the electron energy distribution through de-convolution. Other problems are the sensitivity of the system and possible error sources due to the shielding of the collector.

Towards the described diagnostics tool in 2012 following steps have been done:

1. Experiments: Measurements of X-ray spectra for different quasi-monoenergetic HEBs (helical electron beams). Different electron energies has been realized, and the measured electron spectra has been calculcated. Necessary optimization of the test apparatus and algorithms has been done.
2. Definition of a measurements system to diagnose HEBs with electron energies up to 100 keV, and with beam currents up to tens of amperes.
3. Experiments at the KIT facility at typical operating regimes.

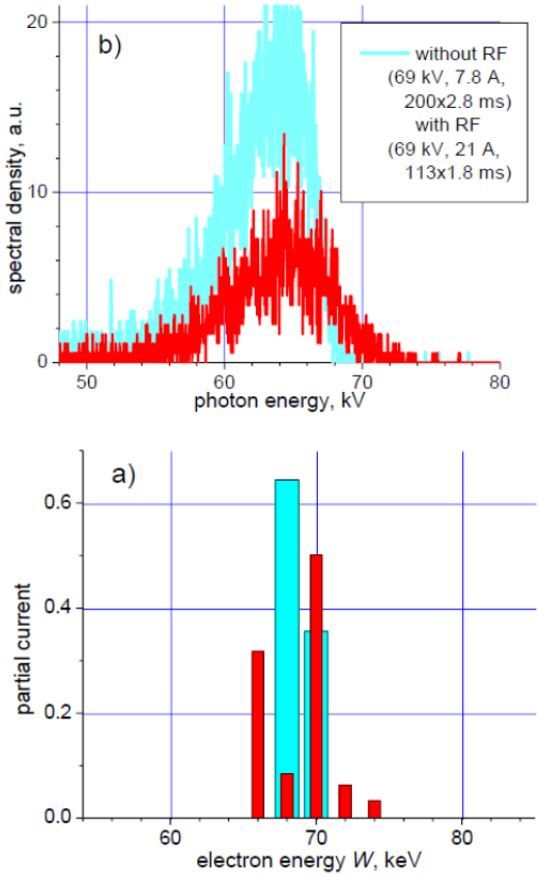

Electron energy distributions (bottom) reconstructed from x-ray spectra (top) for gyrotron regimes with (red curves) and without (blue) rf output via inverse integral transformation.

Above tasks have been done during two experimental campaigns which took place at the IHM gyrotron facility in April and October 2012. The campaigns have been followed by periods of data processing.

The two figures left shows an experimental result which confirms the applicability of the developed technique for diagnostics of gyrotron electron beams. The X-ray flux produced by the investigated gyrotron has been sufficiently intense. The spectral distributions agree with the expectations. The spectral characteristics of the x-rays (high-energy cut-off, spectrum widths) correlate with the gyrotron gun voltage and RF output power. Electromagnetic pick-up signals have little or no effect on the spectrometer performance. However, a magnetic field above a certain threshold makes the spectrometer inoperative, but doesn't visibly affect its performance below the threshold.

Design of a low power gyrotron for the test of a new emitter concept

A 10 kW/28 GHz gyrotron has been designed to evaluate the use of CPR emitters for gyrotron applications. CPR cathodes allow operation with higher current density (up to 50 A/cm^2) and provide much longer life time (~100000 h) compared to conventional emitter materials (LaB6, conventional dispenser cathodes etc.). In addition, the azimuthally segmented emitter ring provides the possibility to generate controlled non-uniform electron beams in order to study the effect of the non-uniform emission on the gyrotron output power and efficiency.

The design of all parts of the gyrotron has been finalized. The drawing of the 10 kW/28 GHz gyrotron is shown in the figure see below on the left side triode type magnetron injection gun (MIG) was preferred in order to increase the range of operating parameters. The cavity and the collector are water cooled to allow CW operation. The tube is also equipped with flanges instead of welded connections for easy exchange of components of the tube. The design of the test stand is nearly finished including water, interlock and power supply systems.

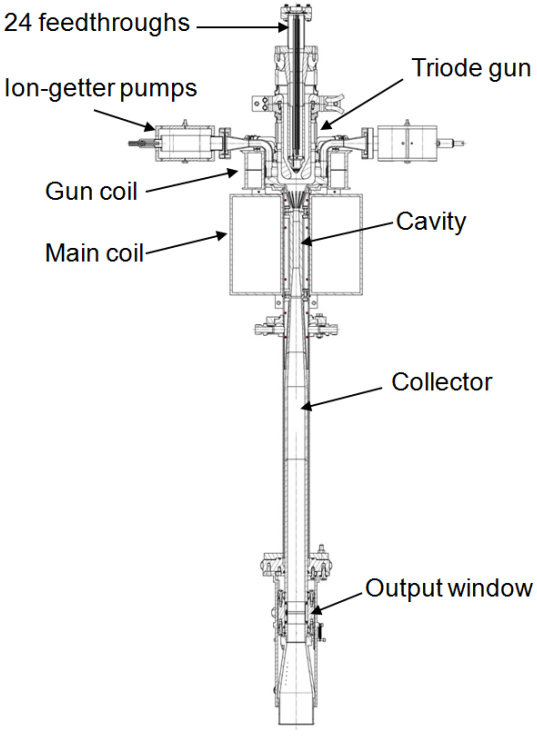

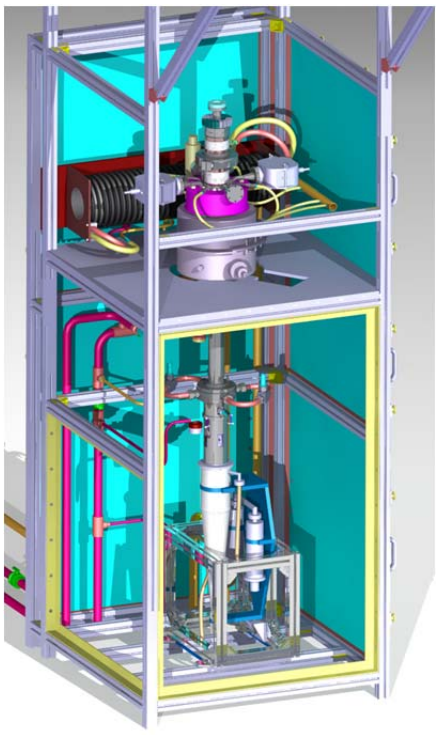

Design drawing of the 10kW/28GHz gyrotron (left), and layout of the test stand (right).

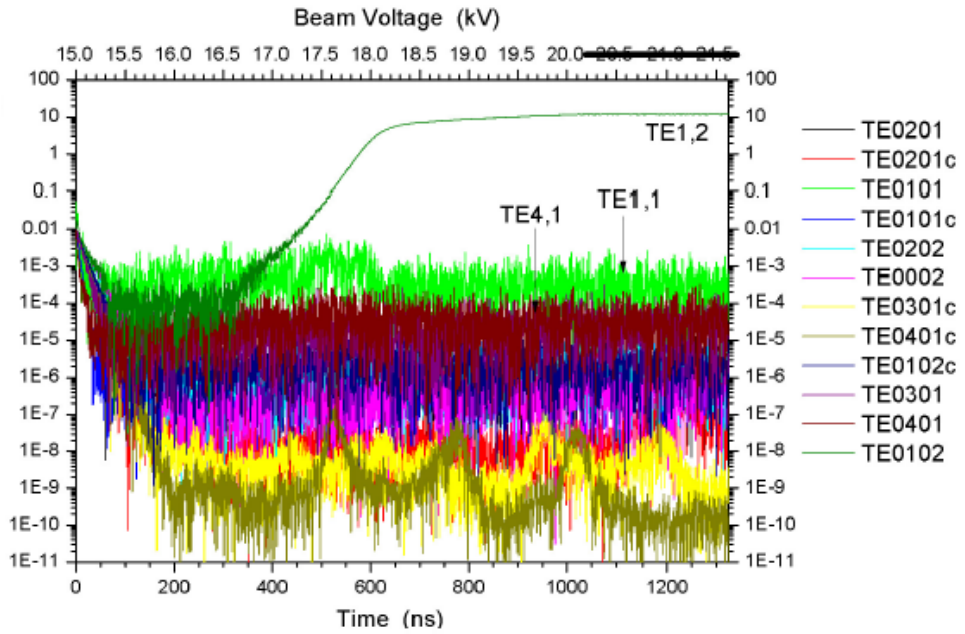

Start-up scenario for the 10kW/28GHz gyrotron (excitation of the mode $TE_{1,2}$).

For the cavity design we selected two modes at the second harmonic of the cyclotron frequency: $TE_{1,2}$ with the cavity radius 9.08 mm and beam radius 3.13 mm and $TE_{3,1}$ with the cavity radius 7.16 mm and the same beam radius as for the $TE_{1,2}$ mode. The optimization of the cavity profile was done by a self-consistent single mode code and the start-up investigations by the non-stationary multi-mode code EURIDICE. In simulations it was shown that for the cavity with $TE_{3,1}$ operating mode it is not possible to avoid the generation of the parasitic mode $TE_{1,1}$ on the first harmonic of the cyclotron frequency. For the cavity with the $TE_{1,2}$ main mode, simulations showed that from optimization of the cavity and magnetic field design it is possible to suppress the mode $TE_{1,1}$, and reach stable operation on the second harmonic $TE_{1,2}$, which can be seen from the figure above, where the start-up scenario of the gyrotron is shown.

Experiments will be performed with two types of emitters, a conventional M-type emitter (with continuous emitter ring) for evaluation of the parameters of the gyrotron and with a controlled porosity reservoir segmented emitter. The manufacturing of the conventional M-type emitter has been finished. For the segmented cathode 8 segments have been built. The assembly of the segmented cathode and preliminary tests are planned in near future. The construction of the segmented cathode and an individual segment are given below.

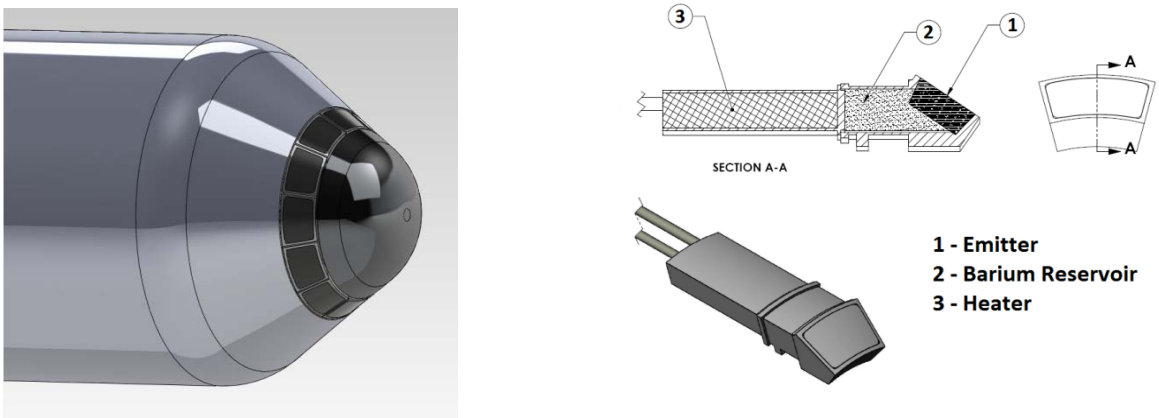

Cathode with the segmented emitter ring (left) and design of an individual segment (right).

– ECR Heating and Current Drive: – Step-Tunable Gyrotron Development –

Introduction

In recent years electron cyclotron resonance heating and current drive (ECRH and ECCD) has been established as a successful instrument in magnetically confined fusion plasmas. Gyrotrons are the unique devices which meet the extraordinary requirements of those applications: output power in the MW range, 100 – 200 GHz output frequency, and pulse length of several seconds up to continuous wave (CW). Due to its excellent coupling to the plasma and the very good localization of the absorbed RF power, ECRH is applied in present day machines and is also foreseen in large forthcoming fusion projects: it will be the main heating system for the stellarator W7-X which is currently under construction and it will play a major role in the ITER tokamak. In particular, advanced tokamaks are and will be operated in plasma regimes where MHD instabilities are probably limiting the performance. To a large extent the stability in a tokamak is influenced by the distribution of the internal plasma currents

which can be manipulated by the injection of RF waves. The location of the absorption of RF waves with the angular frequency ω is dependent on the resonance condition $\omega - k_z v_z = \omega_c$ (k_z: axial(z)-component of the wave number, v_z: electron velocity along z-axis). Thus, by changing the wave frequency ω the absorption can be moved to any radial position where the local cyclotron frequency of the electrons ω_c holds for the expression above.

Today, fusion gyrotrons in the relevant frequency range (between 100 GHz up to 300 GHz (for future devices)) with an output power of minimum 1 MW are designed for fixed frequency operation. Future frequency tunability will require additional optimization of all the major gyrotron components, the electron beam forming optics, the interaction cavity, the quasi-optical mode converter, the RF output window and, finally, the collector.

For experiments on plasma stabilization at ASDEX Upgrade (IPP Garching) with advanced ECRH and ECCD, step-frequency tunable (105 – 143 GHz) 1 MW gyrotrons operating at continuous-wave are strongly requested.

In 2012, major progress has been made in the Brewster angle window technology and in the performance of the gyrotron operation at KIT.

CVD diamond Brewster window development

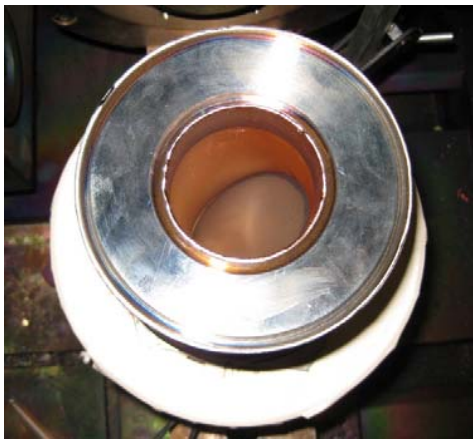

CVD diamond Brewster window after welding into the housing.

For 2012 it was planned to introduce the already brazed CVD diamond window into the housing and to perform an experimental study with a new window using the step tunable gyrotron.

The housing for the new window was designed and produced. But, vacuum tests of the window have shown vacuum tightness only on one side of the brazing. Therefore, that vacuum tight side was used as the inner one.

The copper cuffs of the diamond window were welded using electron beam welding technology to the housing. After successful UHV tests the window was prepared for the installation into the gyrotron.

Low power measurements with new CVD diamond Brewster window

Before installation into the gyrotron, “cold” tests with the full set of quasi-optical system were done, using a vector network analyzer.

Earlier tests using a quartz Brewster window did show , that the spatial distribution of the power in the output beam has multiple maxima, and, as a consequence, a low Fundamental Gaussian Mode Content (FGMC). Related measurements of the multiple maxima had been done using a thermo-imaging camera. As the reason for this beam deterioration the quartz Brewster window itself was suspected. Careful inspection of the surface of the window revealed traces of damages, probably due to overheating. It has been concluded that the inhomogeneity of the window surface disturbs the phase front of the beam and introduces higher order Hermite–Gaussian modes in the field distribution. To compare these results with the results using the diamond window comparative measurements of the quasi-optical system equipped with the quartz Brewster window, the new CVD diamond Brewster window and without window have been performed. In Fig. 2 the power distributions measured with the two types of Brewster windows (quartz and CVD-diamond) and without window are shown. As can be seen, the distribution of the RF power measured after the quartz Brewster window shows multiple maxima. It strongly deviates from the expected Gaussian distribution. This is in agreement with experimental measurements performed earlier using the step tunable gyrotron. In contrary to these results, the RF power distribution measured using the CVD-diamond window, as well as without window show the expected single peak distribution

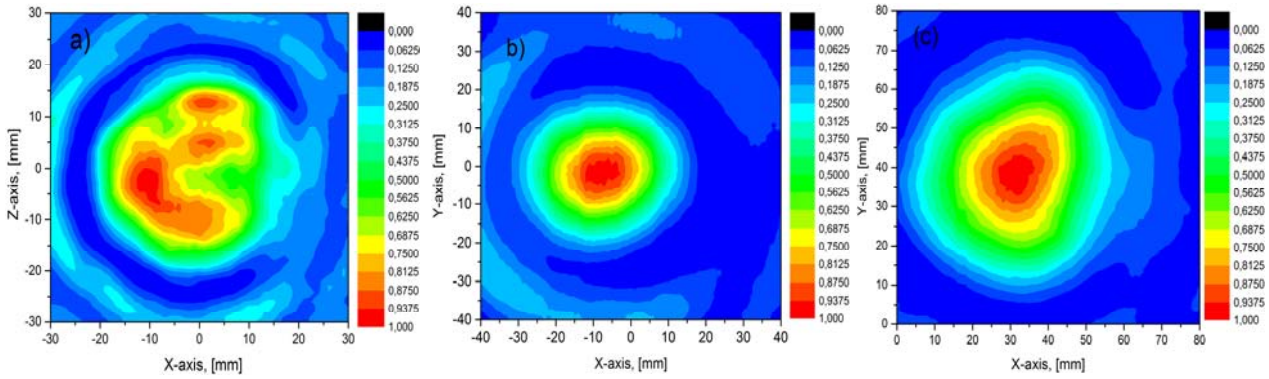

Power distribution measured from: a) quartz Brewster window, b) CVD-diamond Brewster window, c) without window.

Measurements of the gyrotron performance with installed CVD-diamond Brewster window

After low power measurements the CVD-diamond Brewster window was installed in the step tunable gyrotron.

Measurements with 1 MW RF output power were prepared. The basic configuration of the step tunable gyrotron was kept constant, only the quartz window was replaced. Thus, it was possible to compare the final performance of the gyrotron using two those two different types of windows.

Mode	Frequency, [GHz]	Measured FGMC, %	Projected FGMC, %
$TE_{20,7}$	124.1	92.5	93.4
$TE_{22,8}$	140.1	93.9	93.3
$TE_{23,8}$	143.3	96.0	91.7
$TE_{24,9}$	155.92	86.3	--
$TE_{25,9}$	159.2	89.3	--
$TE_{26,9}$	162.5	87.3	--

Measured and predicted FGMC

The measurements using the CVD-diamond Brewster window demonstrated a significant improvement in the Fundamental Gaussian Mode Content (FGMC). A first analysis showed that the values of FGMC are in accordance with the original designed values, which had been verified by numerical simulations using the "Surf3d" code package.

The FGMC measured for the modes $TE_{20,7}$ and $TE_{22,8}$ are in excellent agreement with the predicted values, while for $TE_{23,8}$ the FGNC is even bit better. The quasi-optical system was not projected for $TE_{24,9}$, $TE_{25,9}$ and $TE_{26,9}$, therefore, it has been expected that the beam properties and the final FGMC values are lower in comparison with the operating modes $TE_{20,7}$, $TE_{22,8}$ $TE_{23,8}$. For these modes the QOS had been optimized. The measured intensity of the spatial distributions of the RF power measured with a thermo-imaging camera are shown in the next figure, the picture shows, the profiles from non-optimized modes show larger contribution from side lobes.

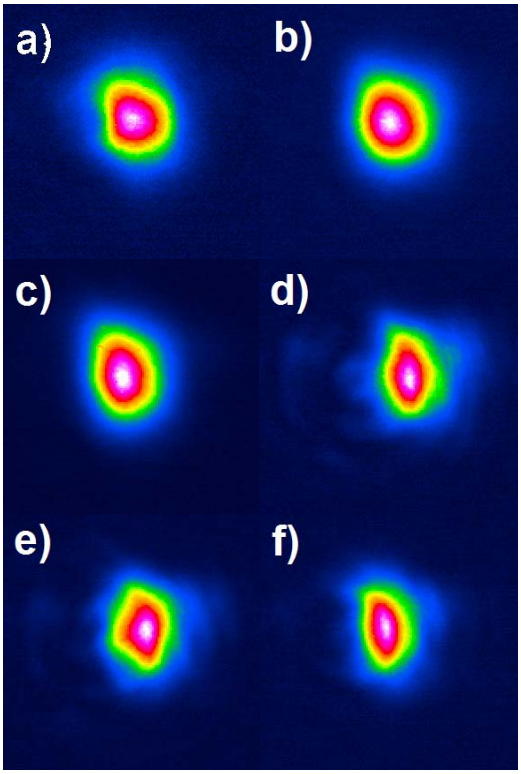

Intensity spatial profile measured by termocamera for : a) $TE_{20,7}$ mode, b) $TE_{22,8}$ mode, c) $TE_{23,8}$ mode, d) $TE_{24,9}$ mode, e) $TE_{25,9}$ mode, f) $TE_{26,9}$ mode

The RF power measurements showed that the gyrotron is capable of producing up to 1.3 MW RF output power in short-pulses. Measurements with beam currents above 50 A were not performed because of the limitation of the power supply used for heating. The transmission of the RF output power through the window was possible without any problem. As an example, see the next figure shows the dependencies of the RF output power on the beam current for $TE_{22,8}$ and $TE_{23,8}$ modes.

The next table shows the dependencies of the RF power and the gyrotron efficiency for a number of experimentally studied modes from the beam current.

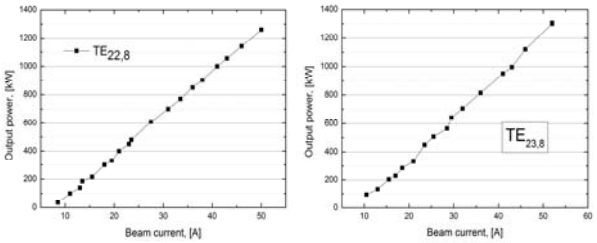

Power dependency on beam current for $TE_{22,8}$ and $TE_{23,8}$ modes.

The total RF output power and gyrotron efficiency are at comparable values as it was observed in the previous studies in 2011 using the quartz-Brewster window. Therefore, the improvement of the gyrotron performance results mainly from the quality of the RF power distribution at the window. Important to note, the operation of the gyrotron with a new CVD diamond Brewster window showed that previously observed parasitic oscillations at lower frequencies (at 5 – 6 GHz lower than the frequency of the working mode) with BWO-like dependence on the cathode voltage and magnetic field did not appear for any measured mode.

Mode	Frequency, [GHz]	U_{cath}, [kV]	I_{beam}, [A]	Power, [kW]	Efficiency, %
$TE_{20,7}$	124.1	91.7	42	900	23.4
$TE_{21,7}$	127.4	90	42	920	23.8
$TE_{22,8}$	140.1	91	40	1000	27.5
$TE_{22,8}$	140.1	91	50	1250	26.5
$TE_{23,8}$	143.3	90.3	40.5	1020	27.7
$TE_{23,8}$	143.3	92.9	52	1300	27
$TE_{25,9}$	159.2	92.3	40	974	26.2
$TE_{26,9}$	162.5	92.3	41	950	25.7

The power and efficiency for a number of experimentally studied modes

The operation of the gyrotron was accompanied by the appearance of parasitic low frequency (LF) oscillations in the region 105 MHz, which was observed in the earlier set-up already. It is assumed, that those parasitics occur due to the oscillation of space charges in the electron beam. In order to get rid of that oscillations, the optimization of electron optics magnetron injection gun would be required.

Investigation of the dependence of the electron beam on the performance of the step tunable gyrotron

An experimental study on the influence of the lateral misalignment between the axis of the annular electron beam and the cavity is performed. The dependence of the output power by the oscillation of $TE_{22,8}$ mode are shown in the next figure. The output power has maximum at optimal alignment of electron beam to the caustic of the mode and gradually reduced with a lateral shifting of the beam away from a maximal coupling. The power of the working mode scales linearly with the cathode voltage also in the case of off-axis beam. In addition, the measurements show that at large beam misalignment the excitation of concurrent counter rotation mode is possible. The data is interpreted qualitatively in the frame of theory. The results of the study will be published in IEEE Transactions on Plasma Science.

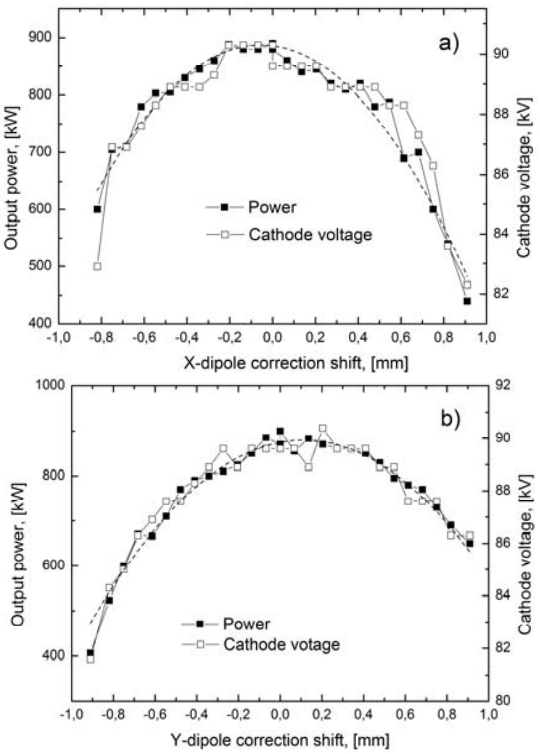

Output power and cathode voltage as a function of applied beam steering: a) – steering in X-direction, b) –steering in Y-direction.

The measured data have a practical application for the development of gyrotrons, because from this data one can obtain an acceptable range of tolerances of the production. This study suggests that the setup of gyrotron in cryostat have to be equipped with X-Y table for an adjustment in the lateral direction perpendicularly to the gyrotron axis.

Development of a new code for numerical simulation of gyrotron performance

A self-consistent time-dependent multimode code with particles has been developed to simulate the interaction in a gyrotron (GyroDyne). The motion of particles is calculated from first principles; therefore the inhomogeneity of the static magnetic field in the resonator region and various beam imperfections can be easily taken into account. The code is based on a model in which the transverse dependence of the radiation field is expanded in a set of waveguide modes. In contrast to standard models based on a such approach, like SELFT, the numbers of assumption to speed up of calculations are removed from the treatment. The code is already used in the design of a technological second harmonic 28 GHz gyrotron.

The code is applied to simulate the power output for various beam shifts. In total 8 modes were taken into account in simulation: $TE_{22,8}$+-, $TE_{21,8}$+-, $TE_{23,8}$+-, $TE_{19,9}$+-, because the frequencies corresponding to oscillations at these cavity modes with such indices were observed in the experiment.

The beam parameters used in simulation are the following: pitch factor 1.3, beam current 40A, no spread of velocity and energy is used.

The next Figure shows the numerical simulation of more steep decay of the power with beam shift in contrast to the experiment. This can be explained by the fact that in the numerical simulation idealized particle beam was used. New numerical simulation are under way where the spread of the guiding center of particles is introduced in addition to the expected spread of

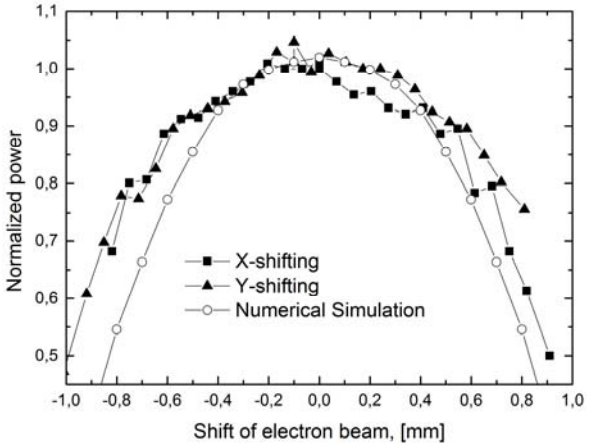

Output power measured experimentally and from simulation by GyroDyne.

velocity and energy, or in other words, to use thicker, more realistic, annular beam.
Further improvements of the code are under way.

Measurement system development for investigation of undesired transient spectral effects in gyrotrons

The field of spectral measurement techniques for gyrotrons has gained interest in the scientific gyrotron community and has also undergone substantial developments throughout the last years. Main focus are parasitic oscillations, but with increasing possibilities other effects like modulation phenomena and mode switching also get into focus.

In last year's report, an early prototype of a new measurement system capable of analyzing the gyrotron's output spectrum for transient effects with a high bandwidth and dynamic range was presented. Throughout the year 2012, the system was continuously developed further and in parallel allowed for the documentation and investigation of highly interesting phenomena.

As depicted in the first figure, the new system is utilizing a fast digital oscilloscope, receiving a downmixed time domain signal with bandwidths exceeding 3 GHz. This permits the calculation of instantaneous spectra, and with a special dual-receiver technique, undesired mixing signals can be safely excluded while actually increasing the usable bandwidth. This is done through a signal post-processing chain, in which the IF spectrograms S1 and S2 are used to reconstruct the original RF data RLSI, RHSI. Through this, the system gains the almost unique feature of unambiguous RF frequency measurement despite receiving in a harmonic-mixer heterodyne setup.

The second figure shows the direct observation of a mode jump, which occurred during the operation of a W7-X gyrotron close to the edge of the stability area of nominal mode TE22,8.

The aforementioned modulation effects can be observed in figure, where alternating modulation patterns in the multiple-MHz range are clearly present.

Second figure: Measurement example of spectrum versus time. It can be seen in the waterfall plot that, after a stable operation with $TE_{28,8}$ at 140.25 GHz, a destabilization and diminuation of the nominal mode occurs, which is accompanied by the start of the azimuthal neighbour mode $TE_{27,8}$ around 137.45 GHz. The example is zoomed for presentation, while the total frequency span of the measurement covers ~7GHz.

Measurement example (see thermocamera profile) of transient modulation during operation with TE27,8. In the spectrogram (left), the highly transient nature of the modulation effect is clearly visible. Instantaneous spectra at two different time positions (A, B) illustrate the strong changes in the modulation pattern.

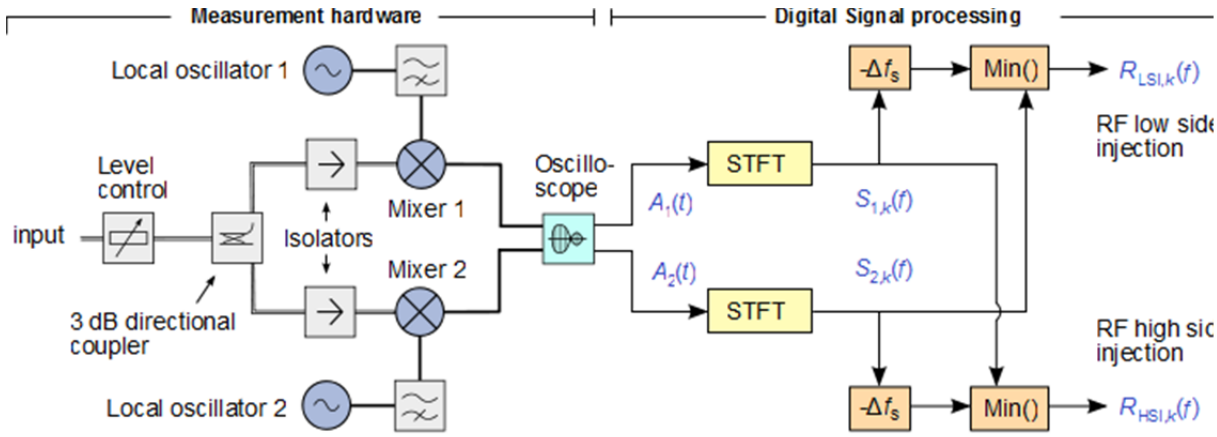

Hardware setup and data flow in new measurement system. From each of the detected time signals $A_i(t)$, through short-time Fourier transform (STFT), an independent IF spectrogram $S_{i,k}(f)$ is created. Through the utilization of the dual-channel arrangement, the unambiguous RF spectrograms $R_{LSI,k}(f)$ and $R_{HSI,k}(f)$ can be obtained.

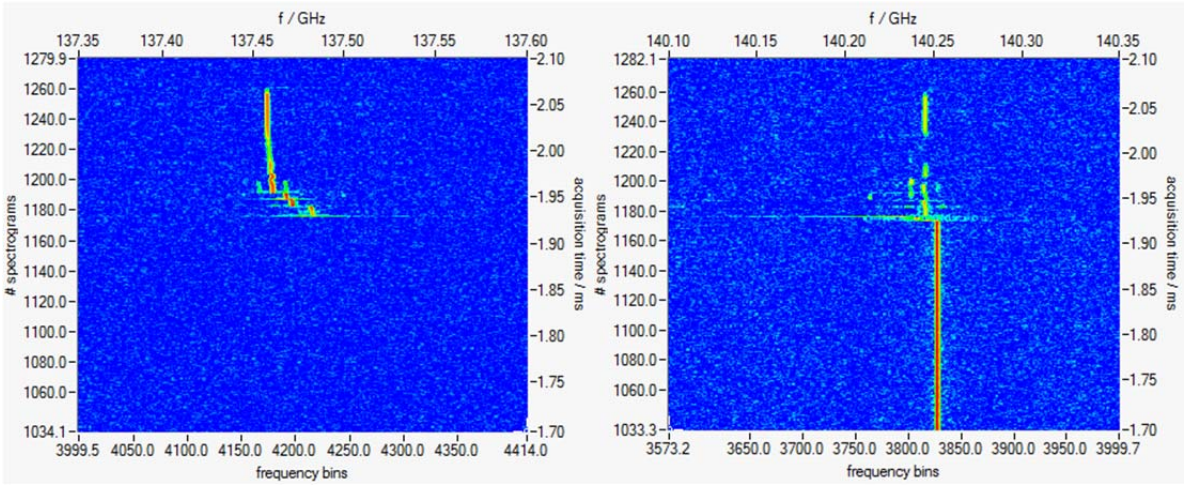

Measurement example of spectrum versus time. It can be seen in the waterfall plot that, after a stable operation with TE28,8 at 140.25 GHz, a destabilization and diminuation of the nominal mode occurs, which is accompanied by the start of the azimuthal neighbour mode TE27,8 around 137.45 GHz. The example is zoomed for presentation, while the total frequency span of the measurement covers ~7GHz.

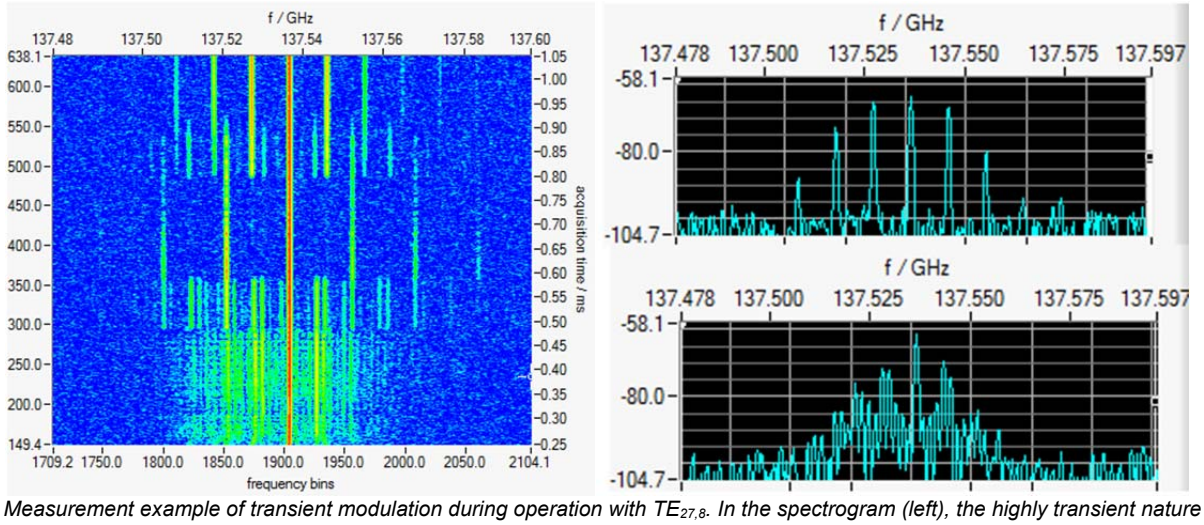

Measurement example of transient modulation during operation with $TE_{27,8}$. In the spectrogram (left), the highly transient nature of the modulation effect is clearly visible. Instantaneous spectra at two different time positions (A, B) illustrate the strong changes in modulation pattern.

Simulations on start-up and parasitic modes analysis in a TE_{12} cavity resonator

In order to evaluate a new type of controlled-porosity reservoir emitter, a 10kW/28GHz gyrotron has been designed. Initially, a self-consistent single-mode code was used to optimize the cavity. Two modes were selected at the second harmonic of the cyclotron frequency: $TE_{1,2}$ with the cavity radius 9.08 mm and beam radius 3.13 mm and $TE_{3,1}$ with the cavity radius 7.16 mm and the same beam radius as for the $TE_{1,2}$ mode. The main competing mode is the $TE_{1,1}$ mode on the first harmonic of the cyclotron frequency. In order to suppress the excitation of this mode, a proper profile of the magnetic field had to be chosen. As a first assumption we took a constant magnetic field along the cavity profile. The fig. 1 shows the efficiency versus magnetic field calculated with the self-consistent single-mode code for the $TE_{1,1}$ (first harmonic) and $TE_{1,2}$ (second harmonic) modes. One can see that from B=0.424 T there is a transition from $TE_{1,1}$ forward wave, to the backward wave. In addition, one can see that at the region of the $TE_{1,2}$ generation there is also the presence of a $TE_{1,1}$ backward wave. The introduction of the non-uniform magnetic field restricts the excitation zone of the mode $TE_{1,1}$ and the mode $TE_{1,1}$ is not exited at magnetic fields for which the the $TE_{1,2}$ mode is excited. In contrast to the $TE_{1,2}$ interaction simulations, calculations of the $TE_{3,1}$ cavity showed that the non-uniform magnetic field does not help to suppress the $TE_{1,1}$ mode.

For multi-mode non-stationary start-up calculations of the gyrotron resonator, the, highly flexible, high-order HALO-PIC code was used. This work and its results represent a new frontier in the exploitation of HALO-PIC potential: conceived as research code Using the HALO-PIC code the $TE_{1,2}$ cavity was discretized by splitting in ~32000 tetrahedrons, the field and particle solvers are set to an 4th order of approximation and the calculations were performed on 128 processors. The results presented in the last figure show the B_z pattern at 150 ns, corresponding to a beam energy of 20 keV. In these simulations it was shown that for the cavity with $TE_{3,1}$ operating mode it is not possible to avoid the generation of the parasitic mode $TE_{1,1}$ on the first harmonic of the cyclotron frequency. For the cavity with the $TE_{1,2}$ main mode, simulations with uniform magnetic field showed the excitation of the parasitic mode $TE_{1,1}$. Simulations for non-uniform magnetic field are in progress.

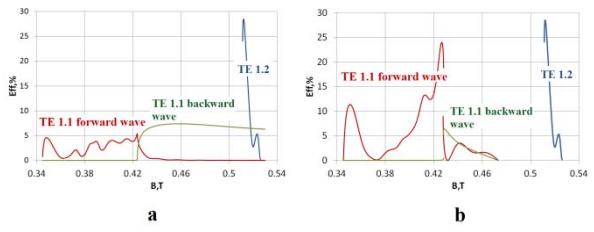

Dependence of the efficiency for the modes $TE_{1,1}$ and $TE_{1,2}$ vs. maximum value of the magnetic field, in the case of (a) constant magnetic field; (b) non-uniform magnetic field.

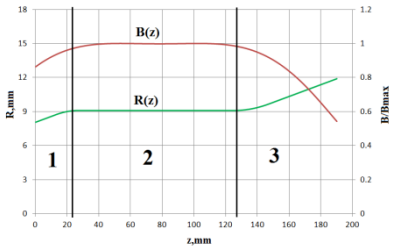

Green line: cavity profile ((1) - down-taper, (2) - constant part, (3) - up-taper); red line non-uniform magnetic field profile.

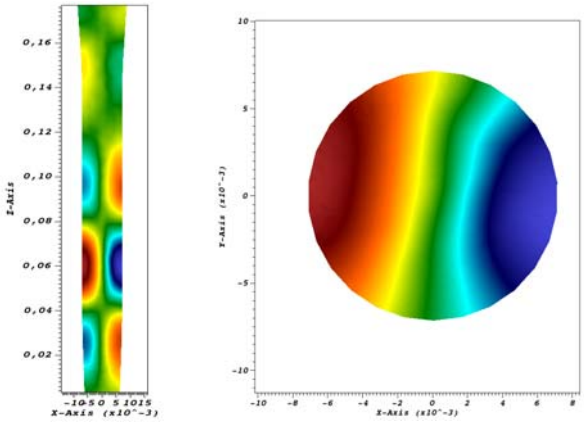

B_z RF field profile in the XZ (left) and XY (right) cross section of the $TE_{1,2}$ resonator showing $TE_{1,1}$ mode

Launcher Handling Test Facility (LHT) development in 2012

The EC H&CD Upper Launcher features some very complex components of which particular ones require basic research and analysis in terms of manufacturing, operation ability and reliability. Therefore a Launcher Handling and Test facility (LHT) is built up and nearly finished in 2012 by financing of German BMBF at KIT which provides an infrastructure for testing of prototypes and launcher components to validate the results from engineering analysis and numerical simulations. Also strategies for acceptance testing can be developed and will be used as an input to procurement, manufacturing, testing and delivery to ITER.

The LHT provides a full scale experimental site with a cooling loop providing water with ITER cooling parameters for several operation scenarios and also bake out conditions. Also the vacuum conditions in the ITER Torus can be mimicked. For analysis and validation a wide range of experimental data can be recorded by various diagnostic systems.

The LHT has a multi-purpose rack for fast installation of the prototypes and an extensive control and Data Acquisition unit (CODAC). Variable protective walls enable safe testing of critical scenarios. All plant components and diagnostics can be controlled and observed from a central switch room. The LHT is arranged as a two-level plant with a total floor space of about 130 square meters.

The LHT cooling circuit offers a wide range of scenarios of the ITER PHTS (Primary Heat Transfer System). Standard operation conditions can be simulated as well as the baking procedure and also particular incidents. The temperature range is from ambient temperature up to 240°C. A water pressure of up to 45 bar can be applied and the maximum flow rate is up to 6 kg/s.

Therefore it is provided with a heater, chillers, pumps, a storage tank and heat exchangers. Numerous valves allow dedicated water flow for individual simulations. All operations can be controlled from the central switch room.

To guarantee realistic test scenarios, a circular stainless steel chamber with a volume of ca. 6 m³ allows testing of typical structural components of up to 2.5 tons under ITER vacuum conditions down to 10^{-9} mbar. The chamber is integrated into the cooling circuit and equipped with feed-throughs and windows for all relevant diagnostic systems.

4 pumps in total as well as racks and a slide system inside the vacuum chamber allow fast and easy setup of the system for tests under realistic conditions.

Involved Staff:

KIT/IHM

K. Baumann
Dr. B. Bazylev
Dr. G. Dammertz
J. Franck
Dr. G. Gantenbein
Dr. H. Hunger
Dr. Yu. Igitkhanov
Dr. S. Illy
Prof. J. Jelonnek
Dr. J. Jin
Dr. S. Kern
Dr. I. Landman
R. Lang
W. Leonhardt
M. Losert
A. Malygin
D. Mellein
A. Meier (KIT, IAM-AWP)
S. Miksch
Dr. I. Pagonakis
A. Papenfuß
Dr. S. Petchanyi
Dr. B. Piosczyk
Dr. T. Rzesnicki
Dr. A. Samartsev
A. Schlaich
Dr. Theo A. Scherer
(KIT, IAM-AWP)
A. Schlaich (KIT CS)
M. Schmid
Dr. R. Schneider
W. Spiess
Dr. D. Strauss
(KIT, IAW-AWP)
J. Szczesny
Prof. M. Thumm
J. Weggen

IPF
(University of Stuttgart)

H. Höhnle
Dr. W. Kasparek
H. Kumric
C. Lechte
R. Munk
F. Müller
Dr. B. Plaum
P. Salzmann
K.H. Schlüter
U. Stroth
S. Wolf
A. Zeitler

(Diploma/Master students)
Z. Popovic
P. Rohmann
D. Tretiak

IPP
(Greifswald/Garching)

B. Berndt
Dr. H. Braune
Dr. V. Erckmann (PMW)
F. Hollmann
L. Jonitz
Dr. H. Laqua
G. Michel
F. Noke
F. Purps
T. Schulz
P. Uhren
M. Weißgerber

Humboldt Universität Berlin:
Prof. G. Fußmann
R. Brose

Eindhoven University of Technology:
J.W. Osterbeek, S. Paquay

Funded by BMBF project 03FUS0010

HGF Program: ENERGY

Renewable Energies (EE)

– Conditioning of Biomass by Pulsed Power Techniques –

For expanding experimental capabilities, microalgae cultivation capacity was increased by a second 26 ltr annular photobioreactor (PBR). Also, in collaboration with IBLT/BVT, a 1000 ltr flat panel PBR to be installed at the greenhouse area of IHM has been designed.

For optimizing downstream processing a detailed study on the lipid yield by ethanolic extraction after PEF treatment was performed after refinement of the biochemical and gravimetric diagnostic methods. A 4-fold increase in lipid extraction yield after PEF treatment could be revealed in average. Solvent extraction efficiency at appropriate treatment energy values was close to 100%. Special emphasis was laid on the extraction from wet biomass, since energy consumption for PEF treatment is low compared to the energy needed in conventional lipid extraction for drying and cell disruption. Furthermore, PEF-processing of microalgae allows for selective extraction of water-soluble components and lipids. In addition to saving processing energy, this may open new processing possibilities for microalgae fractioning.

Nanosecond pulse exposition has been shown to stimulate growth of microalgae cultures. At current state of work an average increase of 10-20% in biomass yield could be achieved by nsPEF-treatment.

Construction and Refinement of a Laboratory Photobioreactor

At KIT, several institutes focus on algae research. The complete chain of use of algae as an energy source, from reactor development to solid-liquid separation and cell disintegration by electroporation to accompanying systems analysis, is covered. At present, institutes involved in algae research are the Bioprocess Engineering Section of the Institute for Process Engineering in Life Sciences, the Microalgae Working Group of the Institute for Technology

Assessment and Systems Analysis (ITAS), and the Bioelectrics Group of the Institute for Pulsed Power and Microwave Technology (IHM).

The algae research at the KIT was presented at the Hannover Messe 2012. For this reason a laboratory photobioreactor PBR was exhibited at the main KIT stand. The reactor had been constructed by IHM. It is an improved copy of a PBR already used for the production of biomass in the IHM laboratory. Like the first PBR, the new one is an annular airlift reactor of 26 litres volume. It can be aerated with CO2 and air. The pH value, temperature, and gas supply can be controlled. The reactor can be cleaned and sterilized in place. After the exhibition the reactor was transferred to the IHM laboratory and adapted to infrastructure and control. With both reactors now it is possible to grow algae under controlled conditions, leading to defined algae biomass, necessary for the pulsed electric field (PEF) treatment experiments.

Since the reactors are only suitable for indoor application they are fitted with illumination devices. The first reactor is illuminated by six fluorescence lamps that supply the reactor with a photosynthetically active radiation (PAR) of about 600 µE/m2/s. The PAR is the photon flux density in the photosynthetical active wavelength range (400 – 700 nm). Since this radiation is not strong enough for high density cultivations, a new illumination device was developed at IHM. It consists of warm white LEDs with a luminous colour of 4500 – 4700 K. Several LEDs are joined to strips and ten LED strips are arranged around the photobioreactor. In order to have a more uniform light distribution at the surface of the photobioreactor, the light is guided by reflectors. The LEDs can be dimmed and the maximum electric input power of the device is 1150 W leading to a maximum PAR of 1030 µE/m2/s. This radiation has been found to be sufficient for the illumination of a PBR and it is half of the PAR of a sunny summer day at noon (2000 µE/m2/s).

Annular airlift photobioreactor with a half shell of the LED illumination at the main KIT stand, Hannover Messe 2012.

Development of a Pilot Flat Panel Photobioreactor

The goal of the algae research at the KIT is the integration, development and analysis of the whole algae production chain. It covers the major processing steps in order to make the application of algae for the production of low value mass products like fuels economically and ecologically feasible in the medium and long term.

In cooperation with the Bioprocess Engineering Section of the Institute for Process Engineering in Life Sciences (BVT), the IHM will build a 1000 l PBR at the campus north. BVT and IHM will undertake large scale algae cultivations in the reactor and the BVT will investigate the transferability of laboratory results to outdoor cultivations. Additionally, the PBR will provide larger amounts of algae biomass to both working groups for scaling-up downstream processing experiments.

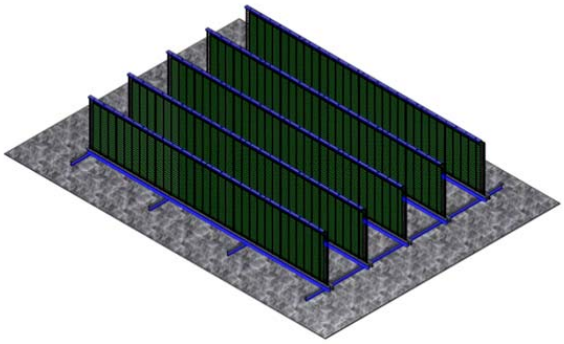

Conceptual design of the 1000 l flat panel photobioreactor, courtesy of C. Steinweg, IBLT-BVT.

The reactor will consist of five flat panels each about 1 m high and 6 m long. The algae will be grown inside a transparent plastic sack that is supported by iron fences. To supply the algae with CO_2 and to avoid algae sedimentation, the reactor will be aerated with an air CO_2 mixture through a tube lying on the bottom of the reactor. Aeration, pH and temperature will be controlled. The reactor is designed for non-axenic cultivations and it can be used in batch or continuous mode. Cultivations will be performed from March to October, since long periods of frost have to be avoided.

Up to now the development of the reactor design is finished and most of the parts necessary for its assembling have been purchased.

Pulsed Electric Field (PEF) Assisted Extraction of Lipids from Microalgae

The establishment and refinement of the Sulfo-Phospho-Vanillin-Reaction within the last two years demonstrated a notable potential of PEF-extraction of lipids from microalgae. This analytical method proved to be very suitable for determination of the lipid content in solvent extracts in screening experiments. On the other hand, the daily working routine revealed some disadvantages of the procedure.

The formation of the oil-content-indicating vanillin complex depends on the existence of C-C double bonds of unsaturated fatty acids. The analysis procedure also requires calibration with an oil standard. A commonly used standard is olive oil, which does not necessarily contain the same amount of double bonds like algal lipids. To make sure that the results obtained with the SPV method actually reflect the lipid yield of the extraction, we developed a gravimetrical analysis procedure. Gravimetric methods of lipid diagnostics require longer processing times and a comparable large amount of biomass per sample but deliver precise results if conducted properly. The experiments were done with 1 g of freeze dried microalgae biomass (Auxenochlorella protothecoides), using 70% ethanol as solvent. After the extraction process, a biphasic solvent system with hexane as major solvent was formed and the crude lipids were transferred into the hexanic phase. After several purification steps, the solvent was

evaporated by a nitrogen gas stream and the residual algae oil was weighed.

The comparison shows that both methods, the gravimetric analysis and the SPV-test, lead to a graph with a very similar shape. In both methods, the application of PEF energy of 50 kJ/kg suspension shows no effect on lipid yield. The increase in amount of extracted lipids at a specific energy of 100 kJ/kg and higher also can be observed with both analytic methods.

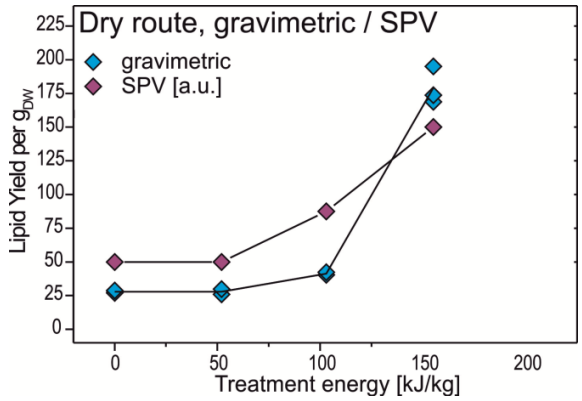

Comparison SPV and gravimetry: Lipid yield from 1 g of freeze-dried biomass, determined by gravimetrical analysis and SPV-test, respectively. Results for SPV-test are given in arbitrary units.

Our results indicate that the Sulfo-Phospho-Vanillin method is well suited for rapid screening of the lipid content in solvent extracts but less suitable for a precise quantification.

In successive studies we determined the influence of treatment energy on lipid yield. Results for two different cultivations are displayed in the following figure. The lipid yield exhibits a strong dependency on the applied treatment energy. Without application of PEFs, the gravimetrically determined lipid content of the algae biomass varies between 25 and 65 mg. At 50 kJ/kg no effect of PEF treatment on lipid yield could be detected. An onset of increase in lipid yield between 70 and 100 kJ/kg_{sus} and finally maximum yield and saturation at 150 kJ/kg_{sus} and higher was observed. The maximum lipid yield of 150-200 mg show that the lipid content of the algae is in the range of 20% of drymass. This is within the scope usually reported for Chlorella type algae. The differences between the cultivations reflect the variations of the biological raw material. Contrary, for a single cultivation and for each set of electrical parameters, the variation between the data points is very small. This proves the low systematic error of the gravimetric lipid quantification method.

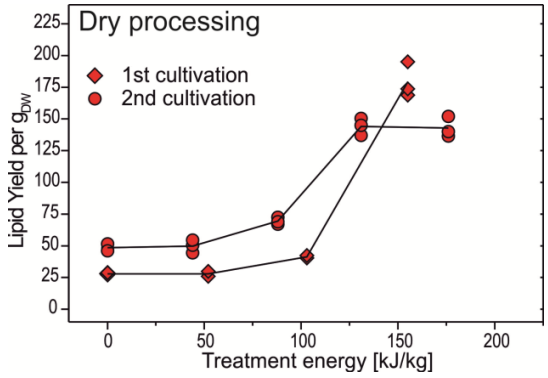

Variation of treatment energy: Lipid yield from 1 g of freeze dried biomass from two different cultivations, treated with different energy values. Extraction was done with 70% ethanol.

PEF treatment at high energy levels (150 kJ/kg) increases lipid yield 2 to 6 fold. These results indicate clearly, that PEF treatment significantly improves the extraction process, most probable caused by a more effective access of ethanol into the cell interior. PEF treatment is also known to improve the release of intracellular water from the cells. Less intracellular water promotes a sufficient high intracellular ethanol concentration for effective lipid extraction.

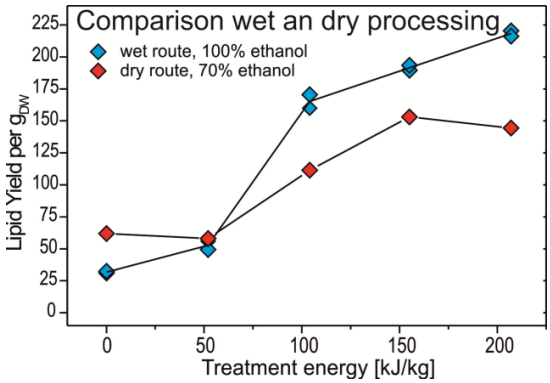

Comparison of wet and dry processing: Lipid yields from 1 g freeze dried and 10 ml wet microalgae biomass, determined with gravimetrical analysis

PEF treatment can also increase the lipid yield of ethanolic extractions from wet microalgae slurry without previous (freeze-) drying. For wet-route processing, pure ethanol was added to the wet microalgae slurry. In the wet extraction process, the lipid yield was more than 3 times higher for PEF-treated algae. We consider this finding very important for future microalgae processing. The wet extraction of lipids from PEF-treated biomass promises economic lipid production, since the energy requirements for PEF-treatment, 1.5 MJ/kgdw, are low compared to the savings in drying energy which are 7 MJ/kgdw in minimum.

Whether or not wet-route solvent extraction in general delivers higher extraction rates cannot be assessed at the current state of work. This needs further statistical verification of the results acquired so far.

Stimulation of algal growth by nanosecond pulsed electric field (nsPEF) treatment

Due to their ability to accumulate considerable amounts of triglycerides, microalgae are considered as the most promising future biomass feedstock for oil production. Pulsed Electric Field (PEF) technology is a low cost process that can be applied to algae suspensions. This treatment is affecting the external membrane of algae cells, increasing the availability of intracellular materials in downstream separation and extraction.

Apart from affecting the membrane, nanosecond Pulsed Electric Fields (nsPEF) can induce growth stimulation on plants and fungi, as we have shown in previous work. In the frame of this study, supported by the Baden-Württemberg Foundation, we try to transpose such growth stimulation process on microalgae in suspension to increase the cultivation yields in order to reduce biomass production costs.

Design of the experimental setup and assessment of diagnostic conditions for a systematic parameter study

Since PEF-treatment of inoculum didn't result in accelerated algae growth, the continuous optical density measurement setup was extended by a continuous flow PEF treatment cell operating in bypass. Optical density measurement of cell culture growth revealed to be a very sensitive diagnostic tool

for determination of the algae growth and algae lethality exposed to PEF treatments.

At first approach, the lethal pulse parameters of PEF treatment of Chlamydomonas reinhardtii algae suspension were determined by monitoring the optical density over the entire cultivation time. In order to treat the algae suspension a transmission line pulse generator providing high treatment field strength was applied. It delivers square pulses with a voltage amplitude between 8 and 20 kV and a pulse duration between 10 ns and 10 µs. To vary the energy of the PEF treatment the treatment time (15 – 180 min) and the pulse duration (25 – 400 ns) were changed whereas the field intensity and the frequency were keep constant at 40 kV/cm and 2.5 Hz, respectively.

We found that the optical density of the C. reinhardtii suspension drops after PEF exposure and that the extent of this drop is related to the energy dose. Furthermore, the cells recovered slower when the cell suspension was treated with higher dose. As a first important result we found that a 30 min long PEF treatment at field strength of 40 kV/cm and pulse duration of 25 ns doesn't affect *C. reinhardtii* growth. In this case the specific energy dose was 1.4 kJ/kg. PEF treatments at specific treatment energies below this limit were considered to be non-lethal.

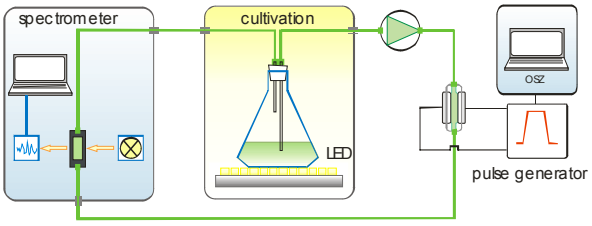

Scheme of the experimental setup for continuous PEF treatment of algae suspension. Microalgae growth is detected by optical density measurement using a spectrometer enclosed into a shielding cabinet. The algae suspension was cultivated in an incubator and continuously exposed to electric pulses generated by a transmission line pulse generator.

For this assay of experiments the orbital shaker with the flasks was placed in the laboratory, thus the cell growth was also influenced by the room temperature and room illumination. Because of the difficulty to keep these external conditions constant during the entire year it was decided to perform further cultivation in an incubator at 25°C, as shown on the scheme. Furthermore, the illumination of the flasks was replaced by a LED panel consisting of an array of 17x19 LEDs which was mounted on the orbital shaker stage. The LED illumination guarantees a uniform and constant illumination of the flasks during the entire cultivation time.

Based on this experimental setup we investigated if the nsPEF treatment with non-lethal dose might stimulate the algae growth. We found that the average value of the growth rate (0.08±0,03 h-1) of nsPEF treated algae suspension doesn't differ significantly from the average growth rate of the sham cultivation (0.07±0,02 h-1) and thus indicates an insignificant stimulation. In addition, as an alternative procedure for growth stimulation of algae, a combined treatment with the growth hormone 2,4-dichlorophenoxy acetic acid and nsPEF was examined. It was found that the optimal nsPEF treatment should be conducted during the exponential growing phase which starts 5 h after inoculation. The combined treatment led to a growth stimulation of algae suspension, as shown in the following figure. The cultivation duration (T_K) was reduced in average by 10%, thus the feasible biomass yield is 1.3-fold higher at same cultivation duration. Under the premise of continuous harvest shortly before approaching the stationary phase, an increase of the biomass yield in the range of 6% to 31% is expected.

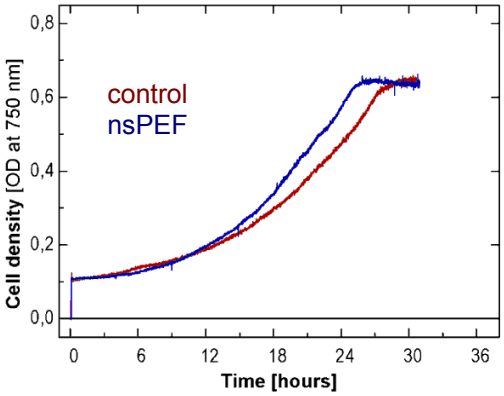

Cell density of algae suspension cultivated in TAP medium which contains 10 µM 2,4-dichlorophenoxy acetic acid: blue line is the cultivation exposed to nsPEF and red the sham. The cultivation duration (T_K) is 10% (2.4 h) shorter for nsPEF treated cultivation than for the sham.

To ensure that algae growth stimulation induced by nsPEF in combination with the hormone is a universal effect a second algae species, *Chlorella vulgaris* has been considered. In the following, the algal lethality of *C. vulgaris* was evaluated by the same procedure as described before. The nsPEF treatment of *C. vulgaris* was performed around 20 h after inoculation corresponding to the starting point of the exponential growing phase. We found that the conditions leading to lethal effect of nsPEF treatment on *C. vulgaris* were very similar to that observed with *C. reinhardtii,* as shown in the diagram. The specific non-lethal nsPEF dose for *C. vulgaris* was also below 1.4 kJ/kg. However *C. vulgaris* recovers faster and the optical density drop observed directly after PEF treatment was lower. One explanation is that C. reinhardtii is more sensitive to nsPEF treatment than *C. vulgaris* and also that the induced effects are of different extent depending on the cell species.

Improvement of the experimental efficiency

The existing experimental procedure was limited to one essay per week, due to the number of spectrometers which were available. An option to increase the number of experiments was to use transmission probes, connected in parallel, instead of continuous flow cuvettes for OD-measurement. These transmission probes are designed for immersion into solutions and allow measuring the OD directly in the cultivation flasks. Hence a multiplexer which distributes the light from each probe to a single spectrometer was purchased and integrated into the experimental setup. The synchronization of the probes and data acquisition was performed with the LabView software.

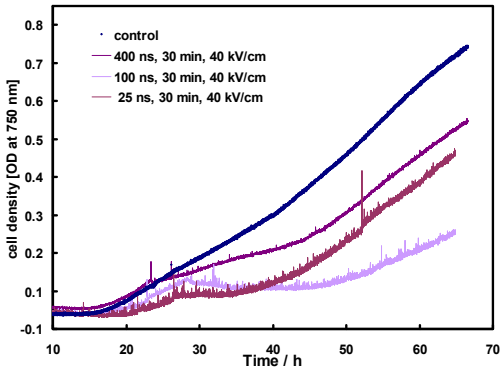

Optical density of algae suspensions, C. vulgaris exposed to different PEF treatment parameters.

In summary, the experimental and diagnostic conditions for efficient systematic parameter studies considerably have been improved. The lethal dose for two different algae species was determined by means of optical density measurements. We found that nsPEF treatment in presence of a hormone increases the biomass yield up to 1.3 fold, so far. Future investigations will focus on alternative algae species.

Monitoring of pulsed electric field induced abiotic stress on microalgae by chlorophyll fluorescence diagnostic

One focus of the work performed in 2012, was layed on stress monitoring of PEF treated microalgae. This subject is of great interest, when the PEF-processed organism must not be killed or even severely harmed, e.g. for soft extraction or growth stimulation.

One possibility to assess green microalgae vitality is to measure the chlorophyll fluorescence emitted from the chloroplasts.

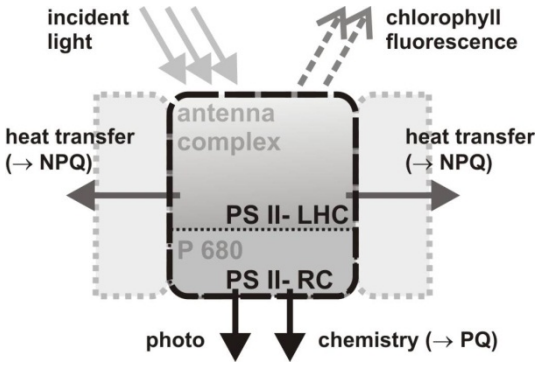

The energy introduced by incident light and captured by the antennae of the photosystem (PS) II light harvesting centers (LHC) of the chlorophyll a molecule, can be converted along three pathways: 1. Photochemical conversion inside the PS II reaction centres (RC)→ photochemical quenching (PQ), 2. Dissipation as heat→ non photochemical quenching (NPQ) and, 3. Excitation of chlorophyll fluorescence.

The required fluorescence parameters F_0 (minimal chlorophyll fluorescence) and F_m (maximal chlorophyll fluorescence) were determined by a pulse amplitude modulated (PAM) measuring device, using the saturation pulse method. The measuring system is equipped with an internal light source for fluorescence excitation, together with an integrated PIN photodiode, which determines the emitted chlorophyll fluorescence. The above mentioned parameters allow to calculate the maximum photochemical quantum yield of photosystem II (PS II): Fv/Fm = (Fm-F0)/Fm.

Fv/Fm proofed to be suitable for evaluating imposed environmental stress on PS II of the photosynthetic apparatus. In consequence, Fv/Fm turned out to be a measure for the vitality status of green plants and microalgae, too. For this reason Fv/Fm serves as benchmark for the stress level of microalgae in this investigation.

To reveal the influence of PEF-stress on microalgae, specimen of Auxenochlorella protothecoides (A. protothecoides) were exposed to electrical pulses of two different pulse lengths (t Imp = 100 / 1000 ns), with constant electric field E Cuv = 40 kV/cm. The applied specific energy was varied from W spec = 2 - 78 kJ/kg for 100 ns pulses and between $2 \leq$ W spec ≤ 20 kJ/kg for 1000 ns pulses, respectively.

The results from one series of experiments were normalized to the initial value of the untreated controls, in each case. Hence, all Δ Fv/Fm values are normalized data, too.

As clearly can be seen in the diagrams, the maximum photochemical quantum yield of PS II of the untreated microalgae samples remained almost constant at a high level of Fv/Fm ~ 0.7, throughout the observation period of 60 minutes (white symbols in the diagrams). The difference in maximum photochemical quantum yields of PS II of the control samples measured at the beginning and the end of the experiment (white symbols) is low, $\Delta F_v/F_m \sim 0.04$, indicating excellent vitality of the microalgae throughout the duration of this experiment of more than 10 hours. To distinguish between time and energy variations of the maximum photochemical quantum yield of PS II, initial changes immediately after PEF treatment are labeled by the index ´ **i** ´ and changes within the observation period subsequent to PEF treatment are labeled by the index ´ **op** ´, followed by the associated specific treatment energy value.

1) 100 ns pulses

When exposing microalgae suspensions to specific energies of $W_{spec} = 2 - 4$ kJ/kg, no significant influence on the maximum photochemical quantum yield of PS II was detected (grey triangles in Fig. above). Even the application of higher treatment energies of $W_{spec} = 8$ kJ/kg and $W_{spec} = 16$ kJ/kg (see squares in Fig. above), had only a minor influence on F_v/F_m and thus on the vitality of the microalgae. The initial F_v/F_m values showed only very small decreases, compared to the untreated controls ($\Delta_{i8} F_v/F_m = 0.040$). Only in the course of the observation period a decrease of $\Delta_{op8} F_v/F_m = 0.113$ became obvious, with a reduction of the gradual slope down to the end (squares in Fig. above). PEF treatment with $W_{spec} = 35$ kJ/kg clearly showed a lower F_v/F_m value at the beginning ($\Delta_{i35} F_v/F_m = 0.226$).

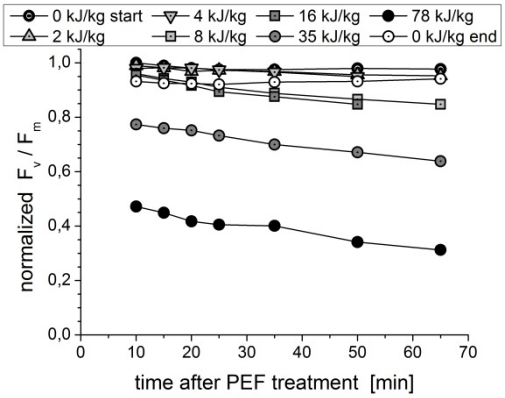

PEF treatment of A. protothecoides: ***t_{Imp} = 100 ns****, E = 40 kV/cm, W_{spec} = 2 - 78 kJ/kg.*

Throughout the observation periode of 60 minutes, a further reduction by $\Delta_{op35} F_v/F_m = 0.135$ could be detected, with a final value of $F_v/F_m = 0.638$ (bright grey circles in Fig. above). In the end this is not really too bad, taking account of the fact that some microalgae are quite healthy in this F_v/F_m-range, under certain cultivation conditions. A serious initial drop of $\Delta_{i78} F_v/F_m = 0.528$, with the W s_{pec} = 78 kJ/kg treatment, was followed by a further decrease leading to a final value of $F_v/F_m = 0.312$ (Fig. above, black circles). Although the gradual slope of the F_v/F_m values seem to reduce towards the end, no higher treatment energies were applied to the microalgae.

2) 1000 ns pulses

Microalgae exposed to 1000 ns PEFs showed a complete different behavior. No influence was visible immediately after PEF treatment with $W_{spec} = 2 - 4$ kJ/kg (grey triangles in Fig. below), compared to the untreated control (white symbols). But at least 20 minutes after treatment, a significant downward trend of the F_v/F_m values became visible. The gradient of decrease was more intensive with the higher treatment energy of $W_{spec} = 4$ kJ/kg (inverted grey triangles in Fig. below), rather than at $W_{spec} = 2$ kJ/kg (grey triangles in

Fig. below). This was surprising, considering the relatively low energy input and compared to the obtained results with the 100 ns treatment, where the curve shape was considerably flatter in the same period (see Fig. above). The experiment with W_{spec} = 4 kJ/kg revealed the strongest decrease in the maximum photochemical quantum yield of PS II, throughout the investigation ($\Delta_{op4} F_v/F_m = 0.431$). Immediately after the PEF treatment, the maximum photochemical quantum yield of PS II was reduced, partially quite considerably, in the experiments with higher energy input (see Fig. below). During the 1000 ns experiments, the lowest energy where an initial drop of the maximum photochemical quantum yield of PS II could be observed was W_{spec} = 6 kJ/kg (grey diamonds in Fig. below), with a $\Delta_{i6} F_v/F_m = 0.169$. The decrease during the observed 60 minutes was similar to the W_{spec} = 4 kJ/kg experiment, $\Delta_{op6} F_v/F_m = 0.401$. The initial drop of F_v/F_m at W_{spec} = 8 kJ/kg (bright grey squares in Fig. below) and W_{spec} = 20 kJ/kg (dark grey squares in Fig. below), was more pronounced. However, in the subsequent course of time the characteristic curve was less steep, compared to the curve gradient of the 100 ns pulses (see Fig. above). The W_{spec} = 20 kJ/kg experiment gave evidence of extraordinary stress to the microalgae, starting with $F_v/F_m = 0.189$ decreasing down to $F_v/F_m = 0.034$ in the end. With $\Delta_{i20} F_v/F_m = 0.811$ the W_{spec} = 20 kJ/kg experiment displayed the largest initial drop of all experiments in this investigation.

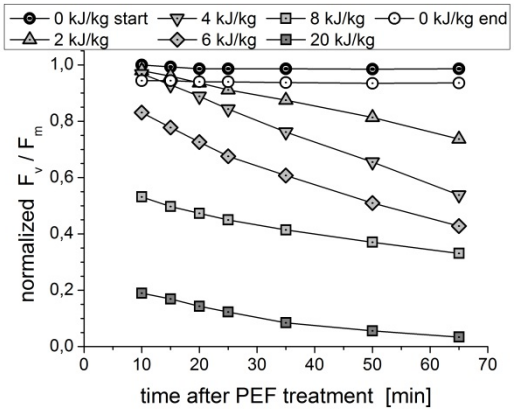

PEF treatment of A. protothecoides: ***t_{Imp} = 1000 ns****, E = 40k V/cm* W_{spec} *= 2 - 20 kJ/kg.*

The experiments show a clear and direct link between the imposed PEF-stress and the response of the maximum photochemical quantum yield of PS II. It can be summarized that the PAM device in combination with the saturation pulse method proved to be a reliable instrument to monitor PEF-stress of green microalgae.

The results indicate that A. protothecoides are more sensitive to long, rather to short PEFs, in particular at low specific treatment energies. The microalgae exposed to t Imp = 1000 ns pulses started with significant lower Fv/Fm values, in comparison to experiments with t Imp = 100 ns and showed a notable faster decline over time. In summary the examined microalgae are more sensitive on PEF stress for µs-pulses compared to 100ns-pulses. This contradicts existing theories where intracellular effects, i.e. PEF impact on chloroplasts, are supposed to be more pronounced for nanosecond pulse exposure.

Transmembrane potential measurements on the mammalian cell line DC-3F

A new mammalian cell line (DC-3F, Chinese hamster lung tissue) was brought to the laboratory. The specific equipment for mammalian cells culture was acquired and the cultivation protocol was established.

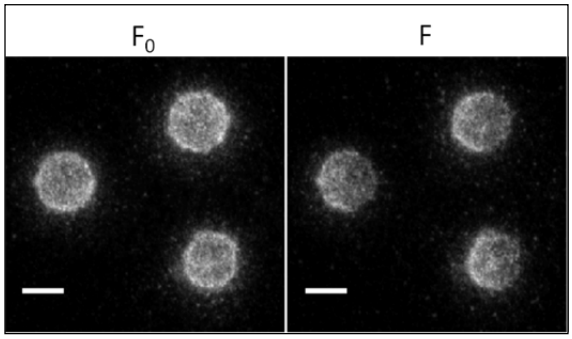

DC-3F cells stained with ANNINE-6 and observed in fluorescent light. The fluorescence intensity F_0 of the cells at rest is modulated during exposure to a 2.4 MV/m electric field, image on the right (Scaling bar 10 µm).

Staining protocol with ANNINE-6 (a fluorescent probe sensitive to electric field) was successfully transposed to the DC-3F cell line. Some preliminary results indicate that it is possible to follow the fluorescence change F/F0 during exposure to pulsed electric field as can be seen on the image above. Illumination for image acquisition is performed with a nanosecond laser which ensures a very high temporal resolution.

Despite the small diameter of the cells (13 µm in average), an angular resolution of 10° along the circumference of the membrane can be achieved. The smaller size of the cells imposes however to average a higher number of experiments in order to obtain a satisfactory signal to noise ratio. This point is even more critical when looking at small fluorescence variations. On the example presented on the following image, 66 cells were averaged in order to measure accurately a fluorescence variation bellow 10%.

The possibility to measure low intensity fluorescence is a crucial point since it gives results in the calibrated range of the fluorescence molecule ANNINE-6. The calibration of the molecule can indeed only be performed with patchclamp measurements. Under these conditions, cells are submitted to long electric pulses in the ms range. This long duration narrows considerably the magnitude of the voltage that can be applied. The typical voltage range in which stable patching can be performed in thus between -300 mV and 300 mV which corresponds to a fluorescence variation typically between -20 % and +20 % (according to previous experiments performed in the laboratory on BY2 protoplasts). The experiments at low field values, inducing low transmembrane voltage in the calibration range will thus enable to draw a direct link between transmembrane voltage and external field. Such information will enable to confront the current electromagnetic models of cells which predict evolution of transmembrane voltage under external electric field.

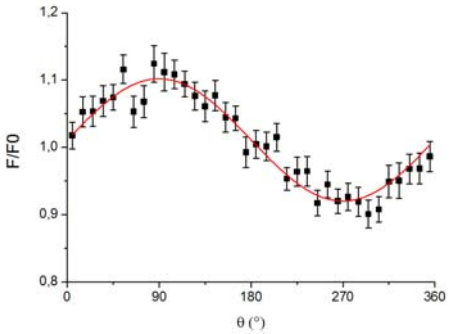

Azimuthal dependence of the relative fluorescence variation F/F0: Results were obtained on DC-3F cells submitted to a 200 µs pulse of 40 kV/m, 10 µs after the onset of the field. The symbols are mean±std error computed on 66 cells. The red curve is the fit of the data with a sine function.

The comparison of the results on the DC-3F cell line with the results previously acquired on tobacco protoplast cells will allow testing the specificity of transmembrane modulation with respect to cell diameter, membrane composition and resting transmembrane potential. Moreover the DC-3F cell line is well suited for survival assay and follow up of cell growth since it is a fast dividing and easy to clone cell line. Thus, this cell line will allow establishing a link between the transmembrane potential modulation immediately induced by electric pulses and secondary effects such as membrane permeabilisation or cell death.

The ability to detect small signal also implies that it is possible to detect the minimum field strength which induces a modification of the membrane such as a conductivity increase. Indeed, a stable fluorescence signal can be interpreted as an unaffected membrane from the conductivity point of view. Only very low voltages on the membrane (and thus low fluorescence variations) can leave the membrane intact. Our current results indicate that a field value of 40 kV/m is low enough to leave the membrane of DC-3F cells intact for at least 50 µs. BY2 protoplasts which is another cell type commonly used in the laboratory appears to be more sensitive. Indeed, a field twice lower (20 kV/m) already induces a modification in the membrane of the protoplasts after only 10 µs. Additional experiments are currently being performed with pulses of different length in order to give more precise values of threshold for different pulse length.

Properties of field-induced pores in tobacco culture cells

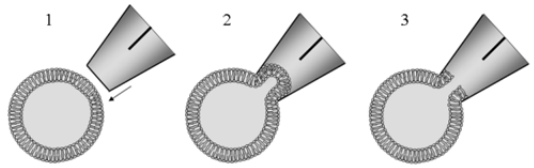

Establishment of the whole cell configuration of the patch clamp technique (see text).

By applying the patch clamp technique in the whole cell configuration, a low-resistance electrical contact with the cell interior is established via a fine-tipped glass microcapillary that contains an Ag/AgCl electrode and is filled with electrolyte solution. To this end, the microcapillary is positioned on the cell

surface, and a membrane 'patch' is aspired into the tip by applying gentle underpressure. When the membrane firmly attaches to the glass surface, a gigaohm resistance ('gigaseal') is obtained that minimizes currents by-passing the cell. Application of a brief underpressure pulse leads to mechanical breaking of the membrane patch encircled by the capillary tip and, in turn, to an establishment of the whole cell configuration. Administration of brief hyperpolarizing and depolarizing voltage pulses and registration of the respective current response allows, among other things, to precisely assess the threshold membrane voltage for electroporation (i.e. minimum polarization of the membrane required to initiate pore formation).

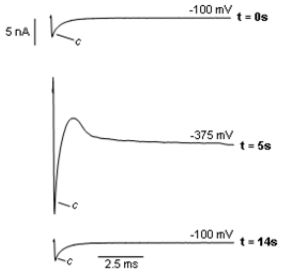

Current response to a sequence of three 10-ms voltage pulses (see individual trans-membrane voltage at the end of each trace; holding potential between pulses: 0 mV) imposed within a few seconds on the same BY-2 protoplast clamped in the whole cell configuration. At -100 mV the current remained constant after relaxation of negative-going capacitive current spikes (indicated by 'c'), whereas at -375 mV inward current increased again with time due to the formation of field-induced membrane pores. Note that top and bottom current traces recorded within seconds before and after membrane electroporation are nearly identical, indicating that pores deactivate rapidly, and membrane integrity is restored within 9 seconds separating pulse 2 and pulse 3.

Experiments reported here were performed on protoplasts prepared from the tobacco cell line 'bright yellow-2' (BY-2). When the cellular membrane is charged beyond threshold voltages for a few ms, an immediate, ~50-fold increase in membrane conductance is observed. Interestingly, within a few seconds after the field pulse the initial status of the membrane was restored and field-induced pores vanished.

In order to investigate which ions carry the large currents recorded in the electroporated state of the plasma membrane, so-called voltage ramp protocols were imposed on cells in the whole cell patch clamp configuration. From these measurements the reversal potential, i.e. the voltage at which no net current is passing through the pores, can be inferred. The voltage protocol was as follows: The membrane was clamped for 10 ms either to a command voltage of -600 mV to establish the electroporated state of the plasma membrane, or to a voltage that would not induce pore formation (-100 mV or -150 mV). The latter treatment served as a control. Subsequently, the command voltage was rapidly changed at a rate of 40 mV/ms. From the current response to the voltage ramp protocol, current-voltage scans of the cell in the electroporated state and in the absence of field induced pores were obtained and superimposed in one plot. The difference of the two IV curves was ascribed to the contribution of field-induced pores, and the voltage at which both curves intersected (the 'intersection potential') was taken as the reversal potential of currents passing through these pores.

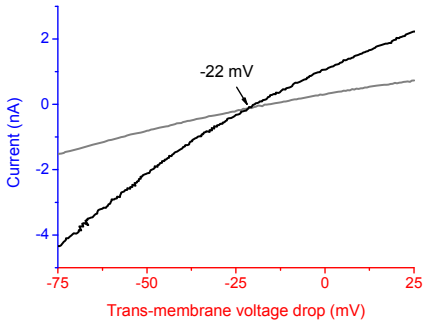

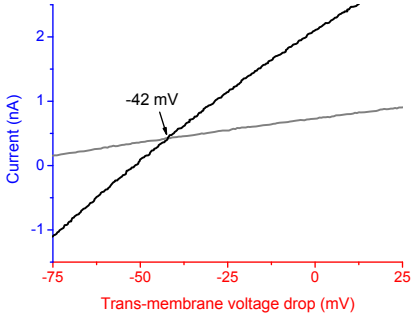

Current-voltage curves obtained from ramp protocols (for details see text) with either 250 mM K+ (top) or Li+ (bottom) in the pipette medium and 12.5 mM K+ in the bath. Voltage ramps were obtained before electroporation (grey traces) and in the electroporated state (black traces). The intersection potential indicating the reversal potential of currents passing through field-induced pores is denoted by arrows. Substituting Li+ for K+ in the cell leads to a negative shift of the intersection potential, indicating that the cellular membrane is more permeable to Li+ than to K+.

Previous work had shown that when an electrolyte gradient was imposed on the membrane, the intersection potential deviated from zero mV and was closer to the Nernst potential of cations (e.g. K+) than those of anions (e.g. Cl- or gluconate-), indicating cation selectivity of field-induced pores. A higher permeability of the porated membrane to K+ compared to the organic cations Tetraethylammonium+ and Tetrabutylammonium+ had demonstrated that cation size matters.

However, the data did not provide a clue whether selectivity was related to the ionic radius, or rather to the hydrodynamic radius of the cation. This was addressed by measuring the relative permeability of Li+ versus K+, since the ionic diameter of Li+ is smaller than that of K+ (0.12 versus 0.27 nm) whereas the hydrodynamic radius is larger due to the large hydration shell surrounding this ion (0.48 versus 0.25 nm). Ramp experiments with either LiCl or KCl (250 mM) in the pipette and KCl in the bath (12.5 mM) were performed to compare the intersection potentials obtained under both conditions. Values of -39±7 mV (n=9) and -24±3 mV (n=18) could be determined with Li^+ and K^+ present in the pipette, respectively. With all other concentration gradients being identical, this difference indicated that pores were more permeable to Li^+ than to K^+. This result provides evidence that the permeability is dependent on the ionic radius rather than on the hydrodynamic radius of the cation. It appears that the hydration shell is stripped off during permeation through the pore.

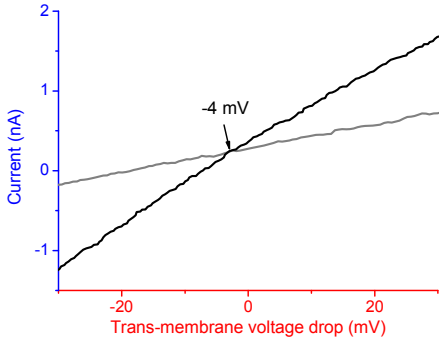

Current-voltage plots obtained from ramp protocols with 253/17.5 mM $CaCl_2$ (pipette/bath), and in the absence of monovalent cations obtained in the electroporated state (black trace) and in the absence of field-induced pores (grey trace). Curves intersect at slightly negative voltages, far more negatve than the Nernst potential of Cl- (+61 mV), indicating that pores are permeable to Ca^{2+}.

Another topic of interest was the permeability of field-induced pores to Ca^{2+}. Indirect evidence for a high Ca^{2+} permeability of the electroporated membrane is available from literature, but no direct measurements have been presented so far. To fill this gap, ramp experiments were performed with monovalent cations in pipette and bath being replaced by Ca^{2+}. An example with 253 mM and 17.5 mM $CaCl_2$ in pipette and bath media, respectively, is shown here. The reversal potential was -6±3 mV (n=7), i.e. slightly negative and strongly deviating from the Nernst potential of Cl^- (+61 mV; calculated from Cl^- activities in pipette and bath, respectively), confirming that pores are permeable to Ca^{2+}. This is also in accordance with pores being predominantly cation-selective.

The NIMEP project – The Non Invasive Microfluidic Electrophysiology Platform

The basic idea of the NIMEP technique is to measure current-voltage relations of individual spherical cells by imposing an external electrical field on a single cell. The current forced through the cell is measured with external electrodes, whereas the voltage drop across the membrane is recorded fluorimetrically by staining the cells with the voltage-sensitive dye ANNINE-6. To this end, the cell is entrapped in a conically formed borehole of a microfluidic structure. This method was patented in 2012 by KIT (patent No. EP 2302375 B1, “Method and device for recording the current voltage curve of a cell”, assigned 12.9.12). Moreover, a ratiometric method was established to measure membrane potentials of tobacco culture cells in the physiological voltage range. Progress could also be made with respect to the design of microfluidic structures to handle and position the cells for NIMEP measurements.

Staff Involved

H. Brüsemeister, Dr. C. Eing, J. Fleig, **Dr. W. Frey**, Dr. C. Gusbeth, Frau DI M. Göttel, K. Leber, E. Menesklou, Dr. G. Müller, K. Paulus, D. Quattrocchi, Frau S. Rocke, Frau Dr. A. Silve, R. Stängle, DI R. Sträßner, **Dr. M. Sack**, **Dr. L. Wegner (KIT-CS)**, R. Wüstner, H. Zimmermann

HGF Program: NUKLEAR

Safety Research for Nuclear Reactors

– Corrosion and Wear Protection for New Reactor Technologies –

To guarantee reliable future electricity supply new types of nuclear reactors are investigated in the frame of GEN IV. The development of technologies required for the safety of fast heavy metal cooled reactors like the Lead Fast Reactor (LFR) is the core area of the work performed at KIT. Especially the development of advanced materials e.g. ODS steels and the investigation and improvements of their compatibility with the proposed coolants are in the focus of this work.

Aim of the institute’s contribution is the development of corrosion barriers to improve the compatibility of new structural materials with liquid Pb or PbBi. Pulsed large area electron beams (GESA - process) are used to modify surfaces such that they satisfy the demands of their targeted environment. Corrosion test facilities for specimen exposure under relevant conditions and for combined loads like fretting or erosion together with corrosion are developed, built and used at the IHM. The conditioning and control of the required oxygen level in the liquid metal is an additional task of the work.

The entire activity is integrated in European and international projects and cooperation, e.g. LEADER, GETMAT, ESFR.

The ELSY project was finished in 2010 and a follow-up project for the development of a Pb cooled fast demonstration reactor LEADER was started in the FP7 frame. The main tasks there are the transfer of the GESA FeCrAl process developed for fuel claddings to heat exchanger geometry,

continuing the investigation of candidate pump materials and to develop oxygen control and purification strategies for a real reactor. In the ESFR project (development of a fast Na cooled European reactor) ideas to engineer Co-free wear resistant coatings were started and will be continued. In the GETMAT project four different tasks have to be fulfilled: corrosion stability of ODS, T91 and mixed welds in Pb; procurement of 12Cr ODS steel bought in Japan, improvement of GESA FeCrAlY process and fretting investigation of fuel clad materials in Pb environment.

The most important results obtained in the reporting period are briefly presented:

Definition of the stability domain of the alumina, grown as protective scale on Fe-Cr-Al-base model alloys during their exposure to oxygen-containing (10^{-6} wt. %) molten lead, in the temperature range 400 - 600 °C:

Fe-Cr-Al alloys are of large interest for practical applications at high-temperatures in reactive environments, thanks to their corrosion resistance, which is due to the formation of an alumina protective scale at the surface. In the energy production industry this alloy system is proposed to be used either as coatings or as bulk oxide-dispersed strengthened steels in the advanced CO_2-free systems using, as working fluid, a heavy liquid metal – HLM - (e.g. Pb, Pb-alloys). However, the phenomena occurring during the Fe-Cr-Al alloys exposure to HLM containing very small amounts of dissolved oxygen is scarcely documented.

Our objective was to define the minimum Al content for the formation of an alumina scale as corrosion barrier on Fe-rich, Fe-Cr-Al-base alloys during their exposure to oxygen (10^{-6} wt%) containing lead at 400, 500 and 600°C.

Based on the state of the art oxide maps concerning oxidation behaviour of Fe-Cr-Al-base alloys at 800 and 1000°C in oxygen atmosphere 10 compositions, belonging to this alloy system, were designed in order to tap the borders of the alumina stability domain.

Eight alloys, Fe6Cr6Al, Fe8Cr6Al, Fe10Cr5Al, Fe14Cr4Al, Fe16Cr4Al, Fe6Cr8Al, Fe10Cr7Al and Fe12Cr5Al, were found to be protected against corrosion in oxygen containing lead, either by a duplex layer (Fe_3O_4 + $(Fe_{1-x-y}Cr_xAl_y)_3O_4$) or by $(Fe_{1-x-y}Cr_xAl_y)_3O_4$, depending on the temperature at which they were exposed.

Two alloys namely Fe12Cr7Al and Fe16Cr6Al were found to form transient aluminas, κ-Al_2O_3 (at 400 and 500°C) and θ-Al_2O_3 (at 600°C), as protective oxide scale against corrosion in oxygen containing lead.

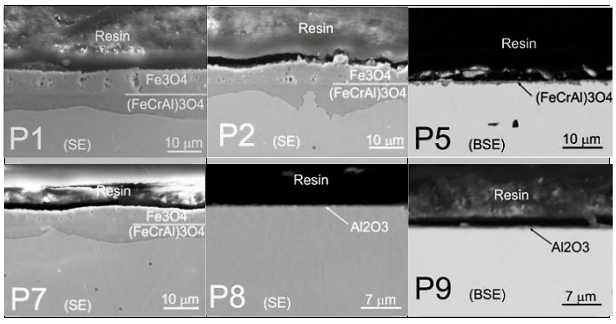

Cross sections of samples made of Fe-Cr-Al-base alloys exposed to oxygen containing liquid lead for 1830 h at 600°C: P1(Fe6Cr6Al),P2(Fe8Cr6Al),P5(Fe16Cr4Al),,P7(Fe10Cr7Al), P8(Fe12Cr7Al), P9(Fe16Cr6Al), P1 to P2, P7 are covered by duplex scale (Fe_3O_4+$Fe(Cr,Al)_2O_4$). P5 is covered by thin $(Fe_{1-x-y}Cr_xAl_y)_3O_4$ layer. P8 and P9 are covered by thin Al-rich scale.

An oxide map illustrating the stability domain of alumina grown on Fe-Cr-Al- alloys when exposed to molten, oxygen containing lead was drawn. The alumina stability domain border shifts with lower temperatures to higher chromium and aluminium concentrations. When (C_{Cr} 12-25 wt%), the minimum concentration of Al required to form alumina scale on Fe-Cr-Al alloys exposed at 400-600°C in molten Pb is:

$C_{Al} = 1.523978 - 0.80805\ (C_{Cr}) + 0.01561\ (C_{Cr})^2$ [wt%].

For the temperature range and exposure times used during the current evaluation, the growth rate of the alumina scale was low. No area with detached scale was observed and no trace of α-Al_2O_3 was detected.

The map includes also additional points extracted from literature and corresponding to alumina forming alloys when exposed to HLMs, which fit very well with our findings.

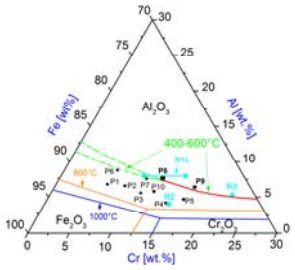

Oxide "map" for the oxidation of Fe-Cr-Al-base model alloys exposed to oxygen contain-ing molten lead, in the temperature range 400 – 600 °C, containing also data from literature: line at 800 °C, line at 1000°C (in oxygen atmosphere), R1s, R2 and R3 (in lead and lead-bismuth, respectively).

Welds:

In the frame of GETMAT a second run of exposure tests with welds were conducted. Friction stir welds with and without heat treatment, one explosive - and one electromagnetic pulse weld were tested at 550°C in liquid lead with an oxygen content of 10^{-6}wt%. Exposure time was for the frictions stir and explosive welds 1342h and for the electromagnetic pulse weld 2131h. The friction-stir welds with and without heat treatment showed on the entire surface a multilayered oxide consisting of magnetite, spinel and inner oxidation zone (IOZ). While the friction-stir welds without heat treatment show nearly no large changes in the microstructure between the original steel, heat affected zone (HAZ) and the weld, the specimen with heat treatment exhibit larger grains in HAZ. This leads to slower oxygen diffusion into the steel and therefore to a smaller inner oxidation zone. In the case of corrosion a better behavior due to the heat treatment is in this case questionable. No negative effect due to the welding was found for the explosive weld. A < 1µm thin oxide was formed on the weld region, while the oxide layer on the original materials was around 14 µm. Specimen manufactured using electromagnetic pulse welding have at the outer side of the weld a gap between the end capsule and the tube. During exposure the known oxide consisting of magnetite, spinel and diffusion zone was growing in the gap without Pb penetration. From previous test it is known that in small gaps Pb does not penetrates. However, the behavior of the gap and the weld should be tested after longer exposure times.

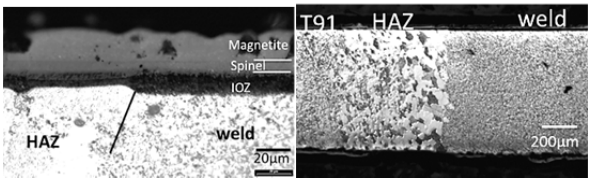

Friction-stir weld with heat treatment: Left: microstructure of the 3 zones, original T91 steel, heat effected zone (HAZ) and joining region; Right: border of HAZ and weld;

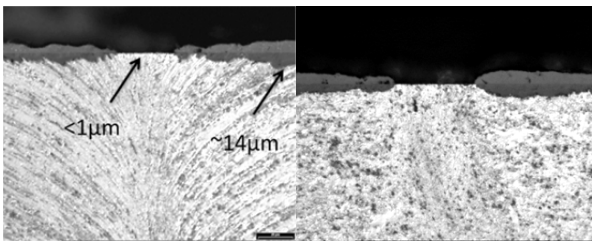

Micrograph (LOM) after etching of the 14Cr ODS steel joint by explosive weld joining cut in rolling direction (left) and perpendicular to the rolling direction (right);

Fretting of fuel clad materials in liquid Pb

The extensive experimental campaign of fretting tests was contiuned for a PhD work in the frame of the GETMAT project. In particular, fretting corrosion tests in accelerated but still reactor relevant conditions (concerning temperature and oxygen content of Pb) were performed to investigate the role of the main affecting parameters, such as temperature, amplitude of the slip and applied load. Three different materials were selected among the candidate alloys for lead cooled nuclear systems, namely: f/m steel T91, austenitic steel 15-15Ti and GESA treated T91 (after LPPS (Low Pressure Plasma Spray) of FeCrAlY powder). The interaction of the fretting process with the corrosion mechanisms occurring in liquid lead and with the protecting oxide scale/corrosion barrier required for reactor components was also matter of study. Based on the concept of fretting maps all obtained data was analysed with respect to the specific fretting coefficient. This data was then applied to prognost parameters like load and amplitude at which tolerable fretting corrosion is expected.

The experimental outcomes underline the fundamental role of the temperature in the fretting process and highlight that temperature has a remarkable influence on the fretting behaviour of the investigated alloys already after 150 hours ($5.4 \cdot 10^6$ cycles). As shown below, increasing the temperature from 450 to 550 °C, the volume loss increases by a factor 4, 2.2 and 1.2 for T91, 15-15Ti and GESA-T91 respectively. The temperature increase enhances significantly the fretting wear, especially for T91 and 15-15Ti, which at 550 °C, already after 150 h, are affected by 30 and 22% of fretting penetration respectively. GESA-T91 is far less susceptible to the temperature increase and the fretting penetration is only 4%.

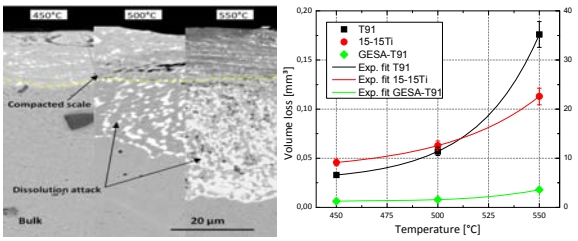

Left: SEM images in BSE mode of 15-15Ti specimens after fretting tests in Pb at 450, 500 and 550 °C for 150 h.
Right: Graph of fretting depth versus temperature for friction pairs of T91, 15-15Ti and GESA-T91.
Test parameters: 75 µm, 50 N, 10 Hz, 150 h, $5.4 \cdot 10^6$ cycles, 10^{-6} [O] wt%.

The exponential law fitting the evolution of the volume loss with the temperature is due to the corrosion processes occurring in liquid Pb (oxidation and dissolution) that are diffusion dependent and hence temperature dependent according to an Arrhenius type relation. The significant increase of the T91 curve (especially at T > 500 °C) can be associated with the extensive oxidation (oxidation enhanced fretting) affecting this steel at 550 °C with 10^{-6} wt% of oxygen. Composition and ferritic/martensitic structure of T91 steel together with the high temperature (550 °C) favour inwards oxygen diffusion and outward metal cations diffusion. As a result, T91 steel is affected by extensive oxidation characterised by the formation of a thick duplex oxide scale and of an internal oxidation zone. Although in the first stage of fretting the fast growing oxide scale might favour a sort of lubricating action, in the long run it likely enhances the material removal. Indeed, oxide scales are less ductile than the original alloy and the thicker the oxide scale the more considerable is this aspect. Moreover, thick oxide scales are generally unstable and tend to spall off. On the contrary, composition and austenitic microstructure of 15-15Ti steel avoid extensive oxidation (at the tested temperature and oxygen content). Up to 500 °C, the dissolution affecting 15-15Ti and the less pronounced oxidation of T91 are likely the reason behind the higher fretting susceptibility of 15-15Ti.
The clear corrosion fretting interaction is also demonstrated in experiments performed in Ni saturated Pb. Volume loss for friction pairs of 15-15Ti tested in Ni-enriched Pb is reduced, for all the exposure times, of about 50 % compared to the results achieved in pure Pb. For 15-15Ti tested in Ni-enriched Pb also the fretting depth is decreased by 54 % (from 47 to 22 µm) after 150 h and by 41 % (from 110 to 66 µm) after 930 h. Besides, friction pairs of 15-15Ti tested in Ni-enriched Pb are even less susceptible to fretting wear than T91. For example, fretting depths plotted for 15-15Ti are from 10 to 40 % lower than the ones measured for T91.

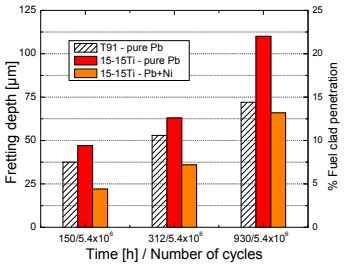

Volume loss for friction pairs of 15-15Ti submitted to fretting test in Ni enriched lead and in pure lead. The values of T91 are also reported for comparison. Test parameters: 75 µm, 50 N, 10 Hz, 450 °C, 10^{-6}wt% [O].

The presence of Ni dissolved in liquid Pb has a remarkable influence on the corrosion behavior of the friction pairs of 15-15Ti. The dissolution attack affecting the bulk material after the fretting test of 930 h at 450 °C and 10^{-6} wt% of oxygen in solution is deeper and more extended in the case of the test performed in pure Pb than for the test performed in Ni-enriched Pb. In pure Pb, dissolution reaches 20-30 µm and is extended on most of the fretted surface. Conversely, in the case of the tests performed in Ni-enriched Pb, the dissolution attack is visible only in few localized places and the maximum dissolution depth is around 15-20 µm. The dissolved Ni clearly reduces the activity for dissolution and by that an improved fretting behaviour is observed.

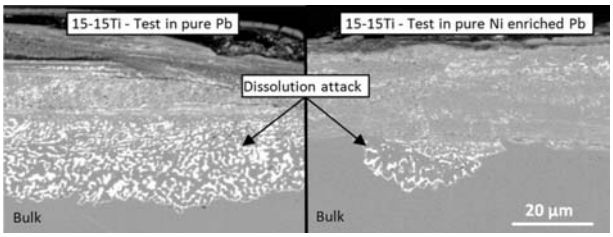

SEM image in BSE mode of the dissolution attack and the compacted scale characterizing friction pairs of 15-15Ti after fretting test of 930 h at 450 °C and 10^{-6} wt% in pure Pb (left side) and Ni-enriched Pb (right side).Test parameters: 75 µm, 50 N, 10 Hz.

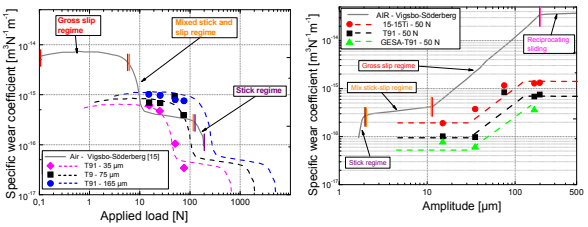

Specific wear coefficient as function of applied load (left) and amplitude (right); fretting regimes are indicated.

The non-monotonic relationship (presence of a turning point) between fretting wear and load indicates a change in the fretting process that is most probably related to a change in the fretting regime. To investigate this aspect, the specific wear coefficient is plotted as function of the applied load for imposed amplitudes of 35 (pink diamonds), 75 (black squares) and 165 µm (blue circles). For friction pairs of T91 (black squares), 15-15Ti (red circles) and GESA-T91 (green triangles), the variation of specific wear coefficient with the amplitude is also shown above together with the curve specific wear coefficient – amplitude for fretting in normal atmosphere (grey line) and fixed applied load.

Fretting in liquid Pb can be considered as a type of fretting occurring at high temperature in lubricating conditions. As a consequence, the fretting wear regimes existing for fretting in air and lubricated fretting are applicable also to the case of fretting in molten Pb. For this reason, a curve specific wear coefficient – load for fretting in normal atmosphere with fixed imposed sliding amplitude is plotted (grey line) for comparison. Adapting this curve to fretting in molten Pb with sliding amplitude of 35 µm, it can be noticed that the experimental points seem to follow the trend proposed. The shift towards lower values of specific wear coefficient is due to the lubricating action of liquid Pb together with the different testing conditions (e.g. amplitude tested > 90 µm) and materials (only austenitic steels) of tests in air. Adapting the curve of reference (grey line) to the other imposed amplitudes (75 and 165 µm), it can be supposed that a load increase tends to bring the contact conditions towards the stick regime, where the specific wear rate (and the fretting wear) is minimized.

The understanding of the amplitude effect on the fretting process was deepened through tests carried out on all the materials under investigation with constant load (50 N) and amplitude variable between 15 and 190 µm. A general increase of fretting wear with amplitude was noticed. Such increase, as explained for fretting in air and as suggested by the variation in fretting depth and specific wear coefficient, is not merely due to an increase of the fretting affected area but must be related to change in the fretting regime. For amplitudes shorter than 35 µm, for all the materials under investigation the specific wear coefficient does not change significantly whereas a significant transition occurs for larger amplitudes. This indicates most likely a change of fretting regime roughly around 35 µm which, according to the reference curve, is supposed to be from gross slip to mixed stick-slip regime. Thus, the sudden increase of fretting wear for amplitudes larger than 35 µm is most likely related to a change of fretting regime.

The influence of amplitude and load on the fretting process can be represented also in 3D fretting maps. These 3D maps were constituted starting from the experimental results and adding to them expected values of specific wear coefficients that are qualitatively predicted according to the expected fretting regimes for friction pairs of T91, 15-15Ti and GESA-T91; full circles correspond to values experimentally measured; empty circles represent the extrapolated values based on fretting regimes interpretation. In this way, a wider overview of the wear process can be provided. In a 3D fretting map, the specific wear coefficient values for friction pairs of 15-15 Ti (red circles) and GESA-T91 (green circles) are compared to the ones of T91 (black circles).

In these fretting maps, it can be clearly noticed that for short amplitudes (e.g. < 35 µm) and high loads (e.g. > 50 N) the fretting damage is minimized. However, in the case of unavoidable large amplitudes (> 75 µm), low loads (< 25 N) can also reduce the fretting damage. Due to the higher fretting and corrosion susceptibility, the experimental points for 15-15Ti are shifted towards higher values of specific wear coefficient. On the contrary, the high wear and corrosion resistance of GESA-T91 leads to a shift towards lower values of the measured specific wear coefficient.

As an alternative comparison approach, the penetration rate can be plotted versus the work rate. Such graph can be used to predict fretting penetration after a certain time. Fretting conditions experimentally tested lead to penetration rates unacceptable for real applications. Even for the lowest measured penetration rates (resulting from an applied load of 50 N and a sliding amplitude of 15 µm), which for 15-15Ti, T91 and GESA-T91 are 0.063, 0.053 and 0.039 µm/h respectively, the penetration limit would be reached after about 800, 950 and 1300 h. Such timing does not meet the targeted operating lifetime for fuel elements, which is about 25000 h.

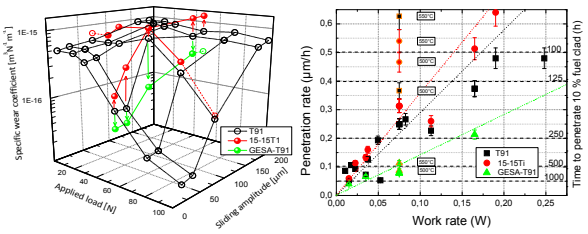

Left: 3D fretting map for friction pairs of 15-15Ti, T91 and GESA-T91. The specific wear rate (z axis) is plotted versus load (axis-x) – amplitude (axis-y) combinations. Test parameters: 450°C, 10^{-6} wt% oxygen.

Right: Penetration rate vs work rate for different fretting conditions in molten Pb for T91, 15-15Ti and GESA-T91.

The fretting tests carried out in this work can be interpreted as a kind of accelerated test that are useful to define the fretting regimes, to extrapolate data for predicting the long time fretting behavior and to provide to the designers indications to prevent a severe fretting damage. A close analysis of the experimental outcomes indicates that it is possible to comply with the mentioned operating requirements by considering the following aspects:

- Fretting is a self mitigating process – data considered from run in period
- Fretting regime required is stick regime ➔high load >75N small amplitude <15µm
- Pre-oxidation lower fretting wear by up to 50%
- Use of surface aluminized material

Characterization of the thermal properties of the oxide scales, grown on T91 steel during the exposure to oxygen-containing (10^{-6} wt%) molten lead

The transfer of the thermal energy from the heat source to the working fluid is the basic process in the energy production industry. This transfer is taking place across a well-defined boundary. The changes in the composition, structure or topology of this boundary will affect the heat transfer.

T91 steel is a ferritic-martensitic steel (~9 wt% chromium) intended to be used for the construction of the heat-exchangers working at one side in HLM.

Our objectives were to determine (i) the thermal properties of the oxide scale grown on T91 steel during the exposure to oxygen-containing (10^{-6} wt%) molten lead and (ii) the thermal contact resistance of the T91/Pb system.

The measurement of the thermal diffusivity (rate of heat transfer) was performed using "laser flash" technique. The technique consists in supplying an energy input on one side (using a high intensity laser energy pulse) and measuring the energy output (using an IR detector) versus time at the other side.

The measurements were performed on samples made of non-oxidized T91, oxidized T91 (scale thickness: ~30 µm) and T91/Pb system.

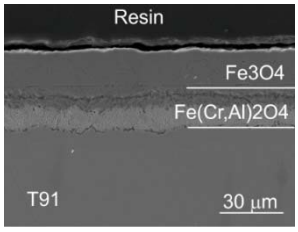

Cross sections of samples made of T91 steel exposed to oxygen containing liquid lead for 2000 hours at 550°C

The figure below contains the values of the thermal diffusivity and thermal conductivity determined at different temperatures and compared with data from literature (L.A. Chapmann et al, NPL Report DEPC-MPE 018 2005).

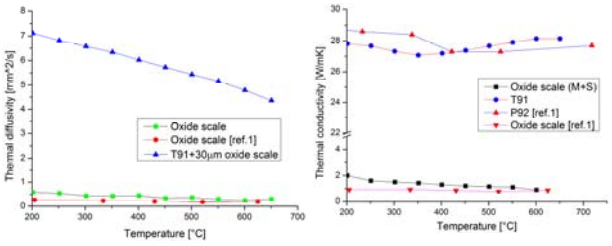

Thermal diffusivity (left) and thermal conductivity (right) of T91 and the oxide scale with a thickness of 30 µm.

The thermal contact resistance at the interface between T91 (with nanometer size oxide scale) and liquid Pb was also determined. The thermal contact resistance depends on the quality of the physical contact between steel surface and liquid lead, which is given by the surface energy between the system elements.

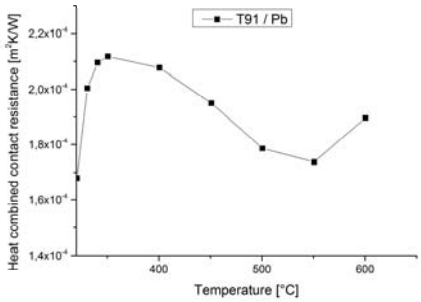

Heat contact thermal resistance of T91/liquid Pb system.

FeCrAlY modified coating for tensile tests

GESA modified FeCrAlY surface layers are known to successfully protect T91 steel from corrosion attack in heavy liquid metals (Pb and Pb/Bi) containing an appropriate amount of oxygen. However, the influence of the FeCrAlY layer on the mechanical properties of the specimens is still under debate. First tensile tests showed improved creep-to-rupture behavior; the creep strength reduction caused by heavy liquid metals is mitigated by the presence of a protective surface layer. Further creep tests are now planned to support or otherwise these preliminary, promising results.

In the reporting period, tensile specimens of T91 steel coated with GESA modified FeCrAlY surface layers were manufactured for testing later on. After deposition of FeCrAlY by LPPS, the specimens were mounted in the treatment chamber of the GESA facility and treated by a planar pulsed electron beam. By subsequent rotation and repeated treatment a homogeneous re-melting of the FeCrAlY layer could be achieved. The tensile specimens were treated as described at two positions to cover their full length.

To allow for later analysis of any changes due to tensile testing, the specimen surfaces were thoroughly analyzed after preparation (prior to the tensile test). Scanning electron microscopy (SEM) was used together with energy dispersive X-ray analysis (EDX) to capture the general aspect and specific features of each specimen in the three regions (left, middle, right) marked in the figure.

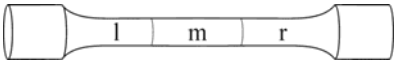

Tensile specimen with three regions

GESA IV beam homogeneity

Influence of self induced magentic field on function of GESA IV

One design specific of GESA IV is the axial current flow along the anode that is most commonly also the specimen. At required energy densities this results in a strong self induced magnetic field with large axial and radial gradients. This magnetic field influences not only the energy distribution along the target but the entire functioning of the accelerator. Especially regarding the further improvement of the GESA IV towards an increasing of the treatment area, the influence of the self induced magnetic field has to be considered.

To investigate the influence of the magnetic field, axial electron currents were measured using specific collectors. Direct beam and reflected electrons receive an axial component of velocity by their interaction wih the magnetic field. The direct beam electrons are deflected from the periphery to the center of irradiation and the reflected ones vice versa. The current collectors are located far out of the irradiation area to minimize any influence by direct beam electrons. At a symmetric set-up the current flow is as expected identical in both axial directions.

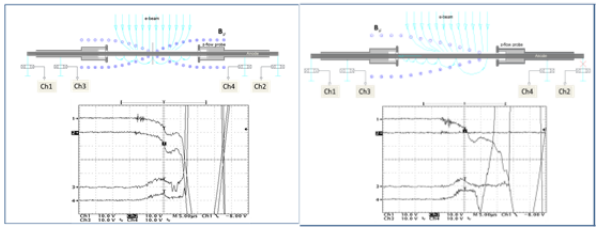

Measurement scheme and signals from symmetric and asymmetric anodic current flow

The collector signal (Ch3 and Ch4) starts simultanously with the pulse and reaches its maximum while the anode current (Ch1 and Ch2) is still rising. Such behavour indicates a magnetic isolation of the reflected electrons. The electrons start in the weak field region and move cycloidally into the stronger field region at the periphery. With increasing magnetic field the radius of the electron paths is decreasing, so that, at a specific anode current (field strength), the reflected electrons are fully depressed and can't reach the collector. An asymmetric anodic current flow re-distributes the magnetic field. In such case measurement signals are generated by different electrons: Sensor Ch4 (right side) by deflected direct beam electrons - Sensor Ch3 (left side) by reflected electrons. The isolation of the reflected electrons is similar to the symmetric configuration. The asymmetric field distribution accelerates plasma out of the irradiation area into the field free regions. Therefore, the right current collector (Ch4) is short circuited to the anode relatively early. The measurements show that the self induced magnetic field influences the behaviour of the reflected electrons strongly. Which configuration results in the best performance has to be investigated in detail.

Measurement of azimuthal energy distribution at GESA IV

The measurement of the GESA IV electron beam homogeneity is one of the most important issues for GESA IV optimization. Therefore, a dedicated test set-up was developed that allows the measurement via X-ray formation using a ring shaped szintillator disc (LuYSiO:Ce) mounted on glas fibre and connected to a high speed camera. A 2mm thick Pb absorber serves to increase the resolution. To achieve an optimized azimuthal resolution the szintillator ring was manufactured with the achievable minimal width (0.5 mm) in house. Parasitic signals from the opposite side are weakened by the Pb absorber placed in the inner ring.

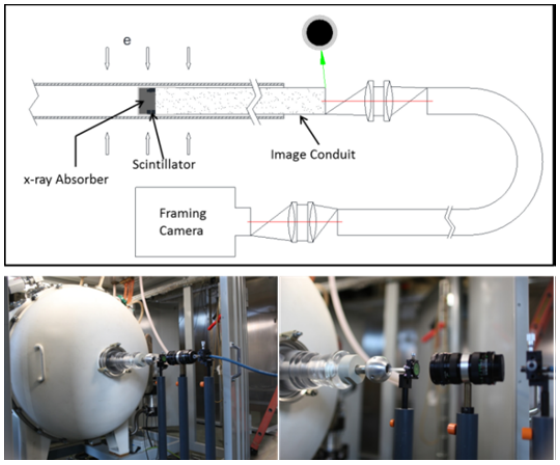

Scheme and photograph of measurement set-up

The szintillator signal is strong enough to distinguish between „real signal" and parasitic fluoresence of glas fibre and projection lenses. Intensity variations that depend on the azimuthal direction are visible, which can be definitely related to inhomogeneities of the electron beam.

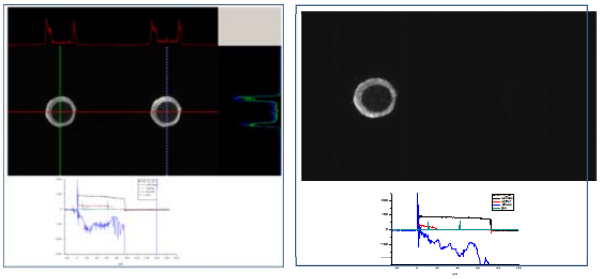

Szintillator signal of typical GESA IV pulses

Remarkable are pulses with missing szintillator signal. When the cathode potential reaches the grid potential by simultanously still high target current no X-ray signal is detected by the szintillator ring. One possible explanation is inhomogeneous cathode plasma; the gap between cathode and grid is short circuited by the plasma. If this happens only localy at the grid, the entire emission surface beside the short circuit area will be excluded. In consequence the anode current is also localized in this area.

Materials and oxygen transport and control in heavy liquid metal cooled subcritical systems (MYRRHA)

Long-living high-level radioactive waste from existing nuclear power reactors should be transmuted in short-living radio nuclides using fast neutrons provided by a spallation target in an accelerator driven subcritical system or by a fast nuclear reactor. The objective is to reduce the final disposal time of high-level radioactive waste (plutonium, minor actinides) from some 10^6 years down to about 1000 years. Lead (Pb) and lead-bismuth (PbBi) are foreseen as spallation-target and coolant of such devices.

The aim of the institute's contribution is the development of a suitable corrosion protection especially for parts under high loads like fuel claddings or pump materials in contact with liquid Pb or PbBi. Pulsed large area electron beams (GESA) are used to modify the surface of steels such that they fulfill the requirements of their surrounding environment. Corrosion test stands for exposure of specimens under relevant conditions are developed and operated. Test facilities for combined loads like erosion and corrosions and fretting corrosion were developed, built and operated. Conditioning the lead with regard to its oxygen concentration and the transport of oxygen in PbBi are additional aspects of the work.

All tasks are embedded in European and international projects and cooperation e.g. MATTER, SEARCH.

The most relevant results obtained in the reporting period are briefly presented:

Corrosion tests of different austenitic steels (MATTER)

Exposure tests with austenitic steels were tested for the EU project MATTER. The steels 316 and the 15-15Ti steel 1.4970 as rod and tube material were tested up to 5000h in PbBi with an oxygen concentration of 10^{-8}wt% as well as 10^{-6}wt% and temperatures of 400, 450 and 500°C. It was shown that the oxidation and dissolution is very similar for the three specimens. With an oxygen concentration of 10^{-8} wt% at 400 and 450°C oxide scales protect the steels up to 5000h, at 500°C dissolution attack was detected after 5000h. While at 10^{-6} wt% at 400°C thin Cr-Oxide layers were growing on the 316 steel, multilayered, thick oxide scales grow at the higher temperatures of 450 and 500°C on this steel. The 1.4970 rod specimen showed a slightly reduced oxidation and reduced dissolution attack in comparison with tube material. In comparison with the 316 steel, the IOZ was more pronounced on the 1.4970 steels due to the smaller grain sizes of the 1.4970 materials.

The experiments showed that if a multilayer oxide is formed due to the diffusion of Fe and Cr, a Ni enrichment under the oxide layer occurs. This can foster a dissolution attack if the oxide layer spalls off especially at an oxygen concentration of 10^{-8}wt% in the liquid metal. Therefore longer exposure tests at this oxygen concentration at 400 and 450°C are running.

Optimisation of the GESA process:

The remelting of metallic specimens using intense pulsed electron beams (GESA) results in a more or less pronounced

waviness of the surface, which may be disadvantageous for some applications. To control the surface topography, basic understanding of the involved physical processes is required. Fast in-situ optical diagnostics performed previously showed the formation of bubbles, up to 300 µm in diameter, around or shortly after melting and their subsequent disappearance prior to beam termination. Around beam termination, at the highest surface temperatures, intense evaporation takes place. The vapor cloud formed above the target surface is partly ionized by beam electrons and plasma is ignited. After beam termination, the target surface temperature decreases rapidly, evaporation ceases, and the plasma decays within a few microseconds.

In the reporting period, in-situ diagnostics was continued and supplemented by a stroboscopic imaging technique and pyrometry.

For the stroboscopic illumination of the target, a laser beam was modulated with the time interval between flashes (20 to 100 µs) much longer than the flash duration (~100 ns), see figure below. The image of the target was recorded by a streak camera, where the width of the observation slit and the streak speed were chosen such that the final micrograph was composed of consecutive, non-overlapping snapshots. In the figure typical micrographs with stroboscopic illumination are shown, recorded prior to, during, and after electron beam irradiation of a stainless steel target. The image taken during exposure is synchronized with the accelerating voltage and current waveforms of the beam and a pyrometer measurement of the target surface temperature. Motion of the liquid surface is visible in this micrograph until solidification occurs. On a larger time scale (time between recording of middle and right image), a further slight deviation of the surface pattern is observed, which can be explained by thermal shrinkage due to cooling.

Using the in-situ diagnostic tools set up in the last year, systematic experiments are now planned to gain more detailed information about the involved processes.

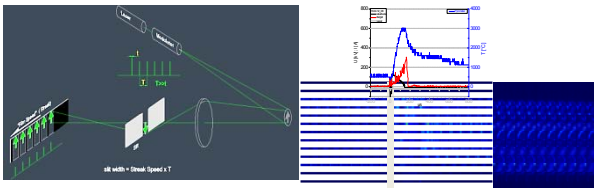

Stroboscopic imaging: (left) experimental setup, (right) micrographs prior to (left), during (middle), and after (right) electron beam irradiation. The micrograph in the middle is synchronized with the beam evolution and pyrometer measurement.

Accompanying the experimental work, simulations of intense electron beam treatment of metal targets were further investigated in the reporting period. The ultimate goal of this study is the numerical prediction of melt motion in order to finally understand and interpret the topography found on the target surface after treatment.

1-D heat transfer simulations were performed and closely compared with experimental results of GESA treated stainless steel, copper, and aluminum targets. For each sample, material loss due to pulsed electron beam treatment was measured and compared with the numerical prediction of evaporation. As shown in the left figure below, material loss is systematically underestimated in the simulations. This might be explained by bubble formation and ejection of droplets observed in the experiments, which are not accounted for in the 1-D simulation code ORION. Then, a cross section was cut from each sample, embedded in resin, grinded, and polished. After a final metallurgical etch the depth of the melted layer could be determined with optical microscopy. The experimental results are in very good agreement with the numerical predictions.

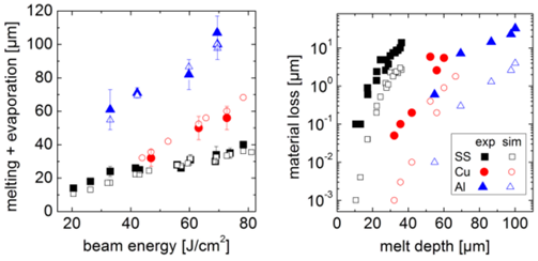

Experimental and simulation results of pulsed electron beam treatment: (left) material loss is underestimated in simulations, (right) melting depth is in very good agreement.

In addition to the code ORION used so far, the code MEMOS was applied to characterize GESA treatment of metal targets. Among further advantages such as 2- and 3-D geometries, MEMOS includes computation of melt motion based on hydrodynamic equations. In the graph below, heat transfer results from ORION and MEMOS are compared with a pyrometer measurement of the surface temperature during GESA treatment of stainless steel. Both simulation codes predict faster initial temperature rise and higher maximum surface temperature than measured in the experiment. Compared to ORION, the code MEMOS predicts more intense evaporation and a lower maximum surface temperature. Thus, MEMOS meets the experimental results more closely than ORION. The main difference of the two simulation codes is the handling of the phase transition: MEMOS solves the moving boundary problem; no melting and solidification plateaus exist.

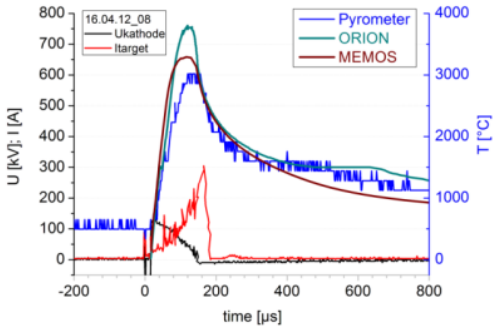

Surface temperature of stainless steel during pulsed electron beam treatment: pyrometer measurement and simulation results from ORION and MEMOS.

Oxygen transport measurements in liquid PbBi (SEARCH)

Within the SEARCH project a dedicated facility to measure adsorption, entrainment of oxides in heavy liquid metals and mass transport phenomena in liquid metals was designed. This facility will be used to measure the transport of oxygen and of metal (oxide) particles. This work was accompanied by CFD calculations performed by colleagues of the IKET already in the design phase. The measurement results finally will be used to qualify and optimize the CFD codes with respect to particle (oxide) transport into and in the liquid PbBi.

The 1st design was changed for an improved and easier experimental handling. Now, three pots, one for conditioning, one for oxgen transport experiments and one for a sacrificial Ni probe (transport of dissolved metals) are selected as final

design. To gurantee a stable PbBi flow over longer times it was decided and proven by CFD calculations to achieve an asymmetric flow pattern, by the use of three orifices at the pump channel. This configuration was fixed and based on CFD calculations the location of the needed dead zone area and of the oxygen sensors were decided. To ensure pure diffusion transport a small box (blue) was implemented close to the wall at the bottom of the pot. Four oxygen sensors, three in the flow to measure the convective oxygen transport and one in the above described box for diffusion transport will be implemented. To measure the PbBi velocity an UDV (ultra sound Doppler velocimeter) will be used at a position determind by CDF calculations. The measurement signals (velocity and oxygen) will be used to assess and optimize the existing transport codes for liquid metals.

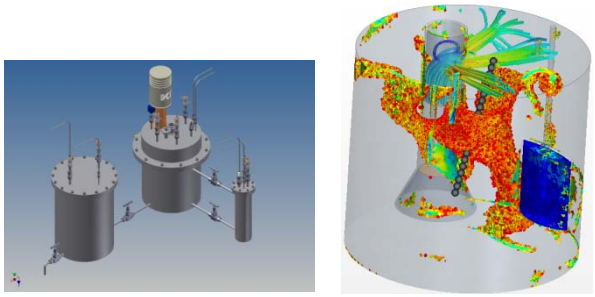

Scheme of actual set-up (right) and CFD calculations of PbBi flow patterns (jets (green, blue) and dead zone (red)).

Staff involved
DP. W. An, R. Beckers, M. Eng. Mattia DelGiacco, Fr. Dr. Renate Fetzer, Fr. Dr. A. Heinzel, DI (FH) F. Lang, Dr. A.Jianu, Dr. G. Müller, Dr. G. Schumacher (Gastwissenschaftler), A. Sivkovich, **Dr. A. Weisenburger**, DI (FH) F. Zimmermann

HGF Program: Energy

Rational Energy Conversion (REUN) –

Major activities in 2012 were related to different BMBF funded joint projects.

– MACOS- Microwave Assisted Ablatation of Contaminated Concrete Surfaces –

The target of this BMBF funded joint project is a design study for a microwave technology that may be used for the ablation of contaminated surfaces, e. g. of nuclear power plants. In collaboration with the Institut für Massivbau und Baustofftechnologie (IMB) a test stand has been developed and built. This system consists of an 10 kW magnetron to which a circulator, an auto-tuner and a WR-340 waveguide based microwave antenna is attached. It is used for systematic variation of process and materials parameters to provide a deep understanding of the ablation.

Result of an ablation experiment. Concrete was exposed to microwave radiation at f=2.45 GHz and an RF power of 8 KW for about 15 s.

The experimental investigation is accompanied by mathematical modeling and simulation. Using a multi-physics model the basic physical principles of the ablation of concrete, in particular the thermal stress and pore pressure shall be understood. The mathematical model includes the partial differential equations for the electromagnetic field and the thermal field inside the concrete coupled with the elastic model describing the thermal stress and pore pressure. It is a multi-scale model acting on different length scales. Simulation results performed with COMSOL Multiphysics are shown in the figure below.

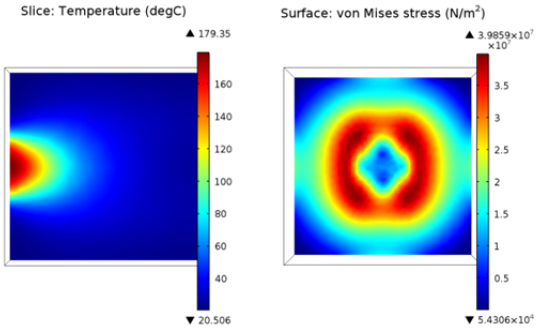

Simulated temperatures and corresponding von-Mises stresses after 20 s of Microwave heating (8 kW RF power).

The detailed knowledge of the dielectric permittivity of concrete with respect to frequency, temperature, moisture content and composition is mandatory to get proper simulation results. Dielectric parameters, such as dielectric constant and loss factor are derived by doing low power measurements with a network analyser and a coaxial probe. Different materials compositions of concrete have been measured. Homogenization methods and electromagnetic mixing rules are used to model the permittivity of the concrete. As can be seen in the following graphs the dielectric properties of concrete are significantly influenced by the moisture content.

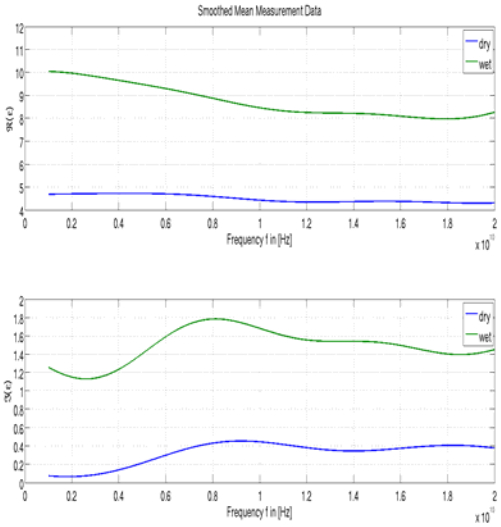

Smoothed dielectric constant (top) and dielectric loss factor (bottom) for dry and wet concrete at room temperature.

– Microwave heating of catalysts for CO_2 reduction –

The BMBF project CO_2RRECT (CO_2-Reaction using Regenerative Energies and Catalytic Technologies) is about the reduction of CO_2 to CO as a precursor for chemical industry using predominantly regenerative energy. The

corresponding chemical reactions, either RWGS (reverse water gas shift) or CO_2 reforming are endothermic. Hence energy in the form of heat has to be supplied continuously.

Using microwaves as heating method has the potential to make this described process significantly more energy efficient. Microwaves penetrate into the catalysts support, getting the heat directly to the location where the reaction takes place, while with conventional heating the heat has to be supplied from the outside, reaching the location of the reaction only by heat conduction and thereby limiting the flow capacity.

A bench-scale microwave applicator, shown in the following sketch was designed. It consists of a quartz tube inside a wave guide with the catalyst support embedded inside. A gas consisting of the reactants flows through the tube with a temperature above 800 C while the catalyst support is heated by the microwave. A resonant approach is used to achieve a high efficient process. The electromagnetic and thermal response of the applicator is simulated using COMSOL Multiphysics tool with the RF and Heat Transfer module considering the mutual coupling between the electromagnetic and thermal field.

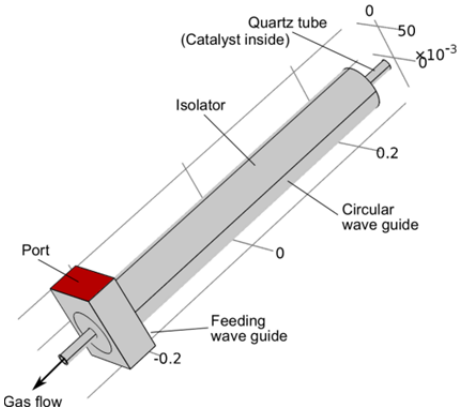

Model of the microwave applicator.

The electric field shows a standing wave pattern that consists of several maxima and minima. This field causes a temperature distribution after a heating time of 70 s as shown in the following. The hot spots give a clue where to place the catalyst, i.e. the chemical active parts.

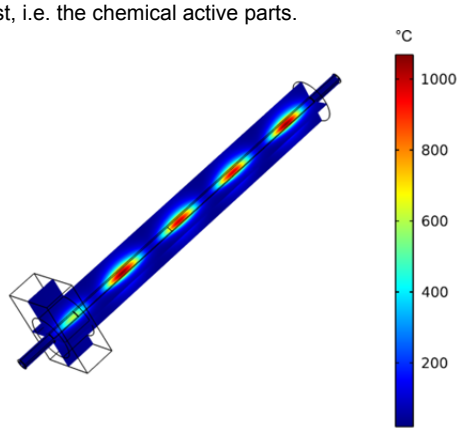

Temperature distribution inside the microwave applicator. The "hot spots" are inside the catalyst support.

This temperature distribution correlates to the electric field standing wave pattern. Due to the gas flow the temperature distribution is homogenized because the gas itself transports the heat along the path by convection. Thereby the hot spots of the temperature distribution get blurred. A velocity of 2 m/s of the gas inside the quartz tube results in the temperature distribution shown next.

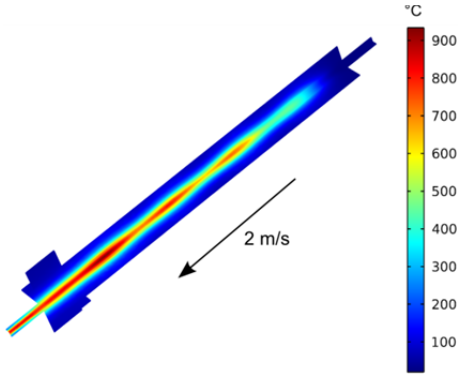

Temperature distribution inside the catalyst support with the presence of a gas flow.

This reactor currently is successfully tested by one of the project partners. For further improvement of the field and temperature homogeneity inside the catalyst, a new applicator design is currently under development.

– Antennas for the Microwave Feeding System of HEPHAISTOS –

Within the BMBF project FLAME one important part is to optimize the microwave feeding system of the HEPHAISTOS oven. The antenna system is coupling the microwaves from the RF sources (magnetrons) into the microwave oven. For the design of the antennas it is mandatory that the antenna system has a sufficient efficiency. More than 99% of the power should be radiated into the oven. As a further requirement the field should be evenly distributed inside the oven. This can be achieved by the proper design and arrangement of the antenna system.

A single antenna consists of a slotted waveguide. Each slot radiates a part of the total microwave power. This approach avoids a single concentrated feed and therefore increases field homogeneity. The slotted waveguide antenna is shown in the figure below.

The slots are covered with a radome made of phlogopite to protect the antenna from any dirt and liquids. The antenna is also designed for the usage inside of a hybrid oven (microwave in combination with convectional heating). For this application temperature resistivity up to 300 C and air-tightness are important requirements. The radome is taken into account in the simulation. It has a significant influence on the antenna performance.

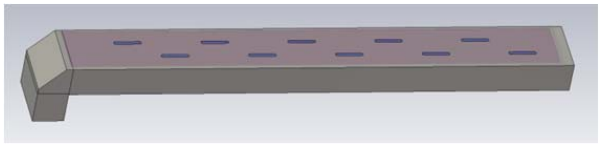

Sketch of a slotted waveguide antenna with 10 slots and a radome of phlogopite

The performance of the antenna is characterized by two properties. First the matching factor S_{11} which is shown next. The matching is better than -20 dB in a broad frequency range around 2.45 GHz. This means more than 99% of the power is radiated.

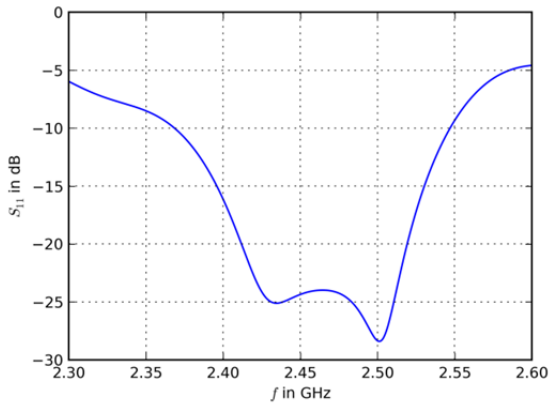

Calculated Matching factor of the antenna.

The second important property is the efficiency which includes coupling of the radiated power to a load inside the oven. To measure this, a special test setup has been constructed which resembles the oven chamber. The main item is a water load inside to measure the calorimetric heat, i.e. the part of the microwave power that is eventually dissipated to heat. The designed antenna holds an efficiency of 75% which is an excellent value compared to previous designs.

A second activity in the FLAME project is related to the development of a microwave heating tool for pultrusion of carbon fiber reinforced profiles. The motivation for the use of microwave technology in this application is a fast and volumetric heating of the thermoset matrix that may allow an energy efficient processing at increased pultrusion speeds. A compact tool has been developed, transparent to microwave and strong enough to hold the tribological and mechanical stress that appears during the pultrusion process. This tool has been successfully tested at the ITV Denkendorf as shown in the following picture.

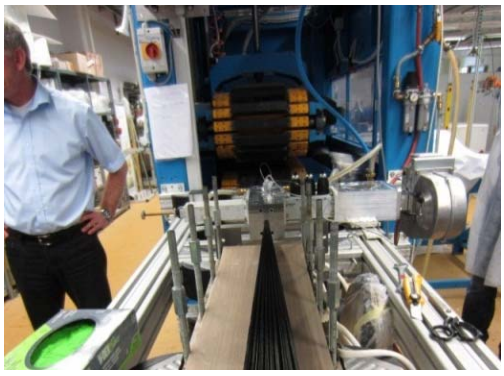

Running experiment for microwave assisted pultrusion of endless CFRP rods with 9 mm in diameter.

– Dielectric measurements –

Since any microwave process is governed by the microwave field and the dielectric response of the material, knowledge of electromagnetic theory and dielectric properties is essential to optimize the microwaves systems and processing of materials. Therefore various test sets for dielectric measurement are currently under development. Beside the reflection method using a coaxial probe as shown before, a transmission reflection method base on the WR-340 waveguide has been developed (see next photo). This allows temperature dependent dielectric measurements up to 200°C for dielectric materials with medium and high loss factor.

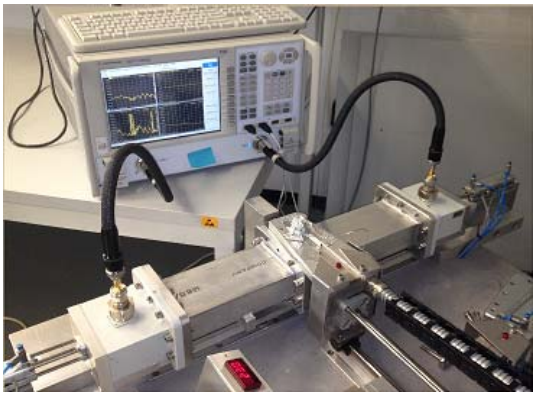

Set-up for temperature dependent dielectric measurement using transmission reflection method.

Samples that fully or partially cover the waveguide cross section can be used to get the dielectric properties with different analysis methods. The temperature of the material under test can be set to predefined temperature values by controlled resistive heating of the sample holder. The heating elements are installed in the waveguide sample holder. Temperature of the material is measured using a thermocouple and synchronized with the scattering parameters measured by the vector network analyzer. Both liquid and solid material can be measured using the setup. First experimental result for two different polymers can be seen in the following graph.

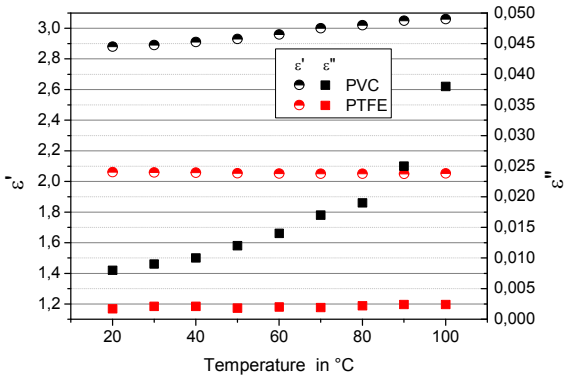

Complex permittivity measurement for PTFE and PVC as a function of temperature at 2.45 GHz.

Another test set, currently under development is the cavity perturbation method. It allows temperature dependent dielectric measurements of low and medium loss materials at 2.45 GHz up to more than 1000°C. Here, a small dielectric perturbation (sample) is placed in the cavity at a position where the electric field is not negligible. Thereby, the cavity resonant frequency and quality factor is changing according to the dielectric constant ε' and loss factor ε'' of the sample

The experimental set-up is presented in the following photo. The cavity is made from standard aluminum WR-340 waveguide. On both sides, the waveguide is closed by a parallel plate with a small iris. The maximum transmission coefficient at resonance and without perturbation for the $TE_{1,0,4}$ mode is -36 dB and the Q-factor is about 12000. Two coaxial waveguide adapters are used to connect the vector network analyzer (VNA) Agilent E5071C to the resonator. To provide an accurate positioning of the material under test (MUT) within the cavity a quartz tube with an outer diameter of 10 mm and an inner diameter of 8 mm is used as the sample holder. This sample holder can be moved between the cavity and a resistive heated tubular furnace that provides the desired temperature to the sample. A pyrometer is

installed at the opposite side of the applicator to get the MUT temperature during the dielectric measurements. Both VNA and pyrometer are connected to a personal computer for remote controlled acquisition and storage of the temperature and the S_{21} data.

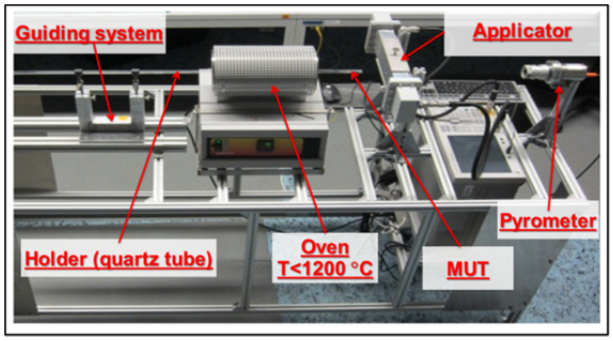

Set-up for temperature dependent dielectric measurement using the cavity pertubations method. (actual state).

The following graph shows an example of first measurement results obtained for MACOR glass ceramic at temperatures up to 550°C. It gives a rather good agreement to published data that was measured at ambient temperatures.

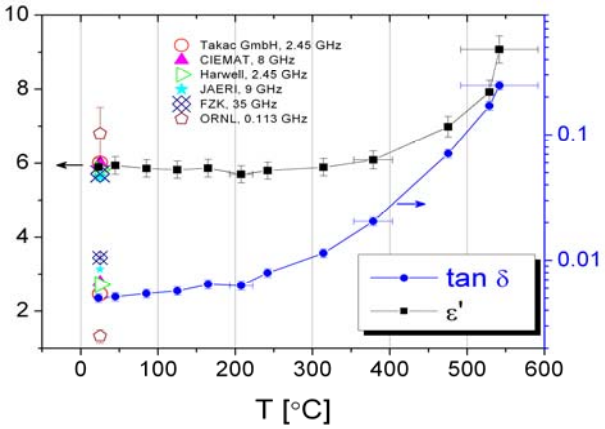

Dielectric properties for MACOR material. Some previously reported data at RT are presented for comparison.

NANOMIKRO

– High temperature microwave processing –

Metal powder sintering

A project on microwave sintering of metal powders compacts is currently running. This project is funded by the German Research Foundation (DFG), in collaboration with the Indian Institute of Technology, Department of Electrical Engineering, Kanpur. Selected metal powders have been investigated, such as Copper (Cu), Stainless Steel 316L and Iron (Fe). Metal powders have been characterized using XRD, XPS and SEM before being sintered using the KIT 30 GHz, 15 kW compact gyrotron system.

The 30 GHz microwave sintering experiments were done in combination with in-situ electrical resistivity measurements via the four-wire method. This four-wire experiment was installed in a modified dilatometer set-up that allows in-situ monitoring of the sintering kinetics as a function of temperature. This setup gives important information about microstructural changes with respect to the inter-particle electrical contacts during the sintering process.

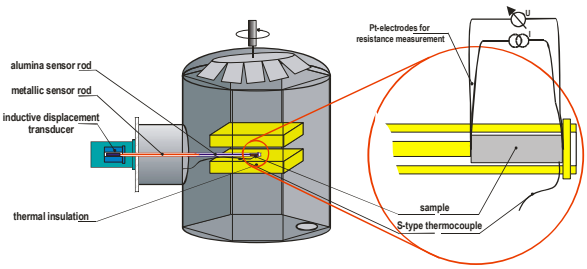

Scheme of the four-wire method in combination with the dilatometer setup.

As shown in the following graphs the electrical resistivity as well as the sintering behaviour, in case of copper metal powder, depend extensively on the environment (i.e. the type of the used gas). So it is believed that microstructural changes with respect to the inter-particle electrical contacts during the sintering process are highly dependent of the sintering environment. In the case where the forming gas was used, the resistance values drop dramatically around 220°C while this trend does not exist when using Argon gas of an identical sample. This temperature range (220°C) is actually matching the reduction reaction of copper oxide using hydrogen gas. So, it is believed that the thin oxide layer that exists on the as received copper particles play an important role. It does interact with the diffused hydrogen gas (in case of forming gas) and forms water vapour. This vapour pressure is causing the large noticeable expansion of the copper sample during sintering in forming gas. This remarkable expansion was not observed for the copper samples sintered in an argon gas environment. This observation highlights the importance of the thin oxide layer that may give some kind of dielectric properties to the green metal powder compact. Thus a volumetric heating during microwave sintering can be explained to some extent. So the dielectric properties calculations and modelling of the copper metal particles should take into account this thin oxide layer and should treat each particle as bi-layer unit in order to predict accurately the dielectric properties of these copper powders and hence to predict the MW absorption and heating profile of these powders.

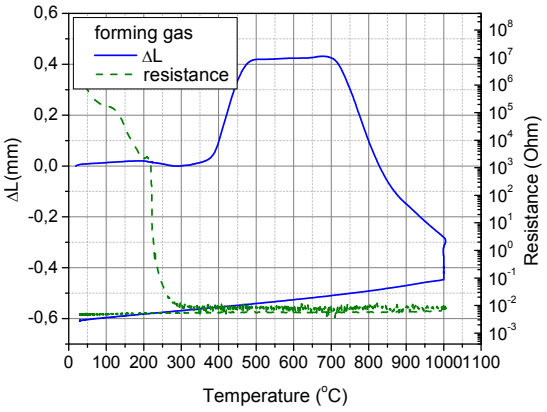

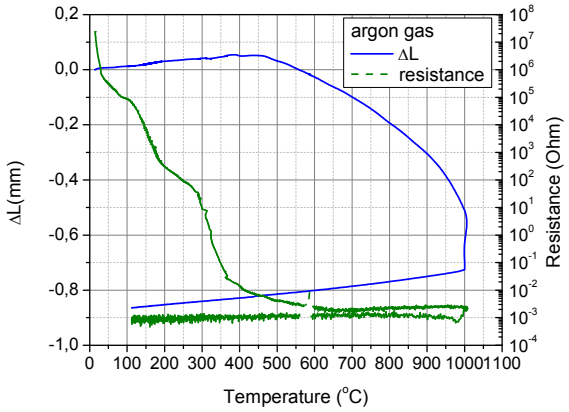

In-Situ resistance and dialtometery measuremnts of copper metal powder compacts sintered at 1000°C (10C/min) 10min in Argon and Forming gas (8%H_2-92%N_2) environments.

The 30 GHz microwave sintered metal samples were characterized using X-ray diffraction (XRD) and optical microscopy. From the XRD and the optical microscopy graphs, it is concluded that 30 GHz microwave processing was used successfully to sinter these copper metal powders. The project is still in progress.

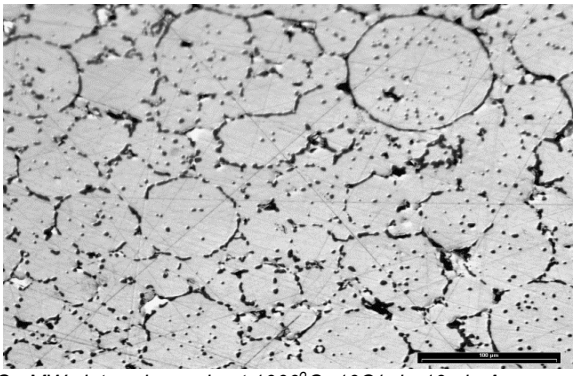

Cu MW sintered sample at 1000°C -10C/min-10min Argon gas.

Microwave assisted glycolysis of cobalt ferrite

Furthermore the synthesis and characterization of Cobalt Ferrite using high frequency microwave processing has been investigated. Cobalt ferrite powder was prepared using high frequency microwave heating via the polyol method using ethylene glycol as a high boiling point solvent as well as a reducing agent. A mixture of cobalt nitrate and ferric nitrate after being dissolved and mixed in ethylene glycol was microwave heated for 2 minutes in a closed container. A compact gyrotron system with a maximum power level of 15 kW was used for temperature controlled heating of the mixture. The so prepared powder samples were characterized using particle size analysis, scanning electron microscope (SEM) and X-ray diffraction (XRD). It is concluded that high frequency (30 GHz) microwave processing was successfully used to synthesize cobalt ferrite material.

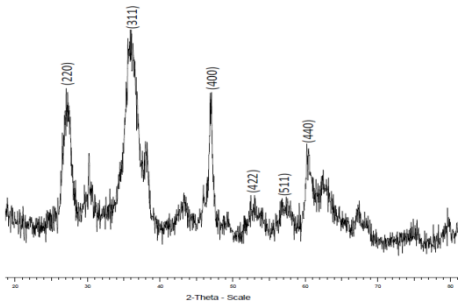

XRD pattern of 30 GHz microwave synthesized Cobalt Ferrite material.

Microwave sintering of doped ZnO nanoceramics

In collaboration with the federal university in Sao Carlos, Brazil systematic studies were performed on microwave sintering of electronic ceramics with submicron and nanoscale microstructures. The material under investigation was ZnO ceramic doped with nanostructured oxides like Bi_2O_3, Mn_3O_4, CoO, Cr_2O_3 and CuO.

Microwave frequency has been reported to influence diffusional processes during sintering. Therefore the project aims to study the influence of dopants and sintering in high frequency microwave fields (30GHz) on the ceramic microstructure and the resulting non-linear current-voltage properties. Comparative sintering studies were performed with the more common microwave frequencies at 2.45 GHz as well. Sintering kinetics were studied by dilatometric experiments at constant heating rates to determine the sintering parameters.

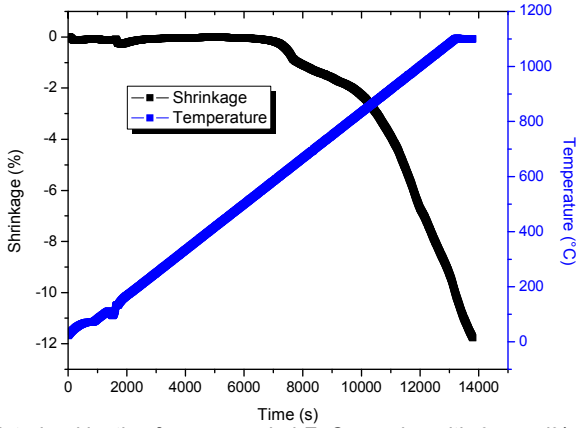

Sintering kinetics for nanoscaled ZnO powder with 0,5 mol% Bi_2O_3, Mn_3O_4, CoO, Cr_2O_3 and CuO dopant each.

Staff Involved:

J. Dittrich, Prof. H. Gemmeke, Prof. J. Jelonnek, Dr. T. Kayser, S. Layer, **Dr. G. Link**, Dr. A. Melcher, V. Nuß, Chr. Ott, T. Seitz, Dr. S. Soldatov, F. Steinhauser, Chr. Zöller

List of Publications

HGF Program: Fusion

Books

Eichmeier, J.A., Thumm, M.K. (Hrsg.)
Handbook of vacuum electronics: components and devices.
Moskva: Technosfera, 2011 (in russ. Sprache)

Faillon, G., Kornfeld, G., Borsch, E., Thumm, M.K.
High frequency electron tubes
Handbook of Vacuum Electronics: Components and Devices
Moskva: Technosfera, 2011, S. 17-95 (in russ. Sprache)

Publications at cross-referenced journals:

Arzhannikov, A.V., Burdakov, A.V., Vyacheslavov, L.N., Ivanov, I.A., Ivantsivsky, M.V., Kasatov, A.A., Kuznetsov, S.A., Makarow, M.A., Mekler, K.I., Polosatkin, S.V., Postuapaev, V.V., Popos, S.S., Sinitsky, S.L., Sklyarov, V.F., Thumm, M.K.A.
Diagnostic system for studying generation of subterahertz radiation during beam-plasma interaction in the GOL-3 facility
Plasma Physics Reports, 38(2012) S. 450-459
DOI: 10.1134/S1063780X12050017

Borie, E.
Lamb shift in light muonic atoms – revisited.
Annals of Physics, 327(2012) S. 733-763
DOI: 10.1016/j.aop.2011.11.017

Ginzburg, N.S., Peskov, N.Yu., Sergeev, A.S., Zaslavsky, V.Yu., Arzhannikov, A.V., Kalinin, P.V., Sinitsky, S.L., Thumm, M.
High selective two-dimensional Bragg resonators of planar geometry: Theoretical, computational, and experimental study.
Journal of Applied Physics, 112(2012 S. 114504/1-12
DOI: 10.1063/1.4766392

Hesch, K., Aktaa, J., Antusch, S., Boccaccini, L.V., Day, C., Demange, D., Fietz, W., Gantenbein, G., Möslang, A., Norajitra, P., Rieth, M.
Technology developments at KIT towards a magnetic confinement fusion power plant.
Transactions of Fusion Science and Technology, 61(2012) S.64-69

Igitkhanov, Yu., Bazylev, B., Landman, I.
CFC and W monoblock first wall concepts for fusion reactor.
Fusion Science and Technology, 62(2012) S.34-38

Igitkhanov, Yu.L.
the effect of non-Coulomb scattering of relativistic electrons on the generation of runaways in multicomponent plasma.
Contributions to Plasma Physics, 52(2012) S. 460-464
DOI: 10.1002/ctpp.201210034

Neudorfer, J., Stock, A., Flamm, J., Hindenlang, F., Gassner, G., Munz, C.D., Schneider, R., Roller, S.
Numerical investigation of high-order gyrotron mode propagation in launcers at 170 GHz.
IEEE Transacations on Plasma Science, 40(2012) S.1512-1521
DOI:101109/TPS.2012.2191575

Pestchanyi, S., Lehnen, M., Huber, A., Landman, I.
JET EFDA Contributors
Verification of TOKES simulations against the MGI experiments in JET.
Fusion Engineering and Design, 87(2012) S.1195-1200
DOI: 10.1016/j.fusengdes.2012.02.107

Shalashov, A.G., Gospodchikov, E.D., Smolyakova, O.B., Bagryansky, P.A., Maliygin, V.I., Thumm, M.
Auxiliary ECR heating system for the gas danamic trap.
Physics of Plasmas, 19(2012), 052503
DOI: 10.1063/1.4717757

Shalashov, A.G., Gospodchikov, E.D., Smolyakova, O.B., Bagryansky, P.A., Maliygin, V.I., Thumm, M.
Auxiliary ECR heating system for the gas danamic trap.
Problems of Atomic Science and Technology.
Series: Plasma Physics 82, No. 6, 49-51 (2012)

Stock, A., Neudorfer, J., Riedlinger, M., Pirrung, G., Gassner, G., Schneider, R., Roller, S., Munz, C.D.
Three-dimensional numerical simulation of a 30-GHz gyrotron resonator with an explicit high-order discontinuous-Galerkin-based parallel particle-in-cell method.
IEEE Transactions on Plasma Science, 40(2012) S. 1860-1870
DOI: 10.1109/TPS.2012.2195509

Other printed publications:

Arkhipov, A., Dvoretskaya, N., Kern, S., Louksha, O., Rzesnicki, T., Sominski, G.
Reconstruction of energy distributions in electron beams on the gases of Bremsstrahlung X-ray spectra.
4th Euro-Asian Pulsed Power Conf. (EAPPC 2012), 19th Internat. Conf. on High-Power Particle Beams (BEAMS 2012), Karlsruhe, September 30 – October 4, 2012
Proc. on CD-ROM
Karlsruhe: Karlsruhe Institute of Technology, 2012

Avramides, K.A., Ram, A.K., Dumbrajs, O., Alberti, S., Tran, T.M., Kern, S.
On the numerical scheme employed in gyrotron interaction simulations
17th Joint Workshop on Electron Cyclotron Emission and Electron Cyclotron Resonance Heating (EC-17), Deurne, NL, May 7-10, 2012
EPJ Web of Conferences, 32 (2012) S. 04017/1-6
DOI: 10.1051/epjconf/20123204017

Avramides, K.A., Pagonakis, I.G., Iatrou, C.T., Vomvoridis, J.L.
EURIDICE: A code-package for gyrotron interaction simulations and cavity design
17th Joint Workshop on Electron Cyclotron Emission and Electron Cyclotron Resonance Heating (EC-17), Deurne, NL, May 7-10, 2012
EPJ Web of Conferences, 32 (2012) S.04016/1-6
DOI: 10.1051/epjconf/20123204016

Bazylev, B., Coenen, J.W., Pitts, R.A., Philipps, V.
Modelling of tungsten armour damage under ITER-like transient head loads
15th Internat. Symp. on Flow Visualization, Minsk, Belarus, June 25-28, 2012, Proc. on CD-ROM

Bazylev, B., Landman, I., Pestchanyi, S., Igitkhanov, Y., Pitts, R.A., Putvinski, S., Arnoux, G., Brezinsek, S., Lehnen, M., Coenen, J.W., Saibene, G., Garkusha, I., Makhlay, W., Stangegy, P., JET EFDA Contributors
Modelling of material damage and high energy impacts on Tokamak PFCs during transient loads
Compilation of the EFDA-JET papers presented at the 24th IAEA Fusion Energy Conf., San Diego, Calif., October 8-13, 2012, CD-ROM Paper ITR/P1-39

Damyanova, M., Balabanova, E., Kern, S., Illy, S., Sabchevski, S., Thumm, M., Vasileva, E., Zhelyazkov, I.
Simulation tools for computer aided design and numerical investigations of high-Power gyrotrons
J. of Physics: Conference Series, 356 (2012) S.012044/1-4
DOI: 10.1088/1742-6596/356/1/012044

Erckmann, V., Kasparek, W., Plaum, B., Lechte, C., Petelin, M.I., Braune, H., Gantenbein, G., Laqua, H.P., Lubiako, L., Marushchenko, N.B., Michel, G., Turkin, Y., Weissgerber, M. and W7-X ECRH Teams at IPP Greifswald, IPF Stuttgart and KIT
Large scale CW ECRH systems: some considerations
17th Joint Workshop on Electron Cyclotron Emission and Electron Cyclotron Resonance Heating (EC-17), Deurne, NL, May 7-10, 2012
EPJ Web of Conferences, 32 (2012) S. 04006/1-6
DOI: 10.1051/epjconf/20123204006

Flamm, J., Jin, J., Thumm, M.
New algorithm for field calculation in tapered gyrotron launchers with adaptive surface perturbation
Internat. Vacuum Electronics and Vacuum Electron Sources Conf., Monterey, Calif., April 24-26, 2012
Proc. on USB-Stick
Piscataway, N.J.: IEEE, 2012, S. 419-420
ISBN 978-1-4673-0187-9

Ginzburg, N.S., Peskov, N.Yu., Sergeev, A.S., Zaslavsky, V.Yu., Arzhannikov, A.V., Kalinin, P.V., Sinitsky, S.L., Thumm, M.
Generation of powerful spatial coherent radiation in masers and lasers with two-dimensional distributed feedback
37th Internat. Conf. on Infrared Millimeter and Terahertz waves (IRMMW-THz 2012), Wollongong, AUS, September 23-28, 2012, Proc. on USB-Stick

Henderson, M.A., Darbos, C., Albajar, F., Alberti, S., debaar, M., Baruah, U., Becket, B., Bigelow, T., Bonicelli, T., Bruschi, A., Caughman, J., Chavan, R., Denisov, G., Farina, D., Fasel, D., Gandini, F., Gassman, T., Goodman, T.P., Hogge, J.P., Jean, O., Kajiwara, K., Kasparek, W., Kern, S., Kobayashi, N., Moro, A., Nazare, C., Oda, Y., Omori, T., Purohit, D., Ramponi, G., Rao, S.L., Rasmussen, D., Ronden, D., Saibene, G., Sakamoto, K., Sauter, O., Shapiro, M., Scherer, T., Singh, N.P., Strauss, D., Takahash, K., Temkin, R., Zohm, H.
Progress in the ITER electron cyclotron system development
17th Joint Workshop on Electron Cyclotron Emission and Electron Cyclotron Resonance Heating (EC-17), Deurne, NL, May 7-10, 2012

Igitkhanov, Y., Bazylev, B., Landman, I.
Modelling of PFC life-time in tokamak fusion reactor
KIT Scientific Reports, KIT-SR 7612 (Mai 2012)

Igitkhanov, Yu.L.
The effect on non-Coulomb scattering of relativistic electrons on the generation of runaways in multicomponent plasma
17th Joint EU-US Transport Task Force Meeting, Padova, I., September 3-6, 2012

Illy, S., Kern, S., Pagonakis, I., Vaccaro, A.
Collector loading of the 2 MW, 170 GHz gyrotron for ITER in the case of power modulation
4th Europ-Asian Pulsed Power Conf. (EAPPC 2012), 19th Internat. Conf. on High-Power Particle Beams (BEAMS 2012), Karlsruhe, September 30 – October 4, 2012
Proc. on CD-ROM
Karlsruhe: Karlsruhe Institute of Technology

Jelonnek, J., Alberti, S., Avramidis, K., Braune, H., Erckmann, V., Gantenbein, G., Hogge, J.P., Illy, S., Jin, J., Kern, S., Noke, F., Pagonakis, I., Piosczyk, B., Purps, F., Rzesnicki, T., Samartsev, A., Schlaich, A., Schmid, M., Thumm, M.
High power gyrotron development at KIT for ECD & CD of fusion plasmas
Internat. Vacuum Electronics and Vacuum Electron Sources Conf., Monterey, Calif., April 24-26, 2012
Proc. on USB-Stick
Piscataway, N.J.: IEEE, 2012, S. 111-112
ISBN 978-1-4673-0187-9

Jelonnek, J., Braune, H., Dammertz, G., Erckmann, V., Flamm, J., Gantenbein, G., Hollmann, F., Jonitz, L., Kasparek, W., Kern, S., Laqua, H.P., Lechte, C., Legrand, F., Leonhardt, W., Litaer, G., Michel, G., Noke, F., Purps, F., Samartsev, A., Schlaich, A., Schmid, M., Thumm, M., Uhren, P.
Progress on 140 GHz, 1 MW, CW series gyrotrons for W7-X
37th Internat. Conf. on Infrared, Millimeter and Terahertz waves (IRMMW-THz 2012), Wollongong, AUS, September 23-28, 2012, Proc. on USB-Stick

Jin, J., Flamm, J., Jelonnek, J., Kern, S., Pagonakis, I., Rzesnicki, T., Thumm, M.
Synthesis of quasi-optical mode converter for $TE_{32,9}$ mode, 1 MW gyrotron
4th Euro-Asian Pulsed Power Conf. (EAPPC 2012), 19th Internat. Conf. on High-Power Particle Beams (BEAMS 2012), Karlsruhe, September 30 – October 4, 2012
Proc. on CD-ROM
Karlsruhe: Karlsruhe Institute of Technology, 2012

Kalaria, P.C., Kartikeyan, V.M., Thumm, M.K.
Output system design for 170 GHz, 0,5 MW gyrotron for ECRH application
Internat. Vacuum Electronics and Vacuum Electron Sources Conf., Monterey, Calif., April 24-26, 2012
Proc. on USB-Stick
Piscataway, N.J.: IEEE, 2012, S. 501-502
ISBN 978-1-4673-0187-9

Kartikeyan, M.V., Kalaria, P.C., Thumm, M.
Studies on a 0.5 MW, 42 GHz CW. Conventional cavity gyrotron
37th Internat. Conf. on Infrared, Millimeter and Terahertz waves (IRMMW-THz 2012), Wollongong, AUS, September 23-28, 2012, Proc. on USB-Stick

Kartikeyan, M.V., Thumm, M.
Feasibility studies of a 1.0 MW, 204 GHz CW, conventional cavity gyrotron for future thermonuclear fusion reactors
37th Internat. Conf. on Infrared, Millimeter and Terahertz waves (IRMMW-THz 2012), Wollongong, AUS, September 23-28, 2012, Proc. on USB-Stick

Kern, S., Hogge, J.P., Alberti, S., Avramides, K., Gantenbein, G., Illy, S., Jelonnek, J., Jin, J., Li, F., Pagonakis, I.Gr., Piosczyk, B., Rzesnicki, T., Thumm, M.K., Tigelis, I., Tran, M.Q. EU Home Team at EGYC
Experimental results and recent developments on the EU 2 MW 170 GHz coaxial cavity gyrotron for ITER
17th Joint Workshop on Electron Cyclotron Emission and Electron Cyclotron Resonance Heating (EC-17), Deurne, NL, May 7-10, 2012
EPJ Web of Conferences, 32 (2012) S. 02011/1-8
DOI: 10.1051/epjconf/20123204009

Malygin, A., Illy, S., Pagopnakis, I., Piosczyk, B., Kern, S., Weggen, J., Thumm, M., Avramides, K., Ives, L., Marsden, D.
Desgin of a 10 kW / 28 GHz gyrotron with a segmented emitter using controlled-porosity reservoir cathodes
Internat. Vacuum Electronics and Vacuum Electron Sources Conf., Monterey, Calif., April 24-26, 2012
Proc. on USB-Stick, Piscataway, N.J.: IEEE, 2012, S. 331-332
ISBN 978-1-4673-0187-9

Malygin, A., Illy, S., Pagonakis, I., Piosczyk, B., Kern, S., Weggen, J., Thumm, M., Jelonnek, J., Avramides, K., Ives, L., Marsden, D.
Design and 3D simulations of a 10 kW / 28 GHz gyrotron with a segmented emitter based on controlled-porosity reservoir cathodes
4th Euro-Asian Pulsed Power Conf. (EAPPC 2012), 19th Internat. Conf. on High-Power Particle Beams (BEAMS 2012), Karlsruhe, September 30 – October 4, 2012
Proc. on CD-ROM
Karlsruhe: Karlsruhe Institute of Technology, 2012

Ortwein, P., Stock, A., Neudorfer, J., Kern, S., Illy, S., Schneider, R., Jelonnek, J., Munz, C.D.
High-accurate numerical full-wave simulation of an auto-modulation phenomenon for a 30 GHz gyrotron resonator
4th Euro-Asian Pulsed Power Conf. (EAPPC 2012), 19th Internat. Conf. on High-Power Particle Beams (BEAMS 2012), Karlsruhe, September 30 – October 4, 2012
Proc. on CD-ROM
Karlsruhe: Karlsruhe Institute of Technology, 2012

Petelin, M., Bongers, W., Bruschi, A., Erckmann, V., Kasparek, W., Olstad, R., Sakamoto, K., Thumm, M.
Problems of high-power millimetre wave beam control
4th Internat. Workshop on Far-Infrared Technologies (IW-FIRT 2012), Fukui, J., March 7-9, 2012
Proc. on CD-ROM Paper 7a-4
University of Fukui, 2012

Rzesnicki, T., Piosczyk, B., Gantenbein, G., Illy, S., Jelonnek, J., Jin, J., Kern, S., Pagonakis, I., Schlaich, A., Thumm, M.
2 MW coaxial-cavity pre-prototype gyrotron for ITER – recent experiments with the modified gyrotron setup
37th Internat. Conf. on Infrared, Millimeter and Terahertz waves (IRMMW-THz 2012), Wollongong, AUS, Sept. 23-28, 2012
Proc. on USB-Stick

Smartsev, A., Gantenbein, G., Jelonnek, J., Malygin, A., Thumm, M.
Multimode numerical code for simulation of gyrotron interaction with inclusion of particle-in-cell method
4th Euro-Asian Pulsed Power Conf. (EAPPC 2012), 19th Internat. Conf. on High-Power Particle Beams (BEAMS 2012), Karlsruhe, Sept. 30 – Oct. 4, 2012
Proc. on CD-ROM
Karlsruhe: Karlsruhe Institute of Technology, 2012

Schlaich, A., Gantenbein, G., Kern, S., Thumm, M.
Dynamic spectral measurements on high-power oscillators in the millimetre-wave domain
7th German Microwave Conf. (GeMiC 2012), Ilmenau, March 12-14, 2012, Conf-Proc. on USB-Stick
Ratingen: IMA e.V., 2012, ISBN 978-3-981668-5-6

Schlaich, A., Gantenbein, G., Kern, S., Thumm, M.
Systematic observation of time-dependent phenomena in the RF output spectrum of high power gyrotrons
17th Joint Workshop on Electron Cyclotron Emission and Electron Cyclotron Resonance Heating (EC-17), Deurne, NL, May 7-10, 2012
EPJ Web of Conferences, 32 (2012) S. 02011/1-8
DOI: 10.1051/epjconf/20123204002

Stober, J., Bock, A., Höhnle, H., Reich, M., Sommer, F., Treutterer, W., Wagner, D., Giannone, L., Herrmann, A., Leuterer, F., Monaco, F., Maraschek, M., Mlynek, A., Müller, S., Münich, M., Poli, E., Schubert, M., Schütz, H., Zohm, H., Kasparek, W., Stroth, U., Meier, A., Scherer, T., Strauß, D., Vaccaro, A., Flamm, J., Thumm, M., Litvak, A., Denisov, G.G., Chirkow, A.V., Tai, E.M., Popov, L.G., Nichiporenko, V.O., Myasnikov, V.E., Soluyanova, A., Malygin, S.A., ASDEX Upgrade Team
ECRH on ASDEX upgrade. System status, feed-back control, plasma physics results
17th Joint Workshop on Electron Cyclotron Emission and Electron Cyclotron Resonance Heating (EC-17), Deurne, NL, May 7-10, 2012
EPJ Web of Conferences, 32 (2012) S. 02011/1-8
DOI: 10.1051/epjconf/20123202011

Stock, A., Neudorfer, J., Schneider, R., Roller, S., Munz, C.D.
A full-wave 3D high-order discontinuous-Galerkin-method-based particle-in-cell code for the simulation of high-power gyrotron resonators
4th Euro-Asian Pulsed Power Conf. (EAPPC 2012), 19th Internat. Conf. on High-Power Particle Beams (BEAMS 2012), Karlsruhe, Sept. 30 – Oct. 4, 2012
Proc. on CD-ROM
Karlsruhe: Karlsruhe Institute of Technology, 2012

Thumm, M.
State-of-the-art of high power gyro-devices and free electron masers: update 2011
KIT Scientific Reports, KIT-SR 7606 (April 2012)

Wagner, D., Stober, J., Honecker, F., Leuterer, F., Monaco, F., Müller, S., Münich, M., Reich, M., Schubert, M., Schütz, H., Treutterer, W., Zohm, H., Thumm, M., Scherer, T., Meier, A., Gantenbein, G., Jelonnek, J., Kasparek, W., Plaum, B., Höhnle, H., Lechte, C., Litvak, A.G., Denisov, G.G., Chirkow, A., Popov, G., Nichiporenko, V.O., Myasnikov, V.E., Tai, E.M., Solyanova, E.A., Malygin, S.A., ASDEX Upgrade Team
The broadband multi-megawatt ECRH system at ASDEX upgrade
37th Internat. Conf. on Infrared, Millimeter and Terahertz Waves (IRMMW-THz 2012), Wollongong, AUS, Sept. 23-28, 2012
Proc. on USB-Stick

Wagner, D., Stober, J., Leuterer, F., Monaco, F., Müller, S., Münich, M., Schubert, M., Schütz, H., Zohm, H., Thumm, M., Scherer, T., Meier, A., Strauss, D., Gantenbein, G., Flamm, J., Kasparek, W., Höhnle, W., Lechte, C., Litvak, A.G., Denisov, G.G., Chirkov, A., Popov, L.G., Nichiporenko, V.O., Myasnikov, V.E., Tai, E.M., Solyanova, E.A., Malygin, S.A., ASDEX Upgrade Team
Operation of the multifrequency ECRH system at ASDEX upgrade
Proc. of the 36th Internat. Conf. on Infrared, Millimeter and Terahertz Waves (IRMMW-THz 2011), Houston, Tex., Oct. 2-7, 2011, Piscataway, N.J.: IEEE, 2011, S. 468-470
ISBN 978-1-4577-0510-6
DOI: 10.1109/irmmw-THz.2011.6105142

Papers or lectures, which are not available in printed form:

Aloisio, M., Van't Klooster, K., Petelin, M., Thumm, M.
Opportunities of phase controlled gyrotrons and quasi-optics for plasma fusion and space communication
24th Joint Russian-German Meeting on ECRH and Gyrotrons, Nizhny Novgorod, Russia, June 11-15, 2012

Arkhipov, A., Louksha, O., Sominski, G.G., Kern, S., Rzesnicki, T.
Development of X-ray diagnostics for determination of energy spectrum of electrons bombarding the collector
24th Joint Russian-German Meeting on ECRH and Gyrotrons, Nizhny Novgorod, Russia, June 11-15, 2012

Bagryansky, P.A., Demin, S.P., Gospodchikov, E.D., Kovalenko, Yu.V, Malygin, V.I., Murakhtin, S.V., Savkin, V.Ya., Shalashov, A.G., Smolyakova, O.B., Solomakhin, A.L., Thumm, M., Yakovlev, D.V.
ECR heating system for the gas dynamic trap
Joint Conference on Open Magnetic Systems for Plasma Confinement (OS) and the International Workshop on Plasma Material Interaction Facilities for Fusion (PMIF), Tsukuba, J, Aug. 27-31, 2012

Bazylev, G., Landman, I., Pestchanyi, S., Igitkhanov, Yu., Pitts, R.A., Putvinski, S., Brezinsek, S., Lehnen, M., Coenen, J.W., Philipps, V.
Modelling of material damage and high energy impacts on TOKAMAK PFCs during transient loads
Alushta-2012 Internat. Conf. –School on Plasma Physics and Controlled Fusion and Adjoint Workshop 'Nano- and Micro-sized Structures in Plasmas', Alushta, UA, Sept. 17-22, 2012
Book of Abstracts, S. 3

Betz, M., Capsers, F., Gasior, M., Thumm, M.
Status report and first results of the microwave LSW experiment at CERN
8th Patras Workshop on Axions, WIMPs and WISPs, Chicago, Ill., July 18-22, 2012

D'Andrea, D., Malygin, A., Jelonnek, J., Kern, S., Schneider, R., Stock, A., Neudorfer, J., Munz, C.D.
Start-up and parasitic modes analysis in TE31 cavity resonator
39th European Physical Society Conf. on Plasma Physics, 16th Internat. Congress on Plasma Physics, Stockholm, S, July 2-6, 2012

Gantenbein, G., Samartsev, A., Dammertz, G., Jelonnek, J., Losert, M., Schlaich, A., Scherer, T., Strauss, D., Thumm, M., Wagner, D.
Experimental investigations on a step-frequency tunable gyrotron with a diamond Brewster angle output window
Workshop on Physics and Technology of RF Heating of Fusion Plasmas, Nara, J, Dec. 11-13, 2012

Garkusha, L., Aksenov, N., Bazylev, B., Chuvilo, A., Chebotarev, V., Landman, I., Sadowski, M., Makhlai, V., Pestchanyi, S., Skladnik-Sadowska, E., Morgal, Y.
Analysis of tungsten dust generation under powerful plasma impacts simulating ITER ELMs and disruptions
24th IAEA Fusion Energy Conf., San Diego, Calif., Oct. 8-13, 2012, Abstracts on USB-Stick, S. 585

Igitkhanov, Yu., Bazylev, B., Boccaccini, L.
Analysis of W /Eurofer blanket lifetime in DEMO reactor
20th Internat. Conf. on Plasma Surface Interactions (PSI-20), Aachen, May 21-25, 2012

Igitkhanov, Yu., Bazylev, B., Pestchanyi, S., Boccaccini, L.
Plasma facing materials lifetime in fusion reactor
27th Symp. on Fusion Technology (SOFT 2012), Liege, B, Sept. 24-28, 2012

Igitkhanov, Yu., Bazylev, B., Landman, I.
Plasma facing materials lifetime in fusion reactor
20th Topical Meeting on the Technology of Fusion Energy (TOFE 2012), Nashville, Tenn., Aug. 27-31, 2012

Illy, S., Kern, S., Pagonakis, I., Thumm, M., Vaccaro, A.
Impact of gyrotron power modulation on the collector of the 2 MW, 170 GHz gyrotron for ITER
39th IEEE Internat. Conf. on Plasma Science (ICOPS 2012), Edinburgh, GB, July 8-12, 2012
Abstract on USB-Stick

Ioannidis, Z.C., Tigelis, I.G., Pagonakis, I.Gr., Illy, S., Schmid, M.
The eddy current effect on the transversal sweeping system of a gyrotron collector
39th IEEE Internat. Conference on Plasma Science (ICOPS 2012), Edinburg, GB, July 8-13, 2012

Jelonnek, J., Alberti, S., Erckmann, V., Gantenbein, G., Hogge, J.P., Illy, S., Jin, J., Kern, S., Pagonakis, I., Piosczyk, B., Rzesnicki, T., Thumm, . and W7-X Teams and EGYC Teams at KIT, EPFL-CRPP, HELIAS, IPF Stuttgart, IPF-CNR and IPP Greifswald
Development of advanced gyrotron
20th Topical Meeting on the Technology of Fusion Energy (TOFE 2012), Nashville, TN, Aug. 27-31, 2012

Jelonnek, J., Roy Choudhury, A., Dammertz, G., Flamm, J., Gantenbein, G., Illy, S., Jin, J., Kern, S., Losert, M., Malygin, A., Pagonakis, I., Piosczyk, B., Rzesnicki, T., Samartsev, A., Schlaich, A., Schmidt, M., Thumm, M.
Summary on gyrotron development at KIT
24th Joint Russian-German Meeting on ECRH and Gyrotrons, Nizhny Novgorod, Russia, June 11-15, 2012

Jelonnek, J., Roy Choudhury, A., Dammertz, G., Flamm, J., Gantenbein, G., Illy, S., Jin, J., Kern, S., Malygin, A., Pagonakis, I., Piosczyk, B., Rzesnicki, T., Samartsev, A., Schlaich, A., Schmid, M., Thumm, M.
Status and prospects of gyrotron development at KIT
2rd ITG Internat. Vacuum Electronics Workshop, Bad Honnef, Aug. 20-21, 2012

Kasparek, W., Holzhauer, E., Kumric, H., Plaum, B., Wacker, R., Zeitler, A., Gantenbein, G.
Three-mirror resonator reflectivity measurement of plane and grooved surfaces: setup, options, results
6th European Conf. on Antennas and Propagation (EUCAP 2012), Praha, CZ, March 26-30, 2012

Landman, I., Bazylev, B., Pitts, R., Saibene, G., Pestchanyi, S., Putvinski, S., Sugihara, M.
Radiation loads on the ITER first wall during massive gas injection
27th Symp. on Fusion Technology (SOFT 2012), Liege, B, Sept. 24-28, 2012

Landman, I.S., Pestchanyi, S.E., Igitkhanov, Y., Pitts, R.
Modelling of massive gas injection with tokamak code TOKES for mitigation of ITER disruptions
20th Internat. Conf. on Plasma Surface Interactions (PSI-20), Aachen, May 21-25, 2012

Laqua, H.P., Braune, H., Erckmann, V., Gantenbein, G., Jelonnek, J., Michel, G., Kasparek, W., Kern, S., Klinger, T., Plaum, B., Lechte, C., Schmid, M., Sunn Pederson, T., Wolf, R.
Status of the Wendelstein 7-X project and the ECRH-system
24th Joint Russian-German Meeting on ECRH and Gyrotrons, Nizhny Novgorod, Russia, June 11-15, 2012

Makhlaj, V.A., Garkusha, I.E., Aksenov, N.N., Byrka, O.V., Chuvilo, A.A., Landman, I., Lebedev, S.I., Shevchuk, P.B.
Plasma-surface interaction and mechanisms of dust production in ITER ELM simulation experiments with QSPA Kh-50
Alushta-2012 Internat. Conf.-School on Plasma Physics and Controlled Fusion and Adjoint Workshop 'Nano- and Microp-sized Structures in Plasmas', Alushta, UA, Sept. 17-22, 2012
Book of Abstracts, S. 67

Malygin, A., Illy, S., Pagonakis, I., Piosczyk, B., Kern, S., Weggen, J., Thumm, M., Avramides, K., Ives, L., Marsden, D.
Investigations towards a segmented emitter based on controlled-porosity reservoir cathodes for gyrotrons
24th Joint Russian-German Meeting on ECRH and Gyrotrons, Nizhny Novgorod, Russia, June 11-15, 2012

Malygin, A., Illy, S., Pagonakis, I., Piosczyk, B., Kern, S., Weggen, J., Thumm, M., Avramides, K., Ives, L., Marsden, D.
Design of a 10 kW / 28 GHz gyrotron with a segmented emitter using controlled-porosity reservoir cathodes
3rd ITG Internat. Vacuum Electronics Workshop, Bad Honnef, Aug. 20-21, 2012

Neudorfer, J., Stock, A., Munz,C.D., Schneider, R.
Parallelization of a 3D high-order particle-in-cell method and numerical simulations of a 179 GHz resonator and launcher
39th IEEE Internat. Conf. on Plasma Science (ICOPS 2012), Edinburgh, GB, July 8-12, 2012
Abstract on USB-Stick

Pagonakis, I.G., Illy, S., Piosczyk, B., Kern, S., Jelonnek, J., Avramides, K.A., Hogge, J.P.
Numerical study of the effects of the magnetic axis misalignment in the EU coaxial cavity gyrotron for ITER
39th IEEE Internat. Conf. on Plasma Science (ICOPS 2012), Edinburgh, GB, July 8-12, 2012, Abstract on USB-Stick

Pestchanyi, S., Arkhipov, N., Landman, I., Poznyak, I., Safronov, V., Toporkow, D.
Simulation of tungsten plasma transport along magnetic field under ELM-like heat loads
20th Internat. Conf. on Plasma Surface Interactions (PSI-20), Aachen, May 21-25, 2012

Pestchanyi, S., Lehnen, M., Huber, A., Gerasimov, S., Igitkhanov, Yu., Landman, I., JET EFDA Contributers
Analysis of energy cross-transport during MGI: JET experiments and TOKES simulations
27th Symp. on Fusion Technology (SOFT 2012), Liege, B, Sept. 24-28, 2012

Polosatkin, S., Astrelin, V., Bazylev, B., Beklemikshev, S., Burdakov, A., Gavrilenko, D., Huber, A., Ivanov, A., Ivanov, I., Kalinin, P., Kandaurov, I., Kreter, A., Landman, I., Postupaev, V., Sinitsky, S., Shoshin, A., Trunev, Yu., Thumm, M., Unterberg, B.
GDMT-T: Superconducting lenear device for PMI studies
Joint Conference on Open Magnetic Systems for Plasma Confinement (OS) and the Internat. Workshop on Palsma Material Interaction Facilities (PMIF), Tsukuba, J, August 27-31, 2012

Roy Choudhury, A., Kern, S., D'Andrea, D., Thumm, M., Jelonnek, J.
Feasibility study of a 240 GHz 2.02.5 MW coaxial cavity gyrotron
4th Euro-Asian Pulsed Power Conf. (EAPPC 2012), 19th Internat. Conf. on High-Power Particle Beams (BEAMS 2012, Karlsruhe, Sept. 30 – October 4, 2012

Schlaich, A., Gantenbein, G., Kern, S., Thumm, M.
Recent improvements in time-variant gyrotron RF output spectrum monitoring
39th IEEE Internat. Conf. on Plasma Science (ICOPS 2012), Edinburgh, GB, July 8-12, 2012, Abstract on USB-Stick

Schmid, M., Erckmann, V., Gantenbein, G., Illy, S., Jelonnek, J., Kern, S., Legrand, F., Samartsev, A., Schlaich, A., Rzesnicki, T., Thumm, M.
Recent achievements on tests of series gyrotrons for W7-X and planned extensions at the KIT gyrotron test facility
27th Symp. on Fusion Technology (SOFT 2012), Liege, B, Sept. 24-28, 2012

Stock, A., Neudorfer, J., Pfeiffer, M., Schneider, R., Fasoulas, S., Munz, C.D.
A high-order discontinuous Galerkin-approach-based particle-in-cell method for the simulation of large scale plasma devices
Scientific Computing in Electrical Engineering (SCEE 2012), Zürich, CH, Sept. 11-14, 2012

Stock, A., Neudorfer, J., Munz, C.D., Schneider, R.
Numerical simulation of a 30 GHz gyrotron resonator with a 3D high-order discontinuous Galerkin approach based particle-in-cell method
39th IEEE Internat. Conf. on Plasma Science (ICOPS 2012), Edinburgh, GB, July 8-12, 2012, Abstract on USB-Stick

Stock, A., Neudorfer, J., Schlaich, A., Kern, S., Schneider, R., Munz, C.D.
Simulation of the W7-X 140 GHz gyrotron resonator with an explicit 3D discontinuous Galerkin method based particle-in-cell scheme
39th European Physical Society Conf. on Plasma Physics, 16th Internat. Congress on Plasma Physics, Stockholm, S, July 2-6, 2012

Strauss, D., Aiello, G.,Chavan, R., Cirant, S., deBaar, M., Farina, D., Gantenbein, G., Goodman, T., Henderson, M.A., Kasparek, W., Kleefeldt, K., Landis, J.D., Meier, A., Moro, A., Platania, P., Plaum, B., Poli, E., Ramponi, G., Ronden, D., Saibene, G., Sanchez, F., Sautter, O., Scherer, T., Schreck, S., Serikov, A., Sozzi, C., Spaeh, P., Vaccaro, A., Zohm, H.
Preliminary design of the ITER ECH upper launcher
27th Symp. on Fusion Technology (SOFT 2012), Liege, B, Sept. 24-28, 2012

Thumm, M.
Development and applications of THz gyrotrons
Plasma Seminar, Budker Institute of Nuclear Physics (BINP), Novosibirsk, Russia, 13. März 2012

Thumm, M.
Mode conversion in overmoded waveguides and HE11 balanced hybrid mode
Seminar Series on HE11 Waveguide Transmission, No. 1, Budker Institute of Nuclear Physics (BINP), Novosibirsk, Russia, April 20, 2012

Thumm, M.
Laboratory of advanced research on millimetre and terahertz radiation
Wissenstransfer - die neue Kernaufgabe von Hochschulen, Deutsch-russisches Symp., Kassel, 24.-25. April 2012

Thumm, M.
Results of laboratory of advanced research on millimetre and terahertz radiation
Plasma Seminar, Budker Institute of Nuclear Physics, Novosibirsk, Russia, December 11, 2012

Thumm, M.K.A.
Millimeter-wave RADAR systems with gyro-amplifiers
Plasma Seminar, Budker Institute of Nuclear Physics (BINP), Novosibirsk, Russia, 6. Nov. 2012

Wolf, R.C., Baldzuhn, J. Beidler, C.D., Bluhm, T., Braune, H., Cardelle, A., Endler, M., Erckmann, V., Gantenbein, G., Hathiramani, D., Heimann, P., Hennig, C.,Hirsch, M., Jelonnek, K., Kasparek, W., König, R., Kornejew, P., Kroiss, H., Krom, J.G., Kühner, G., Laqua, H., Laqua, H.P., Lechte, C., Lewerentz, M., Maier, J., Michel, G., Schacht, J., Sunn-Pedersen, T., Thumm, M., Turkin, Y., Werner, A., Zhang, D., Zilker, M., Wendelstein 7-X Team
Preparation of steady-state operation of the Wendelstein 7-X stellerator
24th IAEA Fusion Energy Conf., San Diego, Calif., October 8-13, 2012

Zohm, H., Angioni, C., Fable, E., Federici, G., Gantenbein, G., Hartmann, T., Lackner, K., Poli, E., Porte, L., Sauter, O., Tardini, G., Ward, D., Wischmeier, M.
On the physics guide lines for a Tokamak DEMO
24th IAEA Fusion Energy Conf., San Diego, Calif., October 8-13, 2012

Zoletnik, S., Buday, C., Dunai, D., Kalvin, S., Krämer-Flecken, A., Liang, Y., Petravich, G., Soldatov, S., Pearson, J., Refy, D., TEXTOR Team
Dynamics of the electron density profile and plasma turbulence during the L-H transition and ELMs in TEXTOR
39th European Physical Society Conf. on Plasma Physics, 16th Internat. Congress on Plasma Physics, Stockholm, S, July 2-6, 2012

HGF Program: NANOMIKRO

Books

Thumm, M.K.A., Agafoncecv, A.M., Arzhannikov, A.V., Astrelin, V.T., Bagryansky, P.A., Burdakov, A.V., Ivanov, I.A., Kalinin, P.V., Kuznetsov, S.A., Makarow, M.A., Makotchenko, V.G., Mekler, K.I., Mikheev, A.N., Morozova, N.B., Paulish, A.G., Pankrushina, N.A., Polosatkin, S.V., Popos, S.A., Postupaev, V.V., Rovenskikh, A.F., Sinitsky, S.L., Sklyarov, V.F., Stepanov, V.D., Vyacheslovov, L.N., Zherikova, K.V.
Megagrant research project: laboratory of advanced research on millimeter and terahertz radiation at Novosibirsk state university
Gorzka, G. (Hrsg)
Knowledge Transfer : The New Core Responsibility of Higher Education Institutions Practice and Perspectives in Russia and Germany, Kassel: Kassel University Press, 2012, S. 131-156 (Ost-West Dialog 13), ISBN 978-3-86219-412-4

Publications at cross-referenced journals:

Arzhannikov, A.V., Ginzburg, N.S., Kalinin, P.V., Malkin, A.M., Peskov, N.Yuj., Sergeev, A.S., Sinitsky, S.L., Thumm, M., Zaslavsky, V.Yu.
Short-wavelength tunable Bragg reflectors based on coupling of propagating and cutoff waves: Modelling and experimental studies
Applied Physics Letters, 101 (2012) S. 083507/1-4
DOI: 10.1063/1.4747149

Morsi, M.M., Folz, D.C., Suchicital, C.T.A., Clark, D.E.
Crystallization of lithium disilicate glass using microwave processing
Journal of the American Ceramic Society, 95 (2012) S.579-585
DOI: 10.1111/j.1551-2916.2011.04936.x

Other printed publications:

Arzhannikov, A., Kuznetsov, S.A., Kalinin, P., Stepanov, V.D., Sinitsky, S., Thumm, M., Ginzburg, N., Peskov, N., Sergeev, A., Zaslavsky, V.
Experimentel study of two-channel planar FEM with 2D distributed feedback
4th Euro-Asian Pulsed Power Conf. (EAPPC 2012), 19th Internat. Conf. on High-Power Particle Beams (BEAMS 2012), Karlsruhe, Sept. 30 – Oct. 4, 1012
Proc. on CD-ROM,
Karlsruhe: Karlsruhe Institute of Technology 2012

Arzhannikov, A.V., Ginzburg, N.S., Zasloavkiy, V.Yu., Zotova, I.V., Kalinin, P.V., Kuznetsov, S.A., Malkin, A.M., Peskov, N.Yu., Sergeev, A.S., Sinitsky, S.L., Stepanov, V.D., Thumm, M.
Development of the two-stage planar FEM for the terahertz band on the basis of the ELMI accelerator
Terahertz Quasi-Optics, 7 (2012) S. 5-14

Arzhannikov, A.V., Ginzbur, N.S., Zasloavkiy, V.Yu., Zotova, I.V., Kalinin, P.V., Kuznetsov, S.A., Malkin, A.M., Peskov, N.Yu., Sergeev, A.S., Sinitsky, S.L., Stepanov, V.D., Thumm, M.
Razrabotka dvukhstadijnogo planarnogo MSE teragercovogo diapazona n osnove uskoritelja ELMI
Vestnik Novosibirskogo Gosudarstvennogo Universiteta: anucnyi Zhurnal, 7 (2012) Nr. 1, S. 5-14

Gupta, D., Sharma, A.K., Link, G., Thumm, M.
Investigation on microstructural characterization of microwave cladding
Singh, J.P. (Hrsg.)
Processing and Properties of Advanced Ceramics and Composites IV: Papers from the Materials Science and Technology 2011 Conf. and Exhibition (MS&T'11), Columbus, Ohio, Oct. 16-20, 2011
Hoboken, N.J. : John Wilex and Sons, 2012, S. 133-144 (Ceramic Transactions 234), ISBN 978-1-118-27336-4

Kuznetsov, S.A., Paulish, A.G., Gelfand, A.V., Astafiev, M.A., Arzhannikov, A.V., Fedorinin, V.N., Thumm, M.K.
Extremely thin metamaterial absorbers for subterahertz waves: from fundamentals towards applications in uncooled bolometric sensors
Boardman, A.D. (Hrsg.)
Metamaterials VII : Proc. of Photonics Europe, Bruxelles, B, April 16-19, 2012, Bellingham, Wash. : SPIE 2012,
S. 84230S/1-15 (SPIE Proceedings Series 8423)
ISBN 978-0-8194-9115-2

Kuznetsov, S.A., Astafyev, M.A., Arzhannikov, A.V., Thumm, M.K.A., Paulish, A.G., Gelfand, A.V.
Microstructured frequency selective quasi-optical components and devices for terahertz applications
Proc. of Internat. Symp. on Frontiers in THz Technology (FFT 2012), Nara, J, Nov. 27-29, 2012; USB-Stick Paper Pos 1.38, Shizuoka: Shizuoka University, FTT 2012

Link, G., Morsi, M.M., Thumm, M.
Dilatometric study and in situ resistivity measurements during millimetre wave sintering of metal powder compacts
Singh, J.P. (Hrsg.)
Processing and Properties of Advanced Ceramics and Composites IV: Papers from the Materials Science and Technology 2011 Conf. and Exhibition (MS&T'11), Columbus, Ohio, Oct. 16-20, 2011
Hoboken, N.J. : John Wilex and Sons, 2012, S. 145-149 (Ceramic Transactions 234), ISBN 978-1-118-27336-4

Morsi, M.M., Link, G., Miksch, S., Thumm, M.
High frequency microwave processing of lithium disilicate glass-ceramic
Singh, J.P. (Hrsg.)
Processing and Properties of Advanced Ceramics and Composites IV: Papers from the Materials Science and Technology 2011 Conf. and Exhibition (MS&T'11), Columbus, Ohio, Oct. 16-20, 2011
Hoboken, N.J. : John Wilex and Sons, 2012, S. 115-122 (Ceramic Transactions 234), ISBN 978-1-118-27336-4

Singh, J.P., Bansal, N.P. Goto, T., Lamon, J., Choi, S.R., Morsi, M.M., Link, G. (Hrsg.)
Processing and Properties of Advanced Ceramics and Composites IV
Papers from the Materials Science and Technology 2011 Conf. and Exhibition (MS&T'11), Columbus, Ohio, Oct. 16-20, 2011
Hoboken, N.J. : John Wilex and Sons, 2012 (Ceramic Transactions 234), ISBN 978-1-118-27336-4

Sinitsky, S.L. Arzhannikov, A.V., Kalinin, P.V., Kuznetsov, S.A., Stepanov, V.D., Ginzburg, N.S., Peskov, N.Yu., Sergeev, A.S., Zaslavsky. V.Yu., Thumm, M.
Synchronous generation of powerful 4-mm radiation in a two-channel planar FEM
37th Internat. Conf. on Infrared, Millimeter and Terahertz waves (IRMMW-THz 2012), Wollongong, AUS, Sept. 23-28, 2012
Proc. on USB-Stick

Stepanov, V., Arzhannikov, A., Kalinin, P., Sinitsky, S., Kuznetsov, S., Ginzburg, N., Peskov, N., Sergeev, A., Zaslavsky, V., Thumm, M.
Experimental study of two-channel planar FEM with 2D distributed feedback
4th Euro-Asian Pulsed Power Conf. (EAPPC 2012), 19th Internat. Conf. on High-Power Particle Beams (BEAMS 2012), Karlsruhe, Sept. 30 – Oct. 4, 2012; Book of Abstracts, S. 121

Takayama, S., Link, G., Morsi, M., Sano, S., Jelonnek, J.
Investigation of frequency effect for making iron process
4th Euro-Asian Pulsed Power Conf. (EAPPC 2012), 19th Internat. Conf. on High-Power Particle Beams (BEAMS 2012), Karlsruhe, Sept. 30 – Oct. 4, 2012; Book of Abstracts, S. 176

Thumm, M.K.A., Arzhannikov, A.V., Astrlin, V.T., Burdakov, A.V., Ginzburg, N.S., Ivanov, I.A., Kalinin, P.V., Kuznetsov, S.A., Makarov, M.A., Mekler, K.I., Paulish, A.G., Peskov, N.Yu., Polosatkin, S.V., Popov, S.A., Postupaev, V.V., Rovenskikh, A.F., Sergeev, A.S., Sinitsky, S.L., Sklyarov, V.F., Stephanov, V.D., Vyacheslavov, L.N., Zaslavsky, V.Yu.
Sub-terahertz emission by magnetized plasma at two-stream instability of REB and by two-channel planar FEM with combined electrodynamic system
4th Internat. Workshop on Far-Infrared Technologies (IW-FIRT 2012), Fukui, J, March 7-9, 2012; Proc. on CD-ROM, Paper 7a-2, University of Fukui 2012

Thumm, M.K.A., Arzhannikov, A.V.,Astrelin, V.T., Burdakov, A.V., Ginzburg, N.S., Ivanov, I.A., Kalinin, P.V., Kuznetsov, S.A., Makarov, M.A., Mekler, K.I., Paulish, A.G., Peskov, N.Yu., Polosatkin, S.V., Popov, S.A., Postupaev, V.V., Rovenskikh, A.F., Sergeev, A.S., Sinitsky, S.L., Sklyarov, V.F., Stephanov, V.D., Vyacheslavov, L.N., Zaslavsky, V.Yu.
Generation of high power THz waves in Relativistic electron beam plasma and two-sheet-beam FEM
Terahertz Science and Technology, 5 (2012), S. 18-39

Thumm, M.K.A., Arzhannikov, A.V.,Astrelin, V.T., Burdakov, A.V., Ivanov, I.A., Kalinin, P.V., Kandaurov, I.V., Kurkuchekov, V.V., Kuznetsov, S.A., Makarow, M.A., Mekler, K.I., Polosatkin, S.V., Popov, S.A., Postupaev, V.V., Rovenskikh, A.F., Sinitsky, S.L., Sklyarov, V.F., Stephanov, V.D., Trunev, Yu.A., Timofeev, I.V., Vyacheslavov, L.N.
Generation of high-power sub-THz-radiation by two-stream instability of electron beams in magnetized plasmas
Proc. of Internat. Symp. on Frontiert in THz Technology (FFT 2012), Nara, J, November 27-29, 2012; USB-Stick Paper TuA2.1; Shizuoka: Shizuoka University, FTT 2012

Papers or lectures, which are not available in printed form:

Arzhannikov, A.V.,Astrelin, V.T., Burdakov, A.V., Ivanov, I.A., Kalinin, P.V., Kandaurov, I.V., Kurkuchekov, V.V., Kuznetsov, S.A., Makarow, M.A., Mekler, K.I., Polosatkin, S.V., Popov, S.A., Postupaev, V.V., Rovenskikh, A.F., Sinitsky, S.L., Sklyarov, V.F., Stephanov, V.D., Trunev, Yu.A., Thumm, M.K.A., Timofeev, I.V., Vyacheslavov, L.N.
Experimental and theoretical investigations of emission of high power MM-wave and THz-radiation from magnetized plasma at two-stream instability of high current electron beams
24th Joint Russian-German Meeting on ECRH and Gyrotrons, Nizhny Novgorod, Russia, June 11-15, 2012

Arzhannikov, V.T., Burdakov, A.V., Ivanov, I.A., Kalinin, P.V., Kuznetsov, S.A., Makarow, M.A., Mekler, K.I., Popov, S.A., Postupaev, V.V., Rovenskikh, A.F., Sinitsky, S.L., Sklyarov, V.F., Stephanov, V.D., Sulyaev, Yu.S., Thumm, M.K.A., Vyacheslavov, L.N
Experimental investigation of generation of high power THz waves in magnetized plasma at two-stream instability of a high current REB
2nd Internat. Conf. 'Terahertz and Microwave Radiation: Generation, Detection and Applications', Moskva, Russia, June 20-22, 2012
Book of Abstracts S. 12

Arzhannikov, V.T., Burdakov, A.V., Burmasov, V.S., Kalinin, P.V., Kuznetsov, S.A., Makarov, M.A., Ivanov, I.A., Mekler, K.I., Popov, S.S., Postupaev, V.V., Rovenskikh, A.F., Sinitsky, S.L., Sklyarov, V.F., Stephanov, Timofeev, I.V., Thumm, M.K., Vyacheslavov, L.N
Experimental and theoretical investigations of high power sub-millimeter wave emission from plasma turbulence pumped by high current REB
4th Euro-Asian Pulsed Power Conf. (EAPPC 2012), 19th Internat. Conf. on High-Power Particle Beams (BEAMS 2012), Karlsruhe, Sept. 30 – Oct. 4, 1012; Book of Abstracts, S. 126

Freitas, M.A., Link, G., Kiminami, R.H.
High frequency microwave sintering of $LaNi_{1-x}Mn_xO_3$ (x = 0 to 1)
2nd Global Congress on Microwave Energy Applications (2GCMEA), Long Beach, Calif., July 23-27, 2012; Book of Abstracts S. 68

Kuznetsov, S., Astafyev, M., Navarro-Cia, M., Gelfand, A., Arzhannikov, A., Thumm, M.
Holographic metasurfaces for terahertz focusing: design, fabrication and experiment
3rd Internat. Conf. on Metamaterials, Photonic Crystal and Plasmonics (META'12), Paris, F, April 19-22, 2012

Kuznetsov, S., Arzhannikov, A.V., Thumm, M.K.A., Paulish, A.G., Gelfand, A.V., Fedorinin, V.N., Beruete, M., Navarro-Cia, M., Sorolla, M.
Ultrathin electromagnetic absorbers for mm- and submm-waves: from fdundamentals towards applications in bolometric sensors
3rd Internat. Conf. on Metamaterials, Photonic Crystal and Plasmonics (META'12), Paris, F, April 19-22, 2012

Link, G., Kayser, T., Lepers, B., Melcher, A., Nuß, V., Soldatov, S., Jelonnek, J.,
Microwave systems and applications at KIT
4th Euro-Asian Pulsed Power Conf. (EAPPC 2012), 19th Internat. Conf. on High-Power Particle Beams (BEAMS 2012), Karlsruhe, Sept. 30 – Oct. 4, 1012; Book of Abstracts, S. 250

Link, G.
Review on microwave materials processing
Indian Institute of Technology, Kanpur, IND, 16 Oktober 2012

Morsi, M.M., Link, G., Akhtar, J., Thumm, M.
High frequency microwave sintering of metal powders
2nd Global Congress on Microwave Energy Applications (2GCMEA), Long Beach, Calif., July 23-27, 2012

Morsi, M.M., Link, G., Schlabach, S., Szabo, D.V.
Symthesis and characterization of cobalt ferrite using high frequency microwave processing
4th Euro-Asian Pulsed Power Conf. (EAPPC 2012), 19th Internat. Conf. on High-Power Particle Beams (BEAMS 2012), Karlsruhe, Sept. 30 – Oct. 4, 1012; Book of Abstracts, S. 228

Morsi, M.M.
Microwave processing of lithium disilicate glass-ceramics
Department of Mechanical and Industrial Engineering, Indian Institute of Technology, Roorkee, IND, 21. März 2012

Morsi, M.M.
Microwave processing of silicate glass-ceramics
Department of Mechanical and Industrial Engineering, Indian Institute of Technology, Roorkee, IND, 16. März 2012

Thumm, M.K.A., Arzhannikov, A.V., Ginzburg, N.S., Kalinin, P.V., Kuznetsov, S.A., Peskov, N.Yu., Sergeev, A.S., Sinitsky, S.L., Stephanov, V.D., Zaslavsky, V.Yu.
Coherent radiation from two-channel planar FEM with 2D distributed feedback
24th Joint Russian-German Meeting on ECRH and Gyrotrons, Nizhny Novgorod, Russia, June 11-15, 2012

Thumm, M.K.A., Arzhannikov, A.V., Astrelin, V.T., , Burdakov, A.V., Ginzburg, N.S., Ivanov, I.A., Kalinin, P.V., Kuznetsov, S.A., Makarow, M.A., Mekler, K.I., Paulish, A.G., Peskov, N.Yu., Polosatkin, S.V., Popos, S.A., Postupaev, V.V., Rovenskikh, A.F., Sergeev, S.A., Sinitsky, S.L., Sklyarov, V.F., Stepanov, V.D., Vyacheslovov, L.N., Zaslavsky, V.Yu
Sub-terahertz emission by two-stream instability of REB in magnetized plasma and by two-channel planar FEM with combined electrodynamic system
3rd ITG Internat. Vacuum Electronics Workshop, Bad Honnef, Aug. 20-21, 2012

HGF-Program: NUKLEAR

Books

Kessler, G., Veser, A., Schlüter, F.H., Raskob, W., Landman, C., Päsler-Sauer, J.,
Sicherheit von Leichtwasserreaktoren: Risiken der Nukleartechnologie
Heidelberg [u.a.] : Springer, 2012, ISBN 978-3-642-28380-9 e-ISBN 978-3-642-288381-9

Kessler, G.
Sustainable and safe nuclear fission energy: technology and safety of fast and thermal nuclear reactors
Berlin [u.a.] : Springer, 2012 (Power Systems)
ISBN 978-3-642-11989-7

Publications at cross-referenced journals:

DelGiacco, M., Weisenburger, A., Spieler, P., Zimmermann, F., Lang, F., Jianu, A., Müller, G.
Experimental equipment for fretting corrosion simulation in heavy liquid metals for nuclear applications
Wear, 280-281 (2012), S. 46-53;
DOI:10.1016/j.wear.2012.01.018

DelGiacco, M., Weisenburger, A., Müller, G.
Fretting corrosion in liquid lead of structural steels for lead-cooled nuclear systems: preliminary study of the influence of temperature and time
Journal of Nuclear Materials, 423 (2012) S. 79-86
DOI:10.1016/j.jnucmat.2012.01.007

DelGiacco, M., Weisenburger, Jianu, A., Lang, F. Müller, G.
Influence of composition and microstructure on the corrosion behaviour of different Fe-Cr-Al alloys in molten
Journal of Nuclear Materials, 421 (2012) S. 39-46
DOI:10.1016/j.jnucmat.2011.11.049

Fetzer, R., Weisenburger, A., Jianu, A., Müller, G.
Oxide scale formation of modified FeCrAl coatings exposed to liquid lead
Corrosion Science, 55 (2012) S. 213-218
DOI:10.1016/j.corsci.2011.10.019

Knyazev, B.A., An, W., Bluhm, H.
Stark spectroscopy of a probe lithium beam excited with two dye lasers as a technique to study a high-power ion-beam diode
Review of Scientific Instruments, 83 (2012) S. 033101/1-9
DOI:10.1063/1.3690384

Weisenburger, A., Jianu, A., An, W., Fetzer, R., DelGiacco, M., Heinzel, A., Müller, G., Markow, V.G., Kasthanov, A.D.
Creep, creep-rupture tests of Al-surface-alloyed T91 steel in liquid lead bismuth at 500 and 550^{0}C
Journal of Nuclear Materials, 431 (2012) S. 77-84
DOI: 10.1016/j.jnucmat.2011.11.027

Other printed publications:

Engelko, V.I., Müller, G.
Microsecond intense electron beams for industrial applications
4th Euro-Asian Pulsed Power Conf. (EAPPC 2012), 19th Internat. Conf. on High-Power Particle Beams (BEAMS 2012), Karlsruhe, Sept. 30 – Oct. 4, 1012; Proc. on CD-ROM Karlsruhe Institute of Technology, 2012

Fetzer, R., An, W., Bazylev, B., Weisenburger, A., Müller, G.
Experimental and numerical investigations of surface dynamics during e-beam treatment
4th Euro-Asian Pulsed Power Conf. (EAPPC 2012), 19th Internat. Conf. on High-Power Particle Beams (BEAMS 2012), Karlsruhe, Sept. 30 – Oct. 4, 1012; Proc. on CD-ROM Karlsruhe Institute of Technology, 2012

Gromov, A.N., Bytzenko, O.A., Engelko, V.I., Tkachenko, K.I., Müller, G., Shulov, V.A., Teryaev, D.A.
Technological aspects of intense pulsed electron-beam application for properties improvements and repair of gas turbine engine blades
Internat. Conf. on High-Power Particle Beams (BEAMS 2012), Karlsruhe, Sept. 30 – Oct. 4, 1012; Proc. on CD-ROM Karlsruhe Institute of Technology, 2012

Heinzel, A., Weisenburger, A., Müller, G.
Corrosion behavior of welds in oxygen containing liquid lead
Jahrestagung Kerntechnik 2012, Stuttgart, 22.-24 Mai 2012 Berlin: INFORUM GmbH 2012, CD-ROM

Müller, G., Fetzer, R., An, W., Weisenburger, A., Engelko, V.,
Development of surface waviness during pulsed electron beam treatment
Elektrotechnica & Elektronica E + E, 47 (2012) S.159-163

Papers or lectures, which are not available in printed form:

An, W., Fetzer, R., Weisenburger, A., Müller, G.
Optical diagnostic of melt motion during electron beam treatment
4th Euro-Asian Pulsed Power Conf. (EAPPC 2012), 19th Internat. Conf. on High-Power Particle Beams (BEAMS 2012), Karlsruhe, Sept. 30 – Oct. 4, 1012; Book of Abstracts, S. 171

DelGiacco, M., Weisenburger, A., Müller, G.
Fretting corrosion of steels for lead alloy cooled ADS
11th Internat. Workshop on Spallation Materials Technology (IWSMT-11), Gent, B, Nov. 5-9, 2012

Fetzer, R., An, W., Müller, G., Weisenburger, A.
Development of surface waviness during pulsed electron beam treatment
76. Jahrestagung der DPG und DPG-Frühjahrstagung, Fachverband Dynamik und Statistische Physik, Berlin, 25.-30. März 2012
Verhandlungen der Deutschen Physikalischen Gesellschaft, R.6, B. 47 (2012), DY 3.7

Fetzer, R., An, W., Bazylev, B., Weisenburger, A., Müller, G.
Waviness on electron beam molten metal surfaces
4th Euro-Asian Pulsed Power Conf. (EAPPC 2012), 19th Internat. Conf. on High-Power Particle Beams (BEAMS 2012), Karlsruhe, Sept. 30 – Oct. 4, 1012

Fetzer, R., An, Weisenburger, A., Engelko, V., Müller, G.
In-situ diagnostics of pulsed electron beam interaction with metal targets
3rd ITG Internat. Vacuum Electronics Workshop, Bad Honnef, Aug. 20-21, 2012

Heinzel, A., Müller, G., Weisenburger, A.
Compatibility of welds and 12 Cr ODS with oxygen containing liquid Pb
Annual Meeting of the American Nuclear Society, 106(2012), S. 1260

Jianu, A., Weisenburger, A., Heinzel, A., Fetzer, R., DelGiacco, M., An, W., Müller, G.,
Investigation of thermally grown oxides on FeCrAl alloys exposed to heavy liquid metals
NUCLEAR 2012 : 5th Internat. Conf. on Sustainable Development through Nuclear Research and Education, Pitesti, R, May 16-18, 2012

Jianu, A., Weisenburger, A., Heinzel, A., Fetzer, R., DelGiacco, M., An, W., Müller, G.
Investigation of oxide scales formed on FeCrAl alloys exposed to heavy liquid metals
Nuclear Materials Conf. (NuMat 2012), Osaka, J, October 22-25, 2012

Jianu, A., Weisenburger, A., Heinzel, A., Fetzer, R., DelGiacco, M., An, W., Müller, G.
Investigation of thermally grown oxides on FeCrAl alloys exposed to heavy liquid metals
EFC Workshop 'Beyond Single Oxidants', Frankfurt, Sept. 19-21, 2012

Jianu, A., Weisenburger, Fetzer, R., DelGiacco, M., Heinzel, A., An, W., Müller, G
Compatibility of structural materials with liquid lead alloys
Workshop 'Materials under Extreme Conditions', Bucuresti, R, Sept. 25-28, 2012

Müller, G., Fetzer, R., An, W., Weisenburger, A., Engelko, V.
Development of surface waviness during pulsed electron beam treatment
10th Anniversary Internat. Conf. on Electron Beam Technologies, Varna, BG, May 31 – June 3, 2012

Müller, G., Jianu, A., Weisenburger, A., DelGiacco, M., Heinzel, A., Fetzer, R.,
Recent results on compatibility of structural materials in liquid lead alloys
Materials Research Society Fall Meeting 2012, Boston, Mass., Nov. 25-30, 2012

Weisenburger, A.
Lead cooled reactors – material issues
NUCLEAR 2012 : 5th Internat. Conf. on Sustainable Development through Nuclear Research and Education, Pitesti, R, May q16-18, 2012

Weisenburger, A., Fetzer, R., DelGiacco, M., Heinzel, A., Jianu, A., An, W., Müller, G., Bruhns, M., Doyle, S.
Pulsed electron beam modification (GESA) for improved corrosion resistance and mechanical behaviour of steels applied in lead alloy cooled reactors
4th Euro-Asian Pulsed Power Conf. (EAPPC 2012), 19th Internat. Conf. on High-Power Particle Beams (BEAMS 2012), Karlsruhe, Sept. 30 – Oct. 4, 1012; Book of Abstracts, S. 178

Weisenburger, A., Bruzzese, C., Class, A., Lang, F., Schroer, C.
Mini-pool reactor to determine interaction and mass transport of oxygen and other impurities in flowing LBE. Design and design supporting CFD calculations
11th Internat. Workshop on Spallation Materials Technology (IWSMT-11), Gent, B. Nov. 5-9, 2012

Weisenburger, A.
Environmental effects: liquid metals coolant
the Joint GETMAT-MATTER Internat. School on Materials Under Extreme Conditions (MUNECO)
Madrid, E, June 11-15, 2012

Weisenburger, A.
Corrosion in HLM systems
Internat. Workshop on Innovative Nuclear Reactors Cooled by Heavy Liquid Metals : Status and Perspectives, Pisa, I, April 17-20, 2012

Weisenburger, A., An, W., DelGiacco, M., Fetzer, R., Heinzel, A., Jianu, A., Müller, G.,
Compatibility of austenitic steels with PbBi at MYRRHA relevant conditions
Internat. Workshop on the Key Material Properties for Myrrha and Astrid, Rome, I, March 7-9, 2012

HGF-Program: ENERGY (EE)

Books

Wegner, L.H.
Using the multifunctional xylem probe for in situ studies of plant water and ion relations under saline conditions
Shabala, S. [Hrsg.] Plant Salt Tolerance – Methods and Protocols, New York: Springer 2012, S. 35-66 (Methods in Molecular Biology, Vol. 913) ISBN 978-1-61779-985-3; also publ. online: e-ISBN 978-1-61779-986-0

Publications at cross-referenced journals:

Sack, M., Müller, G.
Modular trigger generator for an over-voltage triggered Marx generator
IEEE Transactions on Plasma Science, 40 (2012) S. 2618-2624
DOI:10.1109/TPS.2012.2196292

Other printed publications:

Attmann, F., Sack, M., Müller, G.
Experiments for reducing the jitter of an over-voltage triggered spark gap
18th Internat. Pulsed Power Conf., Chicago, June 19-23, 2011; Proc. S. 745-748, Piscataway, N.J. : IEEE 2011; ISBN 978-1-457-70629-5; DOI:10.1109/PPC.2011.6191504

Berghoefer, T., Flickinger, B., Frey, W.
Aspects of plant plasmalemma charging induced by external electric field pulses
Plant Signaling and Behavior, 7 (2012) S. 322-324
DOI:10.4161/psb.19174

Frey, W., Eing, C., Göttel, M., Gusbeth, C., Strässner, R.
Pulsed electric field treatment of microalgae – benefits for microalgae biomass processing
4th Euro-Asian Pulsed Power Conf. (EAPPC 2012), 19th Internat. Conf. on High-Power Particle Beams (BEAMS 2012), Karlsruhe, Sept. 30 – Oct. 4, 1012; Proc. on CD-ROM, Karlsruhe Institute of Technology 2012

Frey, W., Eing, C., Göttel, M., Gusbeth, C., Strässner, R.
Application of pulsed electric field treatment for microalgae processing
Proc. of the Internat. Conf. on Bio and Food Electrotechnologies (BFE 2012), Fisciano, I, Sept. 26-28, 2012
Salerno: ProdAl S.c.a.r.l 2012, S. 237-241, ISBN 978-88-903261-8-9

Jelonnek, J. [Hrsg.]
Annual report 2011 Institut for Pulsed Power and Microwave Technology; KIT Scientific Reports, KIT-SR 7619 (July 2012)

Sack, M., Sigler, J., Stukenbrock, L., Eing, C., Müller, G.
Lab-scale experiments on PEF-treatment of grape mash at different pulse parameters
4th Euro-Asian Pulsed Power Conf. (EAPPC 2012), 19th Internat. Conf. on High-Power Particle Beams (BEAMS 2012), Karlsruhe, Sept. 30 – Oct. 4, 1012; Proc. on CD-ROM, Karlsruhe Institute of Technology 2012

Sack, M., Keipert, S., Hochberg, M., Greule, M., Müller, G.
Design considerations for a fast stacked-MOSFET switch
4th Euro-Asian Pulsed Power Conf. (EAPPC 2012), 19th Internat. Conf. on High-Power Particle Beams (BEAMS 2012), Karlsruhe, Sept. 30 – Oct. 4, 1012; Proc. on CD-ROM, Karlsruhe Institute of Technology 2012

Sack, M., Sigler, J., Stukenbrock, L., Eing, C., Müller, G.
On the variation pf pulse parameters for PEF treatment of graphe mash
Proc. of the Internat. Conf. on Bio and Food Electrotechnologies (BFE 2012), Fisciano, I, Sept. 26-28, 2012
Salerno: ProdAl S.c.a.r.l 2012, S. 223-2227, ISBN 978-88-903261-8-9

Sack, M., Müller, G.
Modular trigger generator for an over-voltage triggered Marx generator
18th Internat. Pulsed Power Conf., Chicago, Ill., June 19-23, 2011; Proc. S. 778-781, Piscataway, N.J. : IEEE 2011, 978-1-457-70629-5, DOI:10.1109/PPC.2011.6191510

Schmidt, O., Schick, A., Sack, M., Sigler, I.
Sesam öffne Dich. Elektroporation von Trauben
Das Deutsche Weinmagazin (2012) Nr. 6, S.32-38

Sträßner, R., Eing, C., Frey, W.
Chlorophyll fluorescence as a diagnostic tool for the monitoring of abiotic stress imposed on microalgae by pulsed electric fields
4th Euro-Asian Pulsed Power Conf. (EAPPC 2012), 19th Internat. Conf. on High-Power Particle Beams (BEAMS 2012), Karlsruhe, Sept. 30 – Oct. 4, 1012; Proc. on CD-ROM, Karlsruhe Institute of Technology 2012

Wang, S., Shu, T., Sack, M., Frey, W., Müller, G.
Study of a miniature pulse generator applied to electroporation of plant cells
4th Euro-Asian Pulsed Power Conf. (EAPPC 2012), 19th Internat. Conf. on High-Power Particle Beams (BEAMS 2012), Karlsruhe, Sept. 30 – Oct. 4, 1012; Proc. on CD-ROM, Karlsruhe Institute of Technology 2012

Wegner, L.H., Schönwälder, S.
Electroporation of plant cells studied with the patch clamp technique
4th Euro-Asian Pulsed Power Conf. (EAPPC 2012), 19th Internat. Conf. on High-Power Particle Beams (BEAMS 2012), Karlsruhe, Sept. 30 – Oct. 4, 1012; Proc. on CD-ROM, Karlsruhe Institute of Technology 2012

Papers or lectures, which are not available in printed form:

Eing, C., Frey, W., Gusbeth, C., Göttel, M., Strässner, R.
Pulsed electric field treatment of the microalgae Auxenochlorella protothecoides for improved lipid extraction performance
4th Euro-Asian Pulsed Power Conf. (EAPPC 2012), 19th Internat. Conf. on High-Power Particle Beams (BEAMS 2012), Karlsruhe, Sept. 30 – Oct. 4, 1012, Book of Abstracts, S. 151

Frey, W., Silve, A.
Behaviour of voltage sensitive hemicyanine dyes on the nanosecond time scale: an explanatory approach for ANNINE-6
9th Internat. Bioelectric Symp., Kumamoto, J, Sept. 5-8, 2012

Frey, W., Göttel, M., Eing, C., Gusbeth, C., Strässner, R., Posten, C., Nick, P.
Pulsed electric field treatment of microalgae. Benefits for downstream processing
Halbjahrestreffen des Netzwerks Algen, Göttingen, 5. Nov. 2012

Göttel, M., Eing, C., Gusbeth, C., Frey, W.
Pulsed electric field (PEF) enhanced extraction of cell ingredients from microalgae
Internat. Conf. on Bio ande Food Electrotechnologies (BFE 2012), Fisciano, I, Sept. 26-28, 2012

Göttel, M., Eing, C., Gusbeth, C., Frey, W.
Pulsed electric field treatment - a promising process for the disintegration of microalgae
4th Euro-Asian Pulsed Power Conf. (EAPPC 2012), 19th Internat. Conf. on High-Power Particle Beams (BEAMS 2012), Karlsruhe, Sept. 30 – Oct. 4, 1012

Gusbeth, C., Eing, C., Strässner, R., Göttel, M., Frey, W.
Stimulation of mircoalgal growth by means of nanoseconds pulsed electric field treatment (nsPEF)
9th Internat. Bioelectric Symp., Kumamoto, J, Sept. 5-8, 2012

Gusbeth, C.A., Strässner, R., Frey, W.
Decontamination of wastewater by pulsed underwater corona discharges: anodes lifetime considerations
4th Euro-Asian Pulsed Power Conf. (EAPPC 2012), 19th Internat. Conf. on High-Power Particle Beams (BEAMS 2012), Karlsruhe, Sept. 30 – Oct. 4, 1012, Book of Abstracts S. 241

Sack, M., Attmann, F., Müller, G.
Over-voltage trigger for Marx generators
Symp., Institut Franco-Allemand de Recherches de Saint-Louis, F, 21-22 Mars 2012

Sack, M., Müller, G.
Design and test of a modular trigger generator for over-voltage triggering of Marx generators
2012 IEEE Internat. Power Modulator and High Voltage Conf., San Diego, Calif., June 3-7, 2012

Silve, A., Leray, I., Mir, L.M.
New insights of the electrical parameters responsible for eletroporation on the nanosecond timescale
4th Euro-Asian Pulsed Power Conf. (EAPPC 2012), 19th Internat. Conf. on High-Power Particle Beams (BEAMS 2012), Karlsruhe, Sept. 30 – Oct. 4, 1012, Book of Abstracts S. 242

HGF-Program: Efficient Energy Use and Conversion (REUN)

Other printed publications:

Kayser, T., Melcher, A., Link, G., Jelonnek, J.
Simulation for microwave heating of catalysis for CO_2 reduction to CO
2012 IEEE / MTT-S Internat. Microwave Symp. Digest (MTT 2012), Proc. of a Meeting, Montreal, CDN, June 17-22, 2012 CD-ROM, Piscataway, N.J., IEEE 2012, ISBN 978-1-4673-1087-1

Melcher, A., Lepers, B., Umminger, M., Kayser, T., Link, G., Haist, M., Jelonnek, J., Müller, H.
Modelling and simulation of microwave heating for spalling of radioactive contaminated concrete
83rd Annual Meeting of the Internat. Associaten of Applied Mathematics and Mechanics (GAMM 2012), Darmstadt, March 26-30, 2012
Proceedings in Applied Mathematics and Mechanics, 12 (2012), S. 351-352
DOI:10.1002/pamm.201210164

Soldatov, S., Kayser, T., Link, G., Seitz, T., Layer, S., Jelonnek, J.
High temperature dielectric measurements based on cavity perturbation approach
4th Euro-Asian Pulsed Power Conf. (EAPPC 2012), 19th Internat. Conf. on High-Power Particle Beams (BEAMS 2012), Karlsruhe, Sept. 30 – Oct. 4, 1012; Proc. on CD-ROM, Karlsruhe Institute of Technology 2012

Papers or lectures, which are not available in printed form:

Kayser, T., Melcher, A.M., Link, G., Jelonnek, J.
CO_2 reduction to CO using a microwave heated catalyst
14th Seminar 'Computer Modeling in Microwave Engineering and Applications', Bayreuth, March 5-6, 2012

Kayser, T., Melcher, A., Link, G., Jelonnek, J.
A microwave heated reactor for reduction of CO_2 to CO
2nd Global Congress on Microwave Energy Applications (2GCMEA), Long Beach, Calif., July 23-27, 2012
Book of Abstracts, S. 68

Link, G.
Some basics in microwave technology
Vortrag, Firma Vötsch Industrietechnik, 24. April 2012

Link, G.
Microwave applications in materials processing
Vortrag, Firma Vötsch Industrietechnik, 24. April 2012

Link, G.
Mikrowellenaktivitäten am KIT
Vortrag, Fraunhofer-Einrichtung für Polymermaterialien und Composite (PYCO), Berlin, 5. September 2012

Link, G.
Activities on microwave materials processing at KIT
Alexander-von-Humboldt-Colloquium, Indian Institute of Technology, Roorkee, IND, October 11, 2012

Link, G., Weiß, R.
Faserverbund Leichtbau mit automatisierter Mikrowellenprozesstechnik hoher Energieeffizienz (FLAME)
Koordinatorentreffen Energieeffizienter Leichtbau, Augsburg, 23-24. Mai 2012

Melcher, A., Umminger, M., Kayser, T., Link, G., Haist, M., Müller, H.S., Jelonnek, J.
Microwave-assisted ablation of contaminated concrete surfaces. Modeling, simulation and experiments
14th Seminar 'Computer Modeling in Microwave Engineering and Applications', Bayreuth, March 5-6, 2012

Prastiyanto, D., Link, G., Thumm, M., Jelonnek, J.
Temperature dependent measurements of dielectric materials at 2.45 GHz
Chancen der Energiewende: 1. Jahrestagung des KIT-Zentrums Energie, Karlsruhe, 19. Juni 2012

The Institute for Pulsed Power and Microwave Technology (Institut für Hochleistungsimpuls- und Mikrowellentechnik (IHM)) is doing research in the areas of pulsed power and high power microwave technologies. Both, research and development of high power sources as well as related applications are in the focus. Applications for pulsed power technologies are ranging from material processing to bioelectrics. Microwave technologies are focusing on RF sources for electron cyclotron resonance heating and on applications for material processing at microwave frequencies.

IHM is doing research, development, academic education and, in collaboration with the KIT Division IMA and industrial partners, the technology transfer. Projects have been conducted within six HGF Programs: Renewable Energies (EE), FUSION, NUKLEAR, NANOMIKRO, Efficient Energy Conversion and Use (REUN) and Technology-Innovation and Society (TIG). R&D work has been done in the following topics: fundamental theoretical and experimental research on the generation of intense electron beams, strong electromagnetic fields and their interaction with plants, materials and plasmas; application of these methods in the areas of generation of energy through controlled thermonuclear fusion in magnetically confined plasmas, in materials processing and in energy technology.

By Sept. 2012, Prof. Dr.-Ing. John Jelonnek has completed his first year as successor of Prof. Dr. Dr. h. c. Manfred Thumm as Director of IHM. The organizational structure of IHM has been adapted. The department for high power microwave technologies is formed by three teams now, the team “gyrotron simulation and components”, headed by Dr. Stefan Illy, the team “gyrotron verification and measurements techniques”, headed by Dr. Tomasz Rzesnicki and the team “materials processing with microwaves” headed by Dr. Guido Link. The team “plasma-wall interactions”, headed by Dr. Igor Landman has been moved to the department of pulsed power technologies.

IHM has organized the 4th Euro-Asian Pulsed Power Conference (EAPPC) in combination with the 19th International Conference on High-Power Particle Beams (BEAMS) which took place at Karlsruhe in September. Chair has been Dr. Georg Müller. The conference has been counted as very successful event. Prof. Manfred Thumm received the “Heinrich-Hertz Preis” of KIT and EnBW Stiftung for his research work in the area of generation, transmission and conversion of high power microwaves for future magnetic confinement nuclear plasma devices. Prof. Manfred Thumm received the “Excellent Teaching Award” for the Embedded Systems Engineering Executive Master Program of the HECTOR School of Engineering and Management at the KIT. DI Andreas Schlaich received the “Student Paper Award – Honourable Mention” at the 39th IEEE Int. Conference on Plasma Science (ICOPS 2012) in Edinburgh, Scotland.

The list of 189 publications in 2012 is enclosed at the end of this report.

ISSN 1869-9669